EXPERIMENTAL STUDY OF SHEET PILE RETAINING WALLS WITH GRANULATED RUBBER REINFORCED BACKFILL

A Thesis Submitted to
the Graduate School of
İzmir Institute of Technology
in Partial Fulfillment of the Requirements for the Degree of

MASTER OF SCIENCE

in Civil Engineering

by

Ali Hamid Khlaif KHLAIF

December 2021

IZMIR

ACKNOWLEDGMENTS

I want to express my gratitude to my supervisor, Prof. Dr. Nurhan ECEMIS ZEREN, for his assistance in this scientific study, guiding me through planning, research, and execution of my thesis, instilling in me with scientific confidence through her knowledge and experience. She was always patience with me and showed a high degree of understanding.

I would like to express my gratitude to the jury members, that is Assoc. Prof. Dr. Volkan Emre UZ, and Assoc. Prof. Dr. ONUR AKAY, for their participation in my thesis defense seminar and for their insightful comments on this work.

I would like to express my gratitude to my family for their unwavering support during my studies, particularly my late father, who always believed in me and encouraged me to pursue graduate studies.

We would like to express our gratitude to Mustafa KARAMAN and my laboratory colleagues Murat ORÜCÜ, Ceren Gizem SARITAS, Hazal TANERI, and Mustafa Sezer ARIK for their support and contributions to my laboratory work.

ABSTRACT

EXPERIMENTAL STUDY OF SHEET PILE RETAINING WALLS WITH GRANULATED RUBBER REINFORCED BACKFILL

Earth retaining structures such as retaining walls, bridge abutment, bulkhead, braced excavation, and mechanically stabilized walls play a critical role in many infrastructural projects and are often subjected to different loading conditions. Performance of retaining walls under static and dynamic loading conditions depends upon the type of backfill soil.

According to the European tire and rubber manufacturers' Association (ETRMA) report about the end-of-life tyers management in 2017, Turkey recovers 0% of scrap tires in the civil engineering, public works, and backfilling category.

This study aims at describing the ability to use granulated rubber sand mix as a backfill material in earth retaining structures.

Therefore, physical model tests were conducted to investigate the deformation characteristics and pressure distribution of granulated rubber-sand mixture backfill behind the sheet pile. At dry and saturated conditions, granulated rubber-sand mixture backfill areas were changed in the physical model tests. Granulated rubber showed promising results that reduced the stiffness and density and increased the shear strength when used with sand. 6%, 8%, 10%, 12, and 15% granulated rubber mixing ratios have been tested using coarse and fine granulated rubber. The optimum ratio was 10% of finely granulated rubber. The maximum dry density reduced by 3.1%, and the maximum shear strength increased by 6.1%.

When the granulated rubber-sand mix was used as a backfill, it reduced the lateral earth pressure and increased the water seepage under the sheet pile. The sheet pile model with granulated rubber sand mix backfill showed higher strength than the clean sand model.

ÖZET

GRANÜL KAUÇUK TAKVİYELİ DOLGUYA SAHİP PALPLANŞ İSTİNAT DUVARLARININ DENEYSEL ÇALIŞMASI

İstinat duvarları, köprü kenar ayağı, perde, ikaslı kazı ve mekanik olarak stabilize edilmiş duvarlar gibi zemin istinat yapıları, birçok altyapı projesinde kritik rol oynar ve genellikle farklı yükleme koşullarına maruz kalır. İstinat duvarlarının statik ve dinamik yükleme koşulları altında performansı, dolgu malzemesinin tipine bağlıdır. İstinat duvarlarının arkasında genellikle temiz granüler kohezyonsuz dolgu malzemeleri tercih edilir. Son zamanlarda, parçalanmış lastik kırıntıları, granüler kauçuk, geofoam, uçucu kül, plastik şişeler vb. gibi yeni geri dönüştürülmüş hafif malzemeler, kohezyonsuz granuler zeminle karıştırılarak kullanılabilir.

Avrupa Lastik ve Kauçuk Üreticileri Birliği'nin (ETRMA) 2017'deki ömrünü tamamlamış lastik yönetimine ilişkin raporuna göre, Türkiye inşaat mühendisliği, bayındırlık işleri ve dolgu alanlarında geri kazanın hurda lastik kullanımını %0 olarak belirtilmiştir. Öte yandan, bazı ülkeler inşaat malzemesini geliştirmek için granül kauçuklar kullanmaktadır. Kalifornya'da, lastikli asfalt kaplama projelerinde 10 milyondan fazla atık lastik kullanmış veya tasarımı optimize edilmiştir.

Bu çalışma, granüler kauçuk kum karışımının zemin istinat yapılarında dolgu malzemesi olarak kullanılabilme becerisini açıklamayı amaçlamaktadır.

Bu nedenle, palplanş arkasındaki granüler kauçuk kum karışımı dolgunun deformasyon özelliklerini ve basınç dağılımını araştırmak için fiziksel model testleri yapılmıştır. Kuru ve doygun zemin koşullarında, fiziksel modelleme testlerinde granül kauçuk kum karışımın dolgu alanları değiştirilmiştir. Granül kauçuk, kumla birlikte kullanıldığında rijitliği ve yoğunluğu azaltan ve kesme mukavemetini artıran umut verici sonuçlar göstermiştir. %6, %8, %10, %12 ve %15 granüler kauçuk karışım oranları, kaba ve ince granüler kauçuk kullanılarak test edilmiştir. Optimum oranın %10 ince taneli kauçuk olduğu belirlenmiştir. Maksimum kuru yoğunluk %3,1 azalmış ve maksimum kesme mukavemeti %6,1 artmıştır.

TABLE OF CONTENTS

ABSTRACT iii

ÖZET iv

TABLE OF CONTENTS v

LIST OF FIGURES viii

LIST OF TABLES xiii

CHAPTER 1. INTRODUCTION 1

1.1. Introduction 1

1.2. Usage of Rubber in Civil Engineering 3

1.3. Aim of The Study 4

1.4. Methodology 5

1.5. Thesis Categories 5

CHAPTER 2. LITERATURE REVIEW 7

2.1. Introduction 7

2.2. Tire Scrap as Soil Improvement Material 7

2.3. Scrap Tires Applications in Civil Engineering 19

2.4. Earth Retaining Structures 27

2.5. Conclusion 30

CHAPTER 3 ROPERTIES OF THE SOIL USED IN THE MODEL TESTS 31

3.1. Introduction 31

3.2. Physical and Mechanical Properties of The Soil Used in The Experiments 31

3.3. Measurement of Moisture Content 32

3.4. Hydrometer Test 37

3.5. Measurement of Specific Gravity of Soil Solids and Granulated Rubber 38
3.6. Compaction Test 40
3.7. Direct Shear Test 42
3.8. Soil Types Under Consideration 44

CHAPTER 4. MODEL TESTS 45
4.1. Introduction 45
4.2. Instruments and Data Acquisition System (DAQ) 46
4.3. Pressure Measurement 50
4.4. Pore Water Pressure Measurement 50
4.5. Load Measurement 51
4.6. Linear Variable Displacement Transducer (LVDT) 52
4.7. Sand Preparation Method and Calibration 52
4.8. Velocimetry of Particle Images (PIV) Method 53
4.9.Physical Model - Testing Setup 56
4.10. Measurements of The Lateral Pressure, Pore Pressure, and Displacement 57
4.11. Testing Program 59

CHAPTER 5. PRESENTATION AND DISCUSSION OF THE TEST RESULTS 62
5.1. Introduction 62
5.2. Direct Shear Test 62
5.2.1.Fine Granulated Rubber-Sand mixture: ..... ……62

5.2.2.Coarse Granulated Rubber-Sand mixture: 66
5.3. Compaction Test Results 69
5.4. Summary 70

CHAPTER 6. PHYSICAL MODEL TESTS RESULTS 72
6.1. Introduction 72
6.2. Dry Soil Models 72
6.2.1. First Model – Clean Sand Backfill Model (Control Model): 72
6.2.2. Second Model 76
6.2.3. Third Model 79
6.2.4. The Fourth Model 83
6.3. Saturated Models 86
6.3.1. First Model - Clean Sand Backfill (Control Model): 86
6.3.2. Second Model 89
6.3.3. Third Model 93
6.3.4. Fourth Model 97
6.4. Summary 101

CHAPTER 7. CONCLUSION 102
7.1.Recommended Future Studies 105

REFERENCES 106

LIST OF FIGURES

Figure **Page**

Figure 1.1. World's biggest tire graveyard, Kuwait (Anadolu Agency) 1
Figure 1.2. Granulated rubber related research since 2000 (ScienceDirect). 3
Figure 2.1. Tire chips that used in the study (Source: Lambert, Bałachowski,and Gotteland, 2005) 9
Figure 2.2. Tire chips ratio effect on the void ratio (Source: D. Pradeep Kumar 2014) 10
Figure 2.3. (a) Deviatoric stress–deviatoric strain; (b) volumetric strain– deviatoric strain curves for sand-tier chips mixtures at different proportions of tier chips; model prediction and experimental data at p0′= 138 kPa (adapted from Mashiri, Vinod, and Sheikh 2016) 11
Figure 2.4. The results of a direct shear test on mixtures of sand and tire chips (Source: AL-Neami, 2018) 12
Figure 2.5. Stress-strain curves for dry sand rubber mixes subjected to multiple static and cyclic triaxial tests (Source: Banzibaganye, Becker, and Vrettos 2019). 14
Figure 2.6. The direct shear testing yielded the following results: shear stress vs. shear displacement for both experimental and computational models (adopted Chevalier, Tsutsumi, and Otani 2019). 15
Figure 2.7. Experimental setup (Source: Kaneda, Hazarika, and Yamazaki, 2018) 20
Figure 2.8. The stress-strain behavior of mixtures of gravel and medium-sized tire shreds (Source: Shariatmadari et al. 2018). 21
Figure 2.9. Improvement of different samples (Source: Shariatmadari et al., 2018) 23
Figure 2.10. Experiment setup (Source: Gill and Mittal, 2019) 24
Figure 2.11. Configuration and monitoring the layout of reinforced soil model walls at a reduced scale (Source: Jamshidi et al. 2010). 28
Figure 2.12. Schematic diagram of test wall configuration (Source: Reddy and Krishna, 2015) 30
Figure 3.1. Minimum sample mass depending on maximum particle size for moisture content assessment. (Source: Kalinski, Michael E., 2011) 33
Figure 3.2. Sieve analysis results. 36

Figure **Page**

Figure 3.3. An equipment used for the hydrometer test; (a) hydrometer, and (b) sample mixer 37
Figure 3.4. Specific gravity test equipment 39
Figure 3.5. Mechanical compacter and C type mold 41
Figure 3.6. Direct shear test device 43
Figure 3.7. Tested sample in the direct shear test device 44
Figure 4.1. Experimental model layout a) Top view, b) Side view 46
Figure 4.2. Schematic view of the dry model configuration 47
Figure 4.3. Schematic view of the saturated model configuration 47
Figure 4.4. Data collecting system 48
Figure 4.5. Sensors' wires connection in the DAQ device 49
Figure 4.6. Example of received load cell data from test one (Load vs. data index) 49
Figure 4.7. Pressure transducer (TML waterproof, PDA-PB) 50
Figure 4.8. Pore water pressure transducer. 51
Figure 4.9. Schematic view of the loadcell 51
Figure 4.10. Linear variable displacement transducer 52
Figure 4.11. Sheet pile and the foundation part. 52
Figure 4.12. Preparing the backfill (Top view) 53
Figure 4.13. The equipment used for the PIV process 54
Figure 4.14. PIV algorithm steps 54
Figure 4.15. PIV analysis results 55
Figure 4.16. Application interface programed by LABVIEW 56
Figure 4.17. Pressure transducers mounted on the sheet pile 57
Figure 4.18. Test setup for the dry model 59
Figure 4.19. Final test setup for the saturated model 60
Figure 5.1. Tested sample shows the fine granulated rubber distribution in the sand-granulated rubber mixture. 62
Figure 5.2. Fine granulated rubber-sand mix's direct shear test results with 20 kg normal force. 63
Figure 5.3. Fine granulated rubber-sand mix's direct shear test results with 50 kg normal force. 64
Figure 5.4. Fine granulated rubber-sand mix's direct shear test results with 100 kg normal force. 65

Figure **Page**

Figure 5.5. Coarse granulated rubber-sand mix's direct shear test results with 20 kg normal force 67
Figure 5.6. Cores granulated rubber-sand mix's direct shear test results with 50 kg normal force 68
Figure 5.7. Cores granulated rubber-sand mix's direct shear test results with 100 kg normal force. 69
Figure 5.8. Compaction test results 70
Figure 6.1. Clean sand backfill model (Control model): 72
Figure 6.2. Load cell data recorded from the first dry model condition 73
Figure 6.3. Lateral pressure data (P2) recorded from the first model dry condition 74
Figure 6.4. Lateral pressure data (P3) recorded from the first model dry condition. 74
Figure 6.5. Applied load and pressure development with the lateral displacement first model dry condition. 75
Figure 6.6. Second model dry condition. 76
Figure 6.7. Load cell data recorded from the second dry model condition 76
Figure 6.8. Lateral pressure data (P2) recorded from the second model dry condition.. 77
Figure 6.9. Lateral pressure data (P3) recorded from the second model dry condition.. 78
Figure 6.10. Applied load and pressure development with the lateral displacement second model dry condition. 78
Figure 6.11. Third model setup dry condition. 79
Figure 6.12. Load cell data recorded from the third dry model condition 80
Figure 6.13. Lateral pressure data (P2) recorded from the third model dry condition. . 80
Figure 6.14. Lateral pressure data (P3) recorded from the third model dry condition. .. 81
Figure 6.15. Applied load and pressure development with the lateral displacement third model dry condition. 82
Figure 6.16. Fourth model setup dry condition. 83
Figure 6.17. Load cell data recorded from the fourth dry model condition 83
Figure 6.18. Lateral pressure data (P2) recorded from the fourth model dry condition.84
Figure 6.19. Lateral pressure data (P3) recorded from the fourth model dry condition. 84
Figure 6.20. Applied load and pressure development with the lateral displacement fourth model dry condition. 85
Figure 6.21 First model setup with clean sand backfill saturated condition (control model). 86

Figure **Page**

Figure 6.22. Load cell data recorded from the first saturated model condition 86
Figure 6.23. Lateral pressure data (P2) recorded from the first model saturated condition. 87
Figure 6.24. Lateral pressure data (P3) recorded from the first model saturated condition. 88
Figure 6.25. Applied load and pressure development with the lateral for first test saturated condition 88
Figure 6.26. pore water pressure changes with lateral displacement for the first model..... 89
Figure 6.27. second model setup saturated condition. 90
Figure 6.28. Load cell data recorded from the second saturated model condition 90
Figure 6.29. Lateral pressure data (P2) recorded from the second model saturated condition. 91
Figure 6.30. Lateral pressure data (P3) recorded from the second model saturated condition. 91
Figure 6.31. Applied load and pressure development with the lateral for second test saturated condition 92
Figure 6.32. pore water pressure changes with lateral displacement for the second model..... 93
Figure 6.33. Third model setup saturated condition 94
Figure 6.34. Load cell data recorded from the third saturated model condition..... 94
Figure 6.35. Lateral pressure data (P2) recorded from the third model saturated condition. 95
Figure 6.36. Lateral pressure data (P3) recorded from the third model saturated condition. 95
Figure 6.37. Applied load and pressure development with the lateral for third test saturated condition 96
Figure 6.38. Pore water pressure with lateral displacement for the third model. 97
Figure 6.39. Fourth model setup saturated condition. 98
Figure 6.40. Load cell data recorded from the fourth saturated model condition 98
Figure 6.41. Lateral pressure data (P2) recorded from the fourth model saturated condition. 99

Figure **Page**

Figure 6.42. Lateral pressure data (P3) recorded from the fourth model saturated condition. 99
Figure 6.43. Applied load and pressure development with the lateral for fourth test saturated condition. 100
Figure 6.44. Pore water pressure with lateral displacement for the fourth model. 101
Figure 7.1. Applied load and lateral displacement response for dry soil models. 104
Figure 7.2. Applied load and lateral displacement response for saturated models. 105

LIST OF TABLES

Table **Page**

Table 2.1. Comparison of the maximum calculated responses for backfills of sand and shredded tire (Source: Ravichandran and Huggins 2014)..... 19
Table 3.1. List of laboratory tests performed and applied ASTM standards..... 32
Table 3.2. Moisture content test results for compaction models 34
Table 3.3. Soil properties..... 36
Table 3.4. Specific gravity values of sand and GR..... 40
Table 3.5. Compaction test results..... 42
Table 3.6. Physical properties of sand used in the model tests..... 44
Table 4.1. Dry mode: Sand and granulated rubber-sand mix weight and volume 59
Table 4.2. Saturated models' sand and granulated rubber-sand mix weight and volume..... 61
Table 6.1. Dry model results..... 101
Table 6.2. Saturated model results..... 101

CHAPTER 1

INTRODUCTION

1.1. Introduction

The disposal of millions of tires that have been abandoned in landfills or kept in an uncontrolled manner is a significant environmental concern for developed and industrialized countries. The disposal of used tires poses a substantial threat to both human health and the environment, necessitating the development of economically feasible scrap tire disposal systems.

Figure 1.1. World's biggest tire graveyard, Kuwait
(Source: Anadolu Agency)

Turkish citizens waste millions of scraps of tire each year. The majority of which has been disposed of or stored. These tires take up precious landfill space, and if not disposed of correctly, they represent a threat to the environment.

End-of-life tires (ELTs) are an excellent supply of readily available, low-cost, and environmentally friendly construction materials with superior engineering qualities. Their reuse (as granulated rubber mixed with soils) in large-scale civil (geotechnical) engineering recycling applications would be beneficial and should be encouraged. Globally, it is estimated that less than 10% of ELTs are reused in geotechnical applications, whereas approximately 40% are recycled as tire-derived fuel. Although numerous studies have been conducted on the material characterization of soil-rubber mixes (SRMs), it appears as though the results of these studies have not been effectively collated and compared, making it difficult to comprehend the potential applicability of SRMs completely. Tier manufacturers claim a small proportion of their output is shredded and headed for the trash. Tiers, because of their high volume-to-weight ratio, take up much room in landfills. Moreover, because rubber has a high added value, tier wastes constitute a substantial revenue loss worldwide. Environmental awareness and rising landfill costs compel companies to reduce waste or find new applications for rubbish that cannot be avoided. These fiber wastes might be utilized to create added value products for soil strengthening, a unique approach to soil improvement. Tire-derived fuel for energy generation, ground rubber, or technical applications such as crash barriers, breakwater and reef construction, and crumb rubber in asphalt pavements are all potential answers to this problem. These restrictions, however, have had little effect on the number of tires in landfills or on the issue of illegal tire disposal. As fills and backfills, tire shreds can be used alone or in combination with soil. Field and laboratory experiments have demonstrated that these tire shreds, alone or with soil, have outstanding friction properties.

One solution to this problem has been the development of methods for recycling tires, including the use of tire-derived fuel to generate electricity, the use of ground rubber or engineering applications such as crash barriers, the construction of breakwaters and reefs, and the incorporation of crumb rubber into asphalt pavements. These attempts, however, have had little impact on the volume of tires in landfills or on the prevalent issue of illegal tire disposal. As fills and backfills, tire shreds can be used alone or in combination with soil. Field and laboratory testing have demonstrated that these tire shreds have good frictional qualities when employed alone or in conjunction with soil.

Soil reinforcement may take several forms; it might be in the shape of strips, sheets, grids, bars, or fibers, or it can have a rough or smooth texture (high such as steel or low such as polymeric fabrics). Traditionally, reinforcements have been long, flexible

galvanized steel strips with a smooth or ribbed surface. This scenario has shifted dramatically in recent years, as other forms of reinforcement have gained more attention and widespread usage in practice. Other options include woven and nonwoven fabrics collectively referred to as geotextiles. These reinforcing textiles, in comparison to metal strips, have a considerably lower modulus. (McGown et al., 1978) made this difference, classifying earth reinforcement into two broad categories: ideally inextensible inclusions and ideally extensible inclusions. The former category comprises metal strips and bars with a high modulus, whereas the latter category contains natural and synthetic fibers, plant roots, and polymeric textiles with a low modulus.

1.2. Usage of Rubber in Civil Engineering

Internally, the tire shreds strengthen the soil, giving stability and resulting in minimal differential settling. Shredded tires offer significant benefits for geotechnical applications due to their low density and excellent durability, their ability to drain freely, their thermal insulation properties, and in many instances, their lower cost when

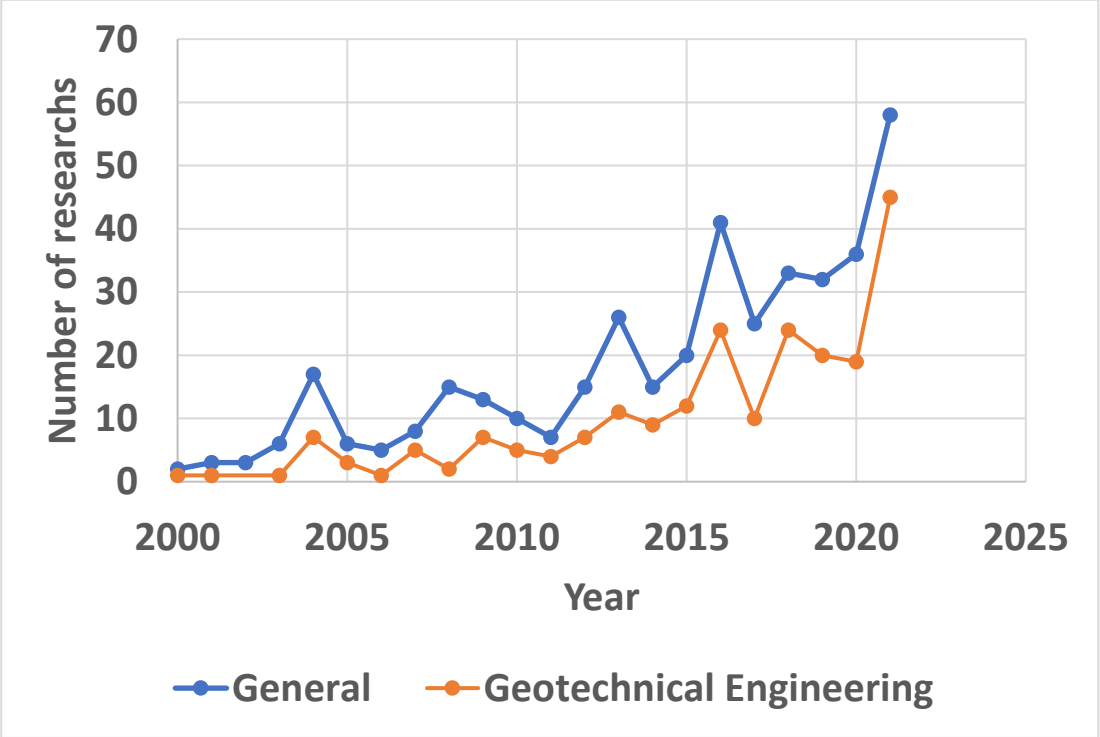

Figure 1.2. Granulated rubber related research since 2000
(Source: ScienceDirect).

Numerous researches have been published in the literature indicating that incorporating granulated rubber and granulated rubber into the soil may substantially improve its engineering characteristics, reducing the lateral earth pressure load-bearing capacity and durability. As shown in Figure 1.2, granulated rubber research, in general, started a stip trend beginning from 2011, and the majority is geotechnical related research.

Masad et al. (1996), Marto et al. (2013), Kaneda et al. (2018), and Al-Neami (2018) showed granulated rubber size and mixing percentage to improve the behavior of sand through direct shear, compaction, and triaxial testing. Research showed that each tire chips type has a different effect on the mixed engineering characteristics. Under the ASTM standard of ASTM D6270-20 (2020), the tier chips fall into four categories.

Although small-scale models are regarded to have restricted applicability since specific critical similarity criteria cannot be fulfilled, these models may be a helpful and low-cost tool to investigate the behavior of geotechnical structures. From testing with small-scale models' experimental observations may be conducted to give a deeper understanding of the deformation process happening in different kinds of boundary issues.

Amshidi et al. (2010) used a series of shaking table tests using the rigid box to study the dynamic response of synthetic fibrous materials-fine sand mix, while others used small scale model to investigate pile group interaction effect different spacing tests (Kim and Lim Yoon, 2011). In the use of recycled material, Reddy and Krishna (2015) investigate the use of granulated rubber -sand mix as lightweight backfill material in retaining wall applications. There is no information in the literature on the physical modeling of recycled carpet waste strips reinforcing under dynamic load, despite laboratory experiments and practical experience demonstrating the usefulness of randomly distributed fibers as sand reinforcement under static or dynamic loading, according to the authors.

1.3. Aim of The Study

The aim of this study is to get a better knowledge of the mechanical behavior of the granulated rubber sand mix and to determine the feasibility of backfilling with shredded tires and sand. Filling material comprised of a mixture of shredded tires and

sand; several small-scale physical test models were constructed to simulate a plain-strain condition inside the different triangular shape that was backfilled.

1.4. Methodology

The volume of all sand-granulated rubber mixing percentages was determined for the known specific gravity of both sand and granulated rubber. Additionally, compaction and direct shear tests were conducted to gain a thorough understanding of the sand-granulated rubber mix's physical and mechanical properties to determine the optimal mixing ratio of sand-granulated rubber. A total of 42 direct shear tests and 4 compaction tests were conducted with various mixing percentages of granulated rubber. Finally, a 0.5-m-high sheet pile model was constructed in the laboratory.

A total of 8 sheet pile models were performed to examine the influence of lightweight backfill volume corresponding to the loading position on the response of sheet pile retaining walls. In this set of tests, the sheet pile was constructed by an acrylic sheet of 10 mm thickness. Part of the sheet pile was driven by 10 cm into the foundation and was free to rotate and translate horizontally. A 1.46m by 0.70m by 0.59m sheet pile models were prepared in a rigid container reinforced by a metallic structure and transparent acrylic sidewalls.

1.5. Thesis Categories

This thesis consists of seven chapters.

Chapter one introduces the research, including a brief description of the problem, objectives of the research, scope of the research, and thesis outline.

Chapter two reviews the previous literature studies and research works related to recycled materials mixed with sand and sheet pile experimental models.

Chapter three presents the tests that were conducted to determine the mechanical and physical properties of the soil and granulated rubber. Moreover, the ASTM standards to perform tests are presented in his chapter.

Chapter four presents the experimental program, which includes a detailed description of the physical models and the instrumentation. The methodology was adopted in conducting different tests.

Chapter five presents the laboratory tests result (mechanical and physical soil properties) and discusses the key differences between each sample that was prepared at different mixing ratios.

Chapter six shows the experimental model test results and shows the results and key findings of each test.

Chapter seven contains the conclusions and the recommendation for future studies.

CHAPTER 2

LITERATURE REVIEW

2.1. Introduction

This chapter presents the literature review of previous research that dealt with scrap tires. The chapter is divided into three categories. The first part presents the previous research that conducted laboratory studies on the tire scraps combined with sandy soil to evaluate the mechanical properties and behavior of the mixture. The second part summarizes the research in which results were based on scrap tires to solve specific geotechnical problems. The last part presents the research in which used tire scrap was used in earth retaining structures

2.2. Tire Scrap as Soil Improvement Material

Historically, when discarded tires were stored or illegally disposed of, they took up space in landfills and served as breeding grounds for mosquitoes and vermin. In 1985, Minnesota passed the nation's first state statute governing the management of waste tires. States have traditionally concentrated their efforts on three areas: (1) programmed management of discarded tires, (2) market development initiatives, and (3) stockpile abatement. Tires that have been shredded or repurposed can be utilized in construction.

Warith, Evgin, and Benson (2004) presented the usage of tire chips in lieu of crushed stone in a landfill's leachate collection system. This study examined Tatlisoz, Benson, and Edil (1997) conducted a study to determine the mechanical properties and behavior of waste tire chips in conjunction with fine and coarse soils. The inquiry made extensive use of laboratory testing equipment on a broad scale. They evaluated the shear strength, deformability, and compressibility. Clean sand, sandy silt, and clay were included in the mixtures. They are more compressible than soils and require a greater amount of deformation to reach their ultimate shear strength. In sand or sandy silt combinations, tire chips as backfill reduce unit weight and increase shear strength.

However, clay-tire chip mixtures are just as robust as pure clay. Strength envelopes for sand-tire chip mixtures can be non-linear with no cohesive intercept. The shear strength envelope is linear and has a cohesiveness intercept for the sandy silt-tire chip mixture. Both instances exhibit similar long-term compression behavior. The strength of sandy silt mixtures grows proportionately to the chip percentage until it reaches 20%, at which point strength remains constant.

The sensitivity of the shredding process to compressibility and hydraulic conductivity responses under diverse applied loads using shredded tires from two separate sources. The maximum normal strain measured in each type of tire chip was found to plateau at a strain level somewhat greater than or equal to 0.5 when vertical loads were applied, resulting in average vertical strains of up to 440 kPa, corresponding to more than 50 m of waste. Permeability studies found an average hydraulic conductivity of 0.67 to 13.4 cm/s when applied normal loads of 60 to 335 kPa, and strain increments of 0.3 to 0.5 were used. These results are significantly more than the 0.01 cm/s hydraulic conductivity normally specified for drainage layers in leachate collection systems.

Lambert, Bałachowski, and Gotteland (2005) performed triaxial tests to determine the mechanical properties of tire chip–sand combinations. Two variables were examined: tire chip content, ranging from 0 to 100% by mass, and tire piece orientation, with four varied orientation conditions. The stress-strain behavior of the various combinations and their volumetric fluctuation during the tests were examined. The friction angle and cohesion angle for each mixture were provided. Additionally, the optimal percentage mass and optimal unit weight that result in the highest shear strength were found.

Figure 2.1. Tire chips that used in the study
(Source: Lambert, Bałachowski, and Gotteland, 2005)

The findings of Lambert, Bałachowski, and Gotteland (2005) support the following conclusions:

1. Without orientation, specimens made entirely of tires exhibit a linear stress-strain relationship.
2. The percentage mass of tires in the mixture has a significant effect on the shear strength. The strength grows as the percentage mass of the tire increases up to an optimum of 34%, at which point the shear strength drops. This optimal value equates to a unit weight of 13.5 kN/m^3.
3. The volumetric variation – axial strain behavior is altered by the tire content. At a percentage mass of 34%, it appears as though the behavior of mixtures switches from sand-like to tire-like.
4. The friction angle equivalent for 100% tire specimens with no orientation is 25°, compared to 41° for sand.
5. The orientation of the tire chips affects the mixture's shear strength.

The samples with horizontally placed tire chips have the highest strength, followed by those with alternatively placed horizontal and vertical tire chips, those with exclusively vertically put tire chips, and finally, those with no orientation of the tire chips.

D. Pradeep Kumar (2014) presented a study in which laboratory experiments were used to determine the optimal tire chip content in sand. The optimal concentration of the

mixture is the concentration at which the greatest benefit can be obtained. The specific gravity and density of the sand tire chip combinations were determined. It was noticed that when the percentage of tire chips in the mixture increases, the specific gravity and unit weights decrease. The corresponding void ratios of the mixtures decreased to nearly 45% when tire chips were added at a 40% weight ratio to sand. However, adding tire chips over 40% increased the void ratio, indicating that adding tire chips above the optimum content reduces the compressibility of the combination, as shown in Figure 2.2.

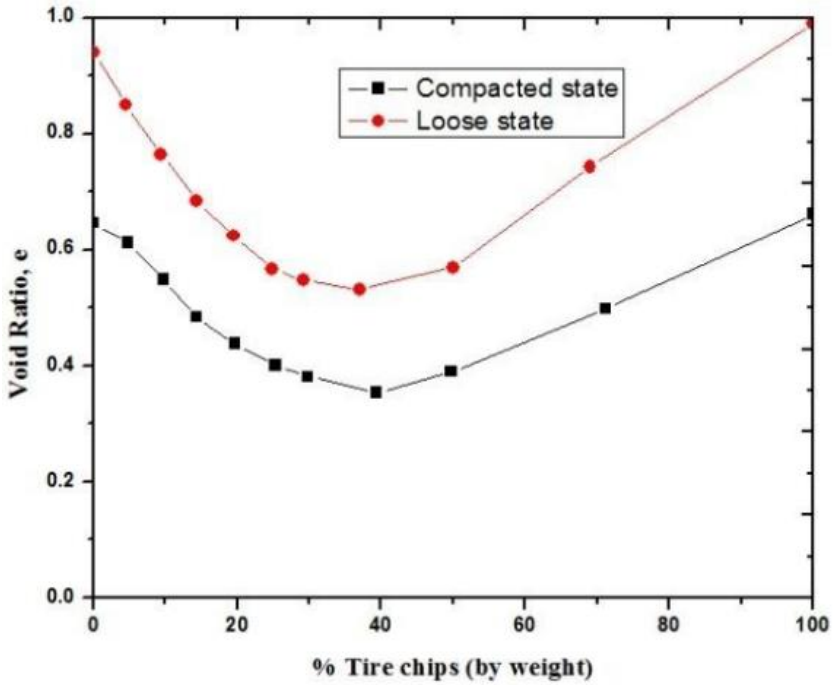

Figure 2.2. Tire chips ratio effect on the void ratio
(Source: D. Pradeep Kumar 2014)

Additionally, a weight volume connection was constructed for the tire chips in the sand tire chip mixtures, which might alleviate the issue of handling the tire chips in the field by weight proportion. It was found that knowledge of the specific gravities of basic materials (in this case, sand and tire chips) is sufficient to determine the specific gravities of proportionate combinations. Thus, the specific gravities of any mixture may be determined using the values of the parent materials' specific gravities (sand and tire chips in this case).

Mashiri, Vinod, and Sheikh (2016) developed a constitutive model to predict the monotonic behavior of sand–tire chip (STCh) mixtures. The model accurately anticipated the hardness and softening of the STCh mixes. This was accomplished by adding the CSR condition to the modified dilatancy and hardness functions, as well as to the changed state

parameters. Validation of the proposed model was performed using data from a series of triaxial laboratory investigations, as shown in Figure 2.3.

The constructed semi-empirical constitutive model for STCh mixes accurately describes the experimental behavior of STCh mixtures at various TCh concentrations (0–40%). Additionally, the semi-empirical constitutive model may readily be modified to account for the effect of various forms of scrap tires (Tier chips, tire shreds, and rubber crumbs) by defining connections between the material properties of various sand–scraps tire mixes.

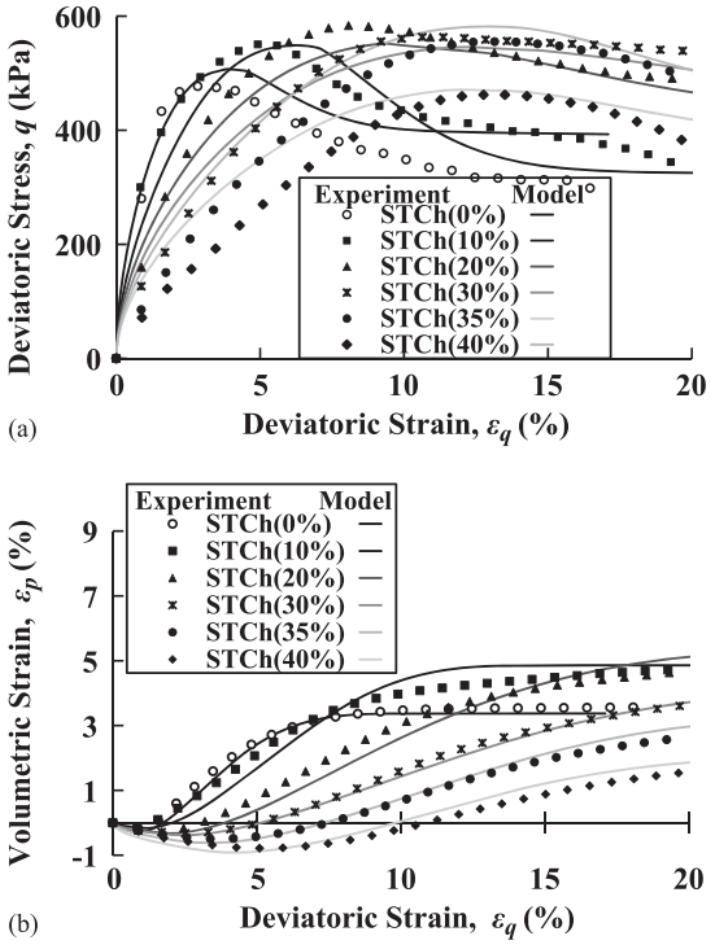

Figure 2.3. (a) Deviatoric stress–deviatoric strain; (b) volumetric strain– deviatoric strain curves for sand-tier chips mixtures at different proportions of tier chips; model prediction and experimental data at p_0'= 138 kPa (Source: Mashiri, Vinod, and Sheikh 2016)

Al-Neami (2018) studied the improvement of sandy soil by replacing waste tire chips with standard soil stabilization chips. The benefits of using locally available

materials to stabilize the sand, various amounts of recycled tire chips are manually combined with dry sand. The geotechnical properties of composite specimens (soil + tire chips) were tested, and the principal findings revealed that scrap tire chips have the capacity to stabilize sand efficiently. The addition of tire chips to sand increased the sand's shear strength, hence increasing both the friction angle and cohesiveness, as shown in Figure 2.4.

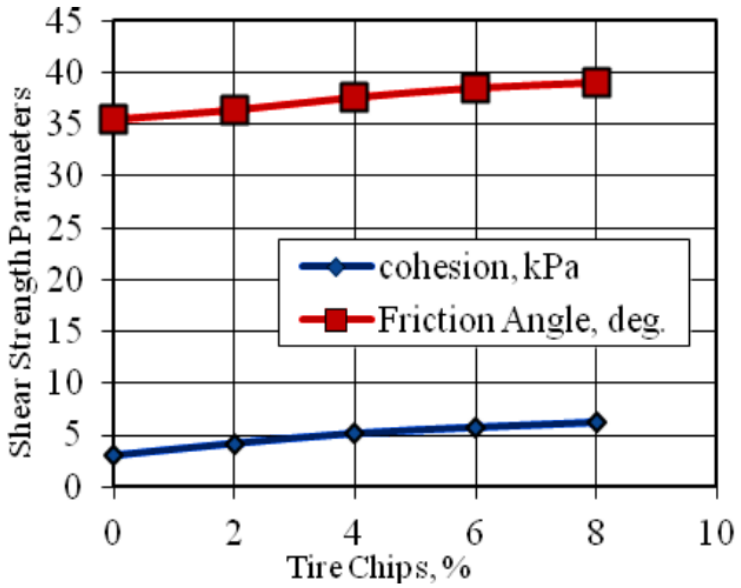

Figure 2.4. The results of a direct shear test on mixtures of sand and tire chips (Source: AL-Neami, 2018)

Tire chips have low unit weight. Increasing their content in sand resulted in a significant reduction in specific gravity and maximum dry density while maintaining appropriate moisture content. Analyses of the CBR test results revealed that sand stabilized with tire chips produced approximately 1.6 times the amount of CBR produced by pure sand, showing that the load-bearing capability of mixed sand has been increased because of the increased physical strength.

Tabrizi et al. (2019) studied the influence of granular rubber particles (GRP) as an addition (up to 50%) on clayey soil behavior by direct shear apparatus. The effects of GRP %, unloading/reloading amplitude, number of cycles, normal stress, and compaction were studied. The internal friction angle increases initially and then reduces after the GRP weight percentage of 20%. Increasing the GRP weight percentage increases permanent horizontal displacement and hardening behavior under high normal loads. The study also

demonstrated that compaction reduces post-repeated loading shear strength, an important economic factor.

Based on the test results Tabrizi et al. (2019),:

1. The void ratio lowers up to 40% GRP but does not vary significantly after that. In GRP, the internal angle of friction rises and then falls somewhat, but cohesiveness declines.
2. Based on the static test results, 20% GRP is optimal. It induces higher horizontal and vertical displacements with increasing loading amplitude.
3. Using GRP is not suggested when considerable amplitudes of repetitive loading are predicted.
4. Maximum permanent deformation occurs in the first cycle of loading, and stiffness declines. Eventually, the particles adjust to new places, and stiffness rises.
5. Compaction has no effect on stiffness under static or repetitive stress.
6. Post-repeated shear strength variations in GRP and non-GRP specimens are opposite.
7. The post-repeated shear strength of specimens subjected to amplitudes greater than 1/3 has a different pattern than specimens subjected to lower amplitudes.

In summary, GRP-soil mixes adapt well to diverse loads (static and repeated). In future studies, in-situ tests such as plate load tests (PLT) or dynamic CBR can be used. Quantitative studies on GRP particle distribution will also be useful.

Banzibaganye, Becker, and Vrettos (2019) performed static and dynamic cyclic triaxial tests on the sand with different rubber chips (5-15 mm in different) amounts. The shear strength of sand enhanced with rubber chips improved in static triaxial tests. With more rubber chips, the maximum shear strength is mobilized at a greater strain level. For medium sand, 20% dry weight chips were found to be ideal. Circular loading of unsaturated sand rubber mixtures increased post-cyclic shear strength.

On dry and moist sand rubber chip mixes, static and dynamic cyclic triaxial tests were conducted. Segregation of the mixture during material mixing was detected for concentrations of more than 20% but was prevented using an appropriate approach. Triaxial tests on dry specimens demonstrated an overall improvement in shear strength when the angle of friction decreased and cohesiveness increased. Changes in the angle of friction were negligible for wet material, and the gain in strength was attributed to enhanced cohesiveness. On the other hand, stiffness reduced as the rubber chip content increased. A chip content of 20% was determined to be optimal for reinforcing

homogeneous medium sand. When the rubber chip content was increased, a substantial rise in cyclic permanent deformation was found. Results are shown in Figure 2.5.

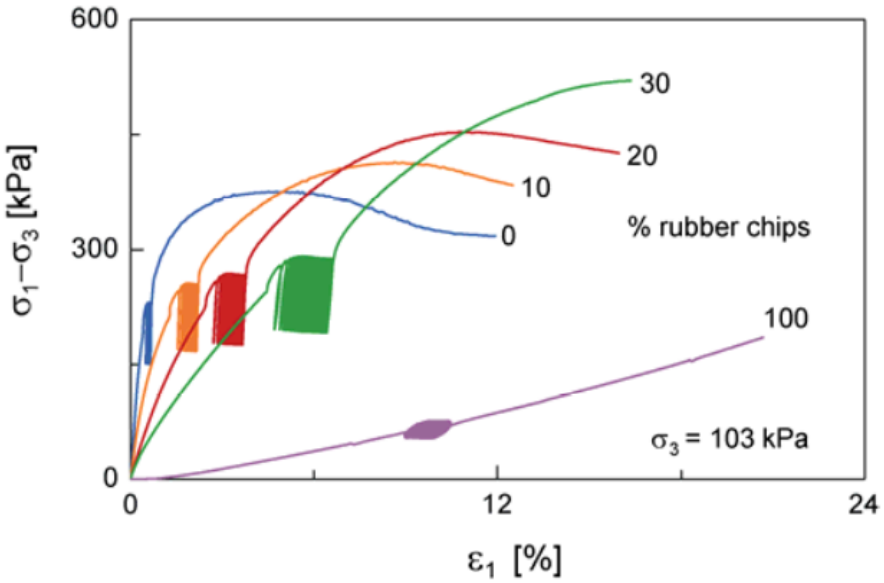

Figure 2.5. Stress-strain curves for dry sand rubber mixes subjected to multiple static and cyclic triaxial tests (Source: Banzibaganye, Becker, and Vrettos 2019).

Chevalier, Tsutsumi, and Otani (2019) studied the direct shear behavior of sands and tire chips as rigid and elastic particles. The near behavior of granular materials is investigated using a microfocus-type X-ray computed tomography (CT) scanner in conjunction with direct shear experiments. To quantitatively discuss the results of CT scanning, a digital image correlation approach is utilized, followed by the measurement of the distribution of displacements in the shear box, shear strain, and volumetric strain using CT data. Additionally, for the same scenarios as the direct shear test, a series of numerical calculations utilizing the discrete element method (DEM), which is frequently used for granular materials, are performed to validate the CT results. Finally, based on a comparison of CT scanning and DEM results as shown in Figure 2.6, the direct shear behavior of several granular materials is explored exactly for the first time using X-ray CT. The addition of tire chips to sand reduces the dilatant behavior under shear stress, and the shear stress peaks are eliminated. Additionally, tire chips appear to inhibit the propagation of shear bands within the material.

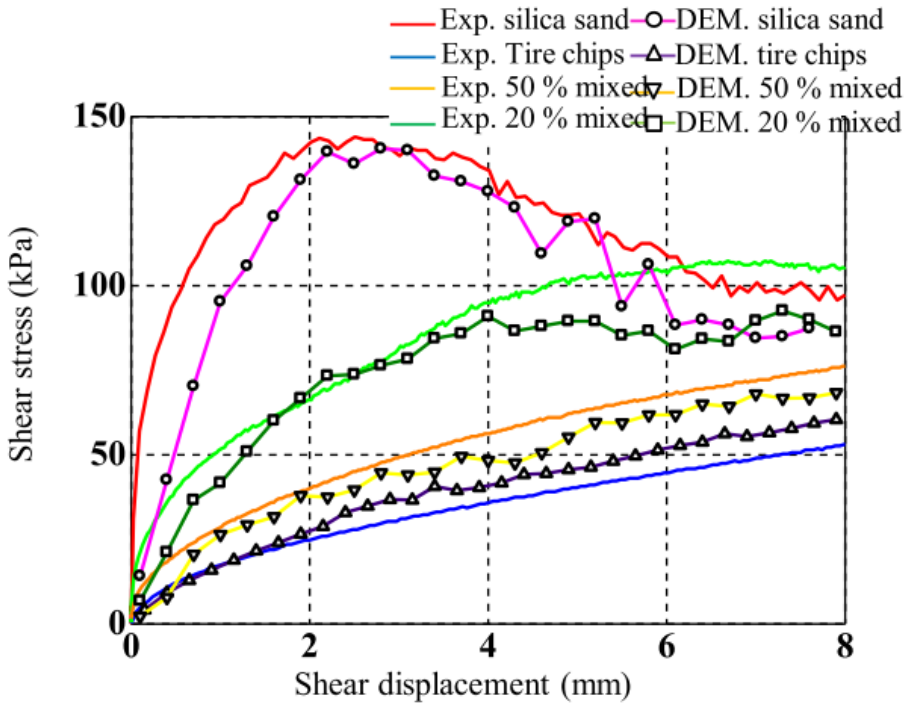

Figure 2.6. The direct shear testing yielded the following results: shear stress vs. shear displacement for both experimental and computational models (Source: Chevalier, Tsutsumi, and Otani 2019).

Liu, Cai, and Liu (2020) studied geotechnical materials' thermal characteristics. Thermal needle tests on recycled rubber-sand mixtures were performed in this paper. It was determined that sand fraction, moisture content, dry density, and particle size affect thermal conductivity. The results indicated that the thermal conductivity of granulated rubber-sand mixes increased parabolically as the dry density increased but linearly when the sand proportion grew. The moisture content of 6% is deemed necessary. The heat conductivity of the mixes increased as the particle size of the sand increased.

The heat transfer process was also studied using scanning electron microscopy (SEM). It was also proposed a simple multiple linear regression (MLR) model for recycled tire rubber-sand mixtures, which showed a satisfactory regression effect (correlation coefficient R2, F, and t-test). For geothermally linked constructions, this research will provide a more suitable thermal parameter for recycled tire rubber-sand mixes. Using waste tires effectively can also minimize pollution and improve sustainable infrastructure.

1. The thermal conductivity of rubber-sand mixtures increases gradually below 20% sand fraction but increases rapidly over 80% sand fraction, reflecting the thermal

characteristics of sand-like particles. A linear increase in dry density is seen with decreasing sand proportion.

2. The thermal conductivity of rubber-sand mixtures changes with moisture content, and 6% is considered essential moisture content. When the moisture content exceeds 6%, the thermal conductivity stabilizes and increases somewhat.
3. The higher the sand particle size, the higher the heat conductivity of the combinations. The primary heat transmission chains of rubber-sand mix transition from rubber-rubber chains (sand fraction less than 20%) to sand-sand chains (sand fraction >80%) using SEM and a schematic diagram.
4. An MLR model for recycled tire rubber-sand combinations is proposed. This model's regression coefficient R2 and F-tests show a good regression effect.

Amanta and Dasaka (2021) examined the effect of tire shards on the sand's physical qualities. Different properties of the materials were studied, including specific gravity, void ratio, water absorption, compressibility, and shear behavior. In addition to the mixtures, the behavior of a single tire chip was examined. According to reports, tire chips are very compressible and have a relatively low shear strength in contrast to sand. The addition of tire chips to sand decreased the shear strength of the mixture while increasing its compressibility. Plastic strains are also detected in combinations containing tire chips. Additionally, optimal sand–tire chip mixture is suggested based on the findings of this investigation.

- Adding TC to the sand reduces the maximum and minimum unit weight of the mixes, but the void ratios behave differently. The maximum and minimum void ratios decreased as the TC content increased up to 30%. Increased TC content reverses the trend, and the void ratio rises steadily. Thus, the TC-30 mix has the densest particle arrangement of all the mixes.
- Total compressive and plastic stresses increase with TC concentration. But TC-30 makes a huge difference in total compression and plastic strain. Mixtures with less than 30% TC showed less compressive behavior, but increasing TC causes a dramatic rise in compression and plastic strain.
- The TC concentration has a big impact on the sand–TC mixtures. Regardless of confining pressure, shear strength decreases with increasing TC.
- Increasing confining pressure raises deviatoric stress for all mixes.

- Like the other stated geotechnical parameters, shear strength behavior changed by over 30% for TC. Mixtures with TC concentration up to 30% revealed very significant deviatoric stresses, which dropped dramatically for TC-40 and higher mixes.
- The shear behavior of the mixes with TC concentration up to 30% behaved more like sand, while the TC-sand mix behaved more like TC.
- The repeatability of TC-30's shear behavior was investigated. The material's behavior is reproducible, with an 8% coefficient of variation.
- Aside from the listed features, it should be noted that the two main components of the mix, sand, and TC, are so dissimilar in size and weight that achieving mix homogeneity beyond a certain percentage is challenging. Material segregation was evident in blends with TC levels over 30%. The optimal sand–TC combination has a reduced void ratio, equivalent strain-strain behavior, and is lighter than sand.

AKSOY, TAHER, and AWLLA (2021) discussed the effect of adding tire chips on the shear strength qualities of high-friction sand. The sand mixed with tire chip at various weight ratios (100: 0, 97.5: 2.5, 95: 5, 92.5: 7.5, and 90:10). The standard proctor test was used to determine the Maximum Dry Density (MDD) and Optimal Moisture Content (OMC) of sand and various sand-tire chip mixes. The samples were generated under OMC and MDD conditions, and the sand and sand-tire chip mixtures were subjected to a direct shear box test under three different axial loads. When the proportion of tire chips reached 5%, the internal friction angle rose by 13.8%, and cohesiveness reduced by 66.48%. Following this point, the internal friction angle was reduced, and cohesiveness was marginally increased.

- Tire chips' low density lowered MDD of sand-tire chip combination.
- Because sand and tire chips have roughly the same particle size, the OMC of the sand tire chip combinations remains almost constant.
- It increases by 13.8 percent when tire chips make up 5% of the weight of the sand-tire chip combination. Then it begins to fall.
- However, it is still lower than unreinforced sandy soil (c) at 5% tire chips. We used dense sand in our trials. Therefore it appears that tire `chips cannot increase the (c). When sandy soil is a worry, (c) is not important.

- This enhancement can be employed in ground improvement applications such as backfill material behind retaining walls and embankment construction, based on the experimental findings of adding a low percentage of tire chips to sand.

Ding et al. (2021) investigated the static and dynamic characteristics of granulated rubber-sand mixtures using consolidated undrained monotonic loading and cyclic loading triaxial tests. Waste tire rubber and sand mixtures are widely used as a new type of railway subgrade filler. The monotonic triaxial tests show that the shear strength of mixes increases with granulated rubber content and peaks at around 10%. A new equation for calculating peak deviatoric stress of mixtures is provided using the equivalent intergranular void ratio theory. The use of granular rubber reduces the production and storage of dynamic pore water pressure and improves mixture liquefaction resistance. The shear modulus changes inversely with granulated rubber content and frequency and directly with confining pressure. The maximum shear modulus is calculated using a revised equation that incorporates the equivalent intergranular void ratio and confining pressure. It is concluded that a granulated rubber composition of less than 20% can meet technical requirements relating to shear stiffness. The damping ratio is proportional to granulated rubber content but not confining pressure or loading frequency. The damping ratio and shear strain follow Hardin and Drnevich's equation. The appropriate granulated rubber percentage should be around 10% based on static and dynamic characteristics of granulated rubber-sand combinations.

The following are the main conclusions of this paper:

1. The shear strength increases up to 10% with granulated rubber content, then drops. A new equation for predicting the peak deviatoric stress of mixes is proposed based on the equivalent intergranular void ratio.
2. This pressure reduces as the granulated rubber content and confining pressure increase during the cyclic stress ratio and frequency increase. Adding granular rubber also improves liquefaction resistance.
3. The shear modulus changes inversely with granulated rubber content and frequency and directly with confining pressure. The comparable intergranular void ratio and confining pressure are also taken into account in the new equation. When the granulated rubber percentage is less than 20%, the shear stiffness meets engineering standards.

4. Inversely associated with confining pressure, the damping ratio is indifferent to loading frequency. Also, granulated rubber-sand mixes can act as seismic and energy dissipation materials. Also, the damping ratio and shear strain follow Hardin and Drnevich's equation.
5. Based on the static and dynamic properties of granulated rubber-sand mixtures, the novel subgrade filler's optimum granulated rubber content is estimated at 10%. The shear strength and liquefaction resistance of the novel subgrade filler are better than pure sand, the shear modulus meets engineering standards, and the damping ratio is significant, providing a good energy dissipation effect. For engineering applications, we urge more research on the mechanical properties of granulated rubber-sand combinations.

2.3. Scrap Tires Applications in Civil Engineering

Ravichandran and Huggins (2014) study the use of Shredded tires as an alternative backfill material for retaining walls, which is an efficient way to recycle tier waste. The engineering properties of shredded tires collected from various sources were collated in this article; retaining walls were developed for static and seismic situations using the average properties calculated using the LRFD method and compared to those of standard granular material. The performance of retaining walls backfilled with shredded tires was then evaluated and compared to that of sand backfill utilizing design seismic acceleration-time histories and advanced finite element software. The results indicate that shredded tire backfill greatly reduces the deflection of the wall tip, the maximum shear force, and the bending moment along the wall, as shown in table 2.1.

Table 2.1. Comparison of the maximum calculated responses for backfills of sand and shredded tire (Source: Ravichandran and Huggins 2014)

Case	Max Wall Deflection (cm)	Percent Savings Max (%)	Max Shear Force (kN/m)	Percent Savings	Max Moment (kNm/m)	Percent Savings (%)
Conventional Sand Backfill	2.16	43.2	244.46	58.8 %	589.52	42.1
Shredded Tire Backfill	1.23		100.66		341.20	

Kaneda, Hazarika, and Yamazaki (2018) performed a numerical analysis to determine the effect of tire chips used as a compressible inclusion in backfill on load reduction against retaining walls, as shown in Figure 2.7.

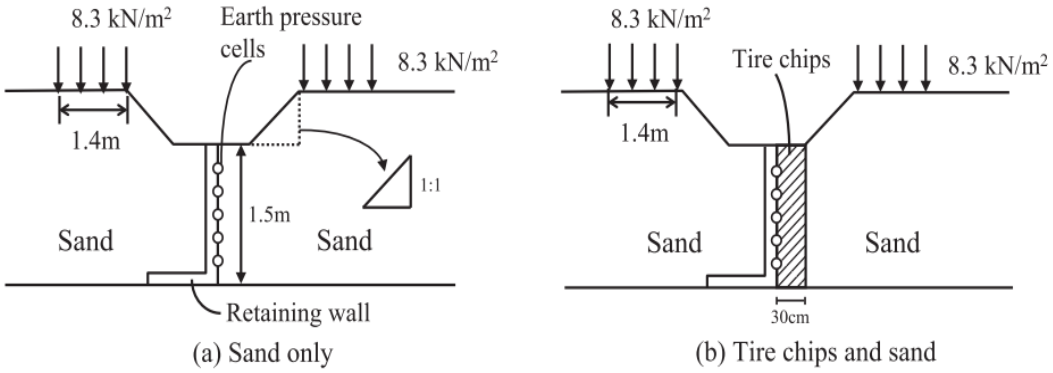

Figure 2.7. Experimental setup
(Source: Kaneda, Hazarika, and Yamazaki, 2018)

It is well established that obtaining a quasi-active or intermediate active state results in a drop in earth pressure in the backfill, and hence a field test of this behavior is numerically simulated herein. By assuming that tire chips may be treated as an elastic body, the effect of the Poisson's ratio and elastic modulus of tire chips on the reduction in ground pressure against retaining walls is investigated. The numerical simulation demonstrates that the active state is predominantly achieved in sandy backfill due to the lightweight nature of tire chips, as well as their low Young's modulus and Poisson's ratio. Additionally, the effect of friction at the bottom of the backfill mass is evaluated, as is the earth pressure reduction mechanism that incorporates this element.

The earth pressure reduction caused by a sandy backfill against retaining walls was numerically simulated using tire chips as a cushion against the retaining structure. The following are some of the study's primary conclusions:

1. When a tire-chip inclusion is implemented, the earth pressure decreases as the backfill transitions to the active state. When the three advantageous qualities of the tire chips are combined (low unit weight, negligible E_0, and small t), a decrease in earth pressure against the wall can be detected.

2. Friction at the base of the mass is necessary for the earth's pressure to be reduced. As the horizontal force is transferred to the ground under the mass, the earth pressure is reduced in the case of friction on the mass bottom.

Shariatmadari et al. (2018) examined the effects of reusing scrap tires in stone columns as a partial replacement for gravel. Three different sizes of tire shreds, including fine, medium, and large, are chosen for this purpose and added to the mixture in three volumetric percentages of 20%, 40%, and 60%.

The effect of tire incorporation on the mechanical characteristics and permeability of the stone column is investigated using large direct shear tests and loading tank testing. The optimal tire content percentage and effective size are calculated, which might be extremely valuable, particularly in field applications. The loading tank test results indicate that a 20% tire shreds mixture has the maximum axial bearing capacity.

The following conclusions are taken from the experiment's results:

1. The shape and proportion of tire material affect the shear strength and axial bearing capacity of stone columns.

2. The unreinforced gravel has an internal friction angle of 49.4^{o} the maximum friction angle is attained by utilizing 20% of the planar-shaped medium tire or 52^{o,} as shown in Figure 2.8.

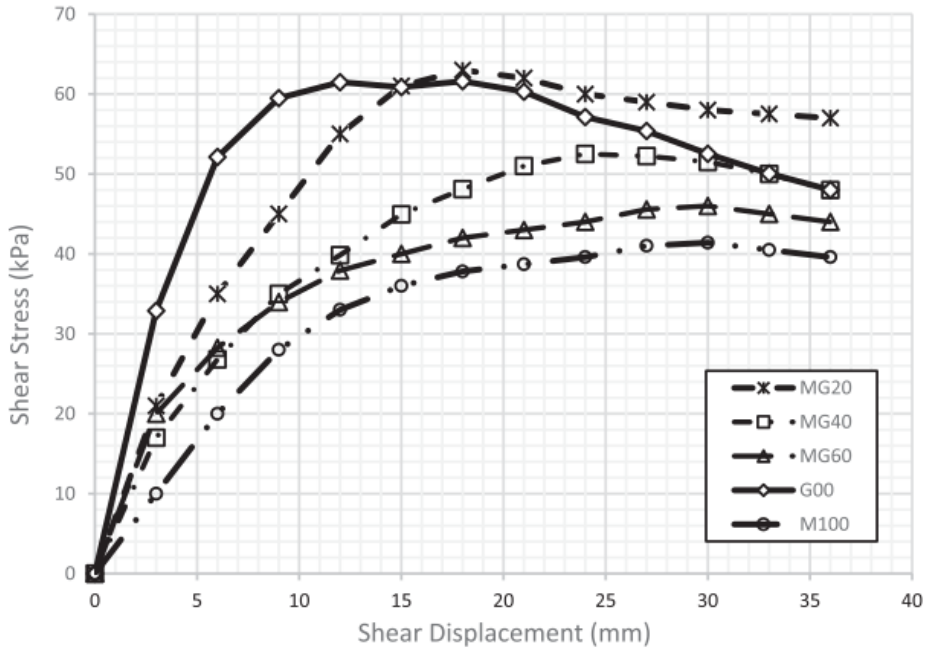

Figure 2.8. The stress-strain behavior of mixtures of gravel and medium-sized tire shreds (Source: Shariatmadari et al. 2018).

3. In terms of tire shred size, replacing 20% of gravel with medium tire shreds of the same size as the gravel results in a 30% increase in bearing capacity. Additionally, the addition of 40% and 60% tire material to each size results in a reduction in bearing capacity. The experimental results are consistent with Hughes and Withers' (1974) formula for bearing capacity.

4. There is no discernible increase in the mechanical and physical qualities of stone columns when using fine granular tires. Additionally, there is little improvement in the shear strength of mixtures and the axial bearing capacity of stone columns when using large cubic tire shreds. Tire shreds with a planar shape are the most effective since their aspect ratio is greater than unity, and their thickness is negligible, allowing them to act as fiber inclusions in reinforced soils.

5. Based on the findings of permeability tests, it can be inferred that mixtures containing 20% tire shreds of the same size as the gravel particles exhibit increased bearing capacity without compromising permeability, as shown in Figure 2.9.

The partial substitution of stone column aggregates with tire shreds is an efficient approach to recycle scrap tires while also safeguarding the environment. It is discovered that stone columns containing tire shreds operate better than the normal ones. Additionally, a reduction in stone column aggregates results in a lighter construction and lower installation costs. It is advised that in-situ experiments on stone columns holding waste tires be used to verify the conclusions of this study. Additionally, dynamic testing such as the shaking table test is advised prior to putting tire shreds in stone columns in the field.

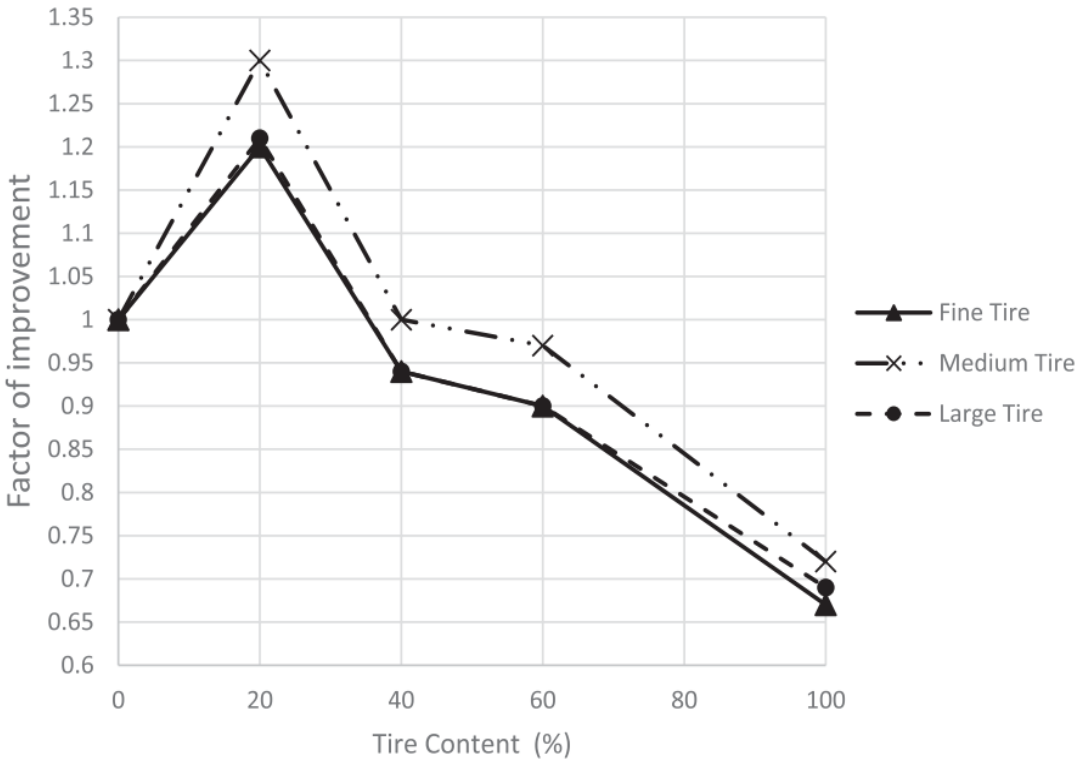

Figure 2.9. Improvement of different samples
(Source: Shariatmadari et al., 2018)

Mittal and Gill (2018) investigated the use of discarded tire chips and geogrid reinforcement to improve sand's load-carrying performance. An investigation on the pressure settlement behavior of Tire Chip Reinforced Sand was carried out in this work (TRS). In the first phase, factors such as tire chip content, TRS Zone reinforcement depth, and TRS relative density were varied on TRS underlying poorly graded sand. The second phase tested Geogrid Reinforced Sand (GRS) and compared the outcomes to TRS. The combined behavior of TRS and GRS was also investigated in the third phase. The results show that adding tire chips increases bearing capacity at low and high strains (s/B 2-5 and 10-20 percent). A BCR of 4.65 and 10.36 was reported at low and high strains, respectively. TRS outperformed GRS at all strain levels. The BCR can be boosted to 11 by using TRS with GRS. Thus, the recommended technique allows for shallow foundations in conditions that need deep foundations or costly ground renovation techniques, allowing for cost savings in construction and safe tire disposal.

1. The addition of discarded tire chips improves the load-carrying capacity of sand. The BCR found for a mixture containing 20% tire chips was 4.11 and 4.75 at s/B of 2%

and 5%, respectively. So, for low strains (s/B 2-5%), use 20% TC and for high strains (s/B 10-20%), 30% TC.

2. Increasing Rd beyond 1B boosts BCR by 30-40% while increasing cost by almost 200%. Hence, Rd above 1B is not advised economically, but if the cost of stockpiling surpasses the extra cost, Rd up to 2B can be provided.
3. Dr increases sand carrying ability, especially in low TC mixes 10%. BCR increased up to 156 % compared to a similar mixture compacted at a lesser density (Dr =30%). However, a higher TC combination does not benefit from an increased density of 20%.
4. In low strains, TRS improved 2-3 times more than GRS, compared to GRS. Thus, it may be a cost-effective alternative to commercial geosynthetic products.
5. Randomly dispersed waste tire chips reinforcement can considerably improve GRS bearing capacity. Adding 20%, TC increased BCR from 2.43 to 10.33.

(Gill and Mittal 2019) discussed the use of tire wastes in shallow footings that are subjected to eccentric loading. Eccentric loads drastically limit the soil's load-carrying capacity. As a result, laboratory model tests on tire chip reinforced sand subjected to eccentric loading conditions were done, as shown in Figure 2.10.

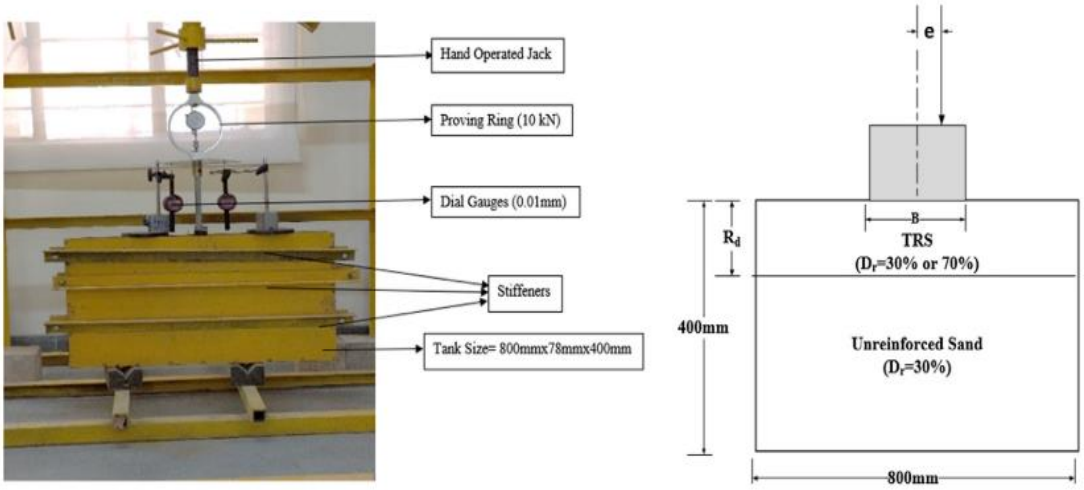

Figure 2.10. Experiment setup
(Source: Gill and Mittal, 2019)

The study examined waste tire chip content, reinforcement depth, and relative density, while the eccentricity of the loading was altered between 0.1B and 0.2B, where B is the footing width. At all strains, a significant improvement in carrying capacity was

noted. According to the experimental results, the optimal amount of tire waste and the appropriate depth of reinforcement are 30% (by weight) and 1B, respectively. The benefits were definite at larger eccentricity, with a bearing capacity ratio of 5.77 kN/m^2 and 7.46 kN/m^2 achieved for low and high stresses, respectively. Additionally, the proposed approach demonstrated beneficial results in both dense and loose states.

Tsiavos et al. (2019) examined the possibility of a low-cost seismic isolation approach for developing countries that uses a deformable granular layer of sand rubber.

Mechanical properties of a putative failure mechanism within the sand-rubber layer are studied. The angle of friction of three different sand-rubber mixtures subjected to varying vertical stresses is measured. The experimentally determined mechanical properties are compared to pure rubber and sand samples. The sliding friction between a sand-rubber layer and a wood interface is identified. The same sand-rubber combinations are tested in direct shear against a timber interface in the foundation casting, subjected to varying vertical loads. The influence of the shear rate and saturation of the sand-rubber mixture on mechanical properties is discussed. The kinetic friction of distinct sliding interfaces against two different sand-rubber mixtures for two different sand-rubber layer heights is measured using a uniaxial shaking table experimental setup. Both harmonic ramp loading and earthquake ground motion excitation are applied to the rigid sliding block against the sand-rubber layer. A lower (and hence better from a seismic isolation standpoint) friction coefficient between the sand-rubber layer and the foundation is the design conclusion of this static and dynamic testing evaluation. It allows for a holistic design of a response modification approach for limiting seismic damage in developing countries.

Direct shear testing is used to determine the ideal sand-rubber grain size ratio for reducing friction and facilitating sliding on a wood interface. The choice of a sand-rubber mixture with $D_{50,r}/D_{50,s} = 2$ is more favorable than the other two tested mean grain size ratios of$D_{50,r}/D_{50,s} = 5$ and $D_{50,r}/D_{50,s} = 10$.

Hazarika et al. (2020) developed A low-cost approach to protect residential buildings from vibration- and liquefaction-induced damage during earthquakes. It incorporates a mixture of tire chips and gravel as horizontal reinforcement material beneath the foundations of residential buildings. The term "horizontal reinforcing inclusion" refers to a horizontal layer of tire chips and gravel laid beneath the foundation. This blend of tire chips and gravel provides the foundation with sufficient bearing capability. A series of small-scale 1 g model shaking table tests was conducted in this

study to determine the technique's efficiency. Additionally, cyclic undrained triaxial tests were used to determine the susceptibility of tire chip-gravel mixes to liquefaction. The findings of the model testing suggested that the technique performs best when the reinforced layer is 10 cm (2 m in prototype) thick and the gravel component (percentage by volume of gravel in the mixture) is 50%. Additionally, the element testing suggested that the gravel fraction is significant. A gravel fraction of 50–60% by volume was found to be the optimal mixing percentage for greatly limiting the rise in excess pore water pressure without jeopardizing the stiffness of the reinforcing inclusion.

Silva Araujo, Suarez Moreno, and Zornberg (2021) studied the utilization of fine lateritic soil combined with TDA's as a substitute composite material for light traffic roads and retaining structures. Experiments were done to characterize materials, compact them, and quantify their shear strength qualities utilizing medium-scale direct shear tests. The direct shear tests were conducted based on the results of the compaction testing, which indicated that the optimal rubber content was 5%. The results indicated that shear strength is significantly dependent on the amount of displacement permitted, which is critical when the analyzed soil has a high proportion of tiny particles and the presence of fractures can limit their use. Finally, the soil examined in combination with TDA's demonstrated the possibility for use in certain civil engineering constructions.

Compaction studies utilizing two distinct compaction efforts (standard and modified Proctor) revealed that as tire shred content increased, the composite's maximum dry unit weight decreased. However, it was shown that variations in the optimal moisture content are only sensitive to compaction effort; the shear strength envelopes, on the other hand, were found to be strongly dependent on the permitted displacement used as a failure criterion. When shear stress at a maximum displacement of 5 mm was used as the shear strength criterion, the composite shear strength decreased. However, when a maximum displacement of 10 mm was used, there was no significant difference in shear strength with varying tire shred percentages. The specimens made entirely of rubber demonstrated the weakest behavior, with high compressibility and low shear strength for all displacements permitted to the samples;

The shear strength values obtained for mixtures containing 5% tire shred were found to be the optimal choice for geotechnical projects involving tropical soils with relatively high fine content, and the investigation demonstrated that tropical soils could be mixed with TDA's in light traffic roads and certain retaining structures.

2.4. Earth Retaining Structures

ERSs are geotechnical structures that are used to retain or support, reinforce, and stabilize soil material. According to the load support mechanism, ERSs can be categorized into two macro-categories: (a) internally stabilized structures and (b) externally stabilized structures. Internally stabilized structures fall into two broad categories: reinforced soil slopes and geosynthetic reinforced soil walls.

Sandford and Cribbs (1997) present the engineering features required to employ tire chips. Grade, specific gravity, compact density, shear strength, compressibility, and coefficient of lateral earth pressure at rest were determined for three vendors' tire chips and presented the benefits of lightweight fill for retaining walls the maximum size of 76 mm and high compressibility of tire chips needed custom-made testing equipment. The experiments revealed that tire chips are made up of equally sized gravel particles that barely absorb a little water. Compacted soils have a density of 0.61 Mg/m^3, whereas theirs is 0.62 Mg/m^3. A large-scale direct shear device assessed shear strength. The friction angle was between 19–25 degrees, and the cohesion intercept was between 8–11kPa. The compressibility studies revealed that tire chips are highly compressible when initially loaded but less so when unloaded and reloaded. The coefficient of lateral earth pressure at rest varied from 0.26 for tire chips with a lot of steel belts exposed at the cut edges to 0.47 for tire chips made entirely of glass-belted tires.

This research has several implications.

1. The three suppliers' tire chips were uniformly graded from 13 to 76 mm in size.
2. The specific gravity of the tier chips ranged from 1.14 to 1.27, somewhat higher than water. Glass-belted tire chips have lower specific gravity than glass-belted tire chips mixed with steel-belted tires.
3. The compacted dry densities of the tire pieces ranged from 0.618 to 0.642 Mg/m^3, indicating its potential as a lightweight fill.
4. Compression tests show that tire chips are highly compressible during the first loading cycle but less so during subsequent unloading and reloading cycles.
5. The tire chips had a friction angle of 19–25 degrees and cohesion of 8–11 kPa.
6. The amount of exposed steel belt appears to affect some engineering properties of tire chips. Large exposed steel belts cause increased compressibility during the first loading

cycle, higher Young's modulus throughout unloading and reloading cycles, lower K_0 coefficient of earth pressure at rest, and lower shear strength during unloading.

7. These laboratory results imply that employing tire chips with exposed steel belts as retaining wall backfill may be advantageous due to their lower K_0.

(Jamshidi et al. 2010) The authors discuss their findings of the influence of synthetic fiber materials on the dynamic characteristics of fine sand. The goal of the project is to convert fibrous carpet waste into a soil reinforcing material. A set of five shaking table tests using a rigid box, shown in Figure 2.11, was performed on Toyoura sand samples reinforced with randomly scattered geotextile bands. The dynamic deformation parameters of reinforced sand are characterized in terms of wall horizontal deformation and rotation. The results indicate that fiber reinforcement considerably enhances the dynamic behavior of fine sand and the deformation properties of a fiber-reinforced sheet pile when subjected to shaking.

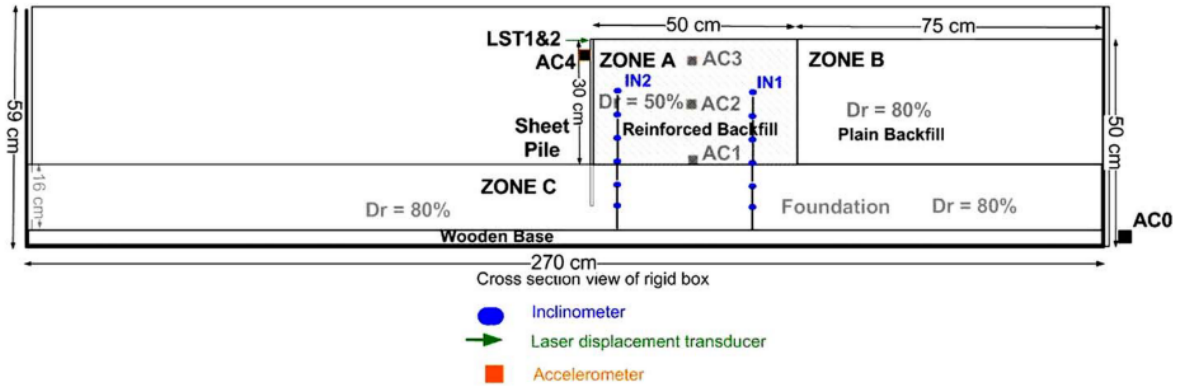

Figure 2.11. Configuration and monitoring the layout of reinforced soil model walls at a reduced scale. (Source: Jamshidi et al. 2010).

- Aspect ratio, fiber length, and fiber content all decreased the maximum residual horizontal displacement.
- Aspect ratio and fiber content increased the amplitude of sheet pile wall rotation.
- The initial acceleration increased as fiber length and/or aspect ratio increased. The input base acceleration's amplitude exceeded the minimum acceleration for every wall.
- The fiber length and aspect ratio led to increasing the stiffness that caused the acceleration amplification factors to decrease.

- Greater shear modulus was achieved by increasing shearing strain amplitude.
- Amplification factors tend to diminish, while shear modulus tends to increase when fiber content approaches 0.5 %. Increased fiber content decreases the composite density and dilutes or eliminates interparticle friction among sand grains. This improvement is laboratory-based and requires more field study. Inclusions with a fiber content of over 1% (weight fraction) become unappealing because they make a combination non compactable. In the field, the fiber content of less than 1% is usually best.

Reddy and Krishna (2015) have investigated the utilization of recycled tire shreds in the sand–tire chip (STC) mixture for retaining wall applications. Small-scale physical model studies on rigid retaining walls with various STC mixes were conducted. In a Perspex container, a rigid retaining wall model with a 600 mm height was made. The wall is constructed entirely of hollow rectangular steel panels. STC mixtures with varying percentages of tire chips, such as 10%, 20%, 30%, 40%, and 50%, were investigated as backfill materials. Concrete blocks were used to apply a static surcharge load of up to 10 kPa. The displacements and earth pressures of model walls have been examined for sand alone (control case), and STC mixes as backfill materials. The experimental results reveal that by employing STC blends as lightweight backfill materials, horizontal displacements and lateral earth pressures are decreased to around 50%–60% of those in the control scenario.

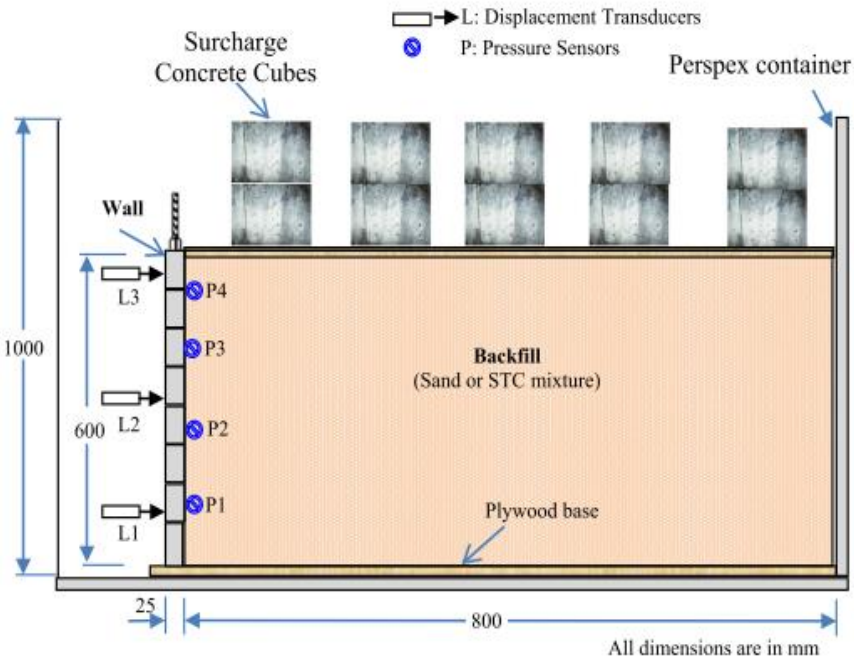

Figure 2.12. Schematic diagram of test wall configuration
(Source: Reddy and Krishna, 2015)

2.5. Conclusion

According to previous research, tire shreds strengthened the soil, increased its permeability, and decreased density. Several types of research have been conducted on the use of tire scraps to solve geotechnical difficulties, such as increasing the bearing capacity of the soil or using them as a lightweight backfill in retaining walls. On the other hand, the researchers assumed that the backfill behind the retaining wall was infinite and overlooked the presence of natural soil in narrow backfills, which is what this research covers with granulated rubber. Recycling used tires contributes to environmental protection, particularly in Turkey, where tires are not recycled in civil works, according to a 2017 report by the European tire and rubber manufactures' association.

The conducted research showed that tire scrap is a promising material to use in the geotechnical field. Increasing strength and permeability decrease in density and stiffness, making it a suitable material to use as lightweight backfill.

CHAPTER 3

PROPERTIES OF THE SOIL USED IN THE MODEL TESTS

3.1. Introduction

This chapter describes the engineering characteristics of the sand and granulated rubber utilized in the investigation and provides an overview of the equipment and testing procedures used in the study.

Generally speaking, the experimental testing program is divided into two main stages. The first stage is dedicated to classifying the soil, defining the engineering properties of the sand-rubber mix, and determining the optimal mixing proportion. A total of 38 direct shear tests and 4 modified compaction tests were performed. The second stage is devoted to the physical model of a sheet pile foundation, which will be explained in detail in chapter four.

3.2. Physical and Mechanical Properties of The Soil Used in The Experiments

Soil may exist as a controlled naturally occurring substance or as a compacted mass. As with other building materials, the soil has mechanical characteristics: strength, compressibility, and permeability. In order to predict how soil will act under loading, measuring the physical and mechanical properties of soil is of higher paramount. This ensures safe soil structure design and also other structures that will be overlaid by the soil. The physical characteristics of soil are quantified in the laboratory via the use of regular laboratory tests shown in Table 3.1. The table also shows the applied ASTM standards.

Table 3.1. List of laboratory tests performed and applied ASTM standards

	Laboratory test	Applied ASTM Standard
Physical properties	Moisture Content of Soil	ASTM D2216
	Specific Gravity of Solids	ASTM D854
	Grain Size Distribution	ASTM D422
	Hydrometer Tests	ASTM D1140
	Laboratory Soil Compaction	ASTM D698, ASTM D1557
Mechanical properties	Direct Shear Strength Test	ASTM D3080

3.3. Measurement of Moisture Content

Moisture content is generally used to calculate weight-volume relationships in soils. Moisture content also provides information about the shrink-swell and strength properties of cohesive soils, as proven by liquid limit and plastic limit testing.

The mass of a given volume of moist soil is equal to the sum of the solids in the soil, M_s, and the water in the soil, M_w. The term "moisture content," abbreviated as *w*, is defined as follows:

$$w = \frac{M_w}{M_s} \times 100\% \tag{3.1}$$

Typically, two decimal points can be used to represent the moisture content in the soil. Moisture content varies significantly between "dry" sands and highly flexible clays, ranging from a few percent to over 100%. Even "dry" soils contain some moisture.

In soils like sands and gravels, the w value ranges between a few percent in dry soils to over 20% in saturated soils. Due to the tendency of clay minerals to absorb water molecules, the range of w in soils, for example, silts and clays, is substantially wider. Moisture content in fine soils varies between 0% to more than 100% in more plastic clays.

When determining the moisture content, possible sources of inaccuracy include insufficient drying less than the range between 12-16 hour drying duration. ASTM stipulates that soil must be dried at 110^o C for 12-16 hours. Nonetheless, in soils holding a considerable quantity of organic matter or hydrous minerals, for example, gypsum, a portion of the water is held in place by soil solids. Excessive drying, on the other hand,

effectively eliminates part of the soil solids, resulting in erroneous results. In these circumstances, the oven temperature should be reduced to 60º C.

Measurements of moisture content and specimen size, the amount of soil taken to make an accurate reading increases as the maximum particle diameter increases, with a minimum of 20 g, as seen in Figure 3.1.

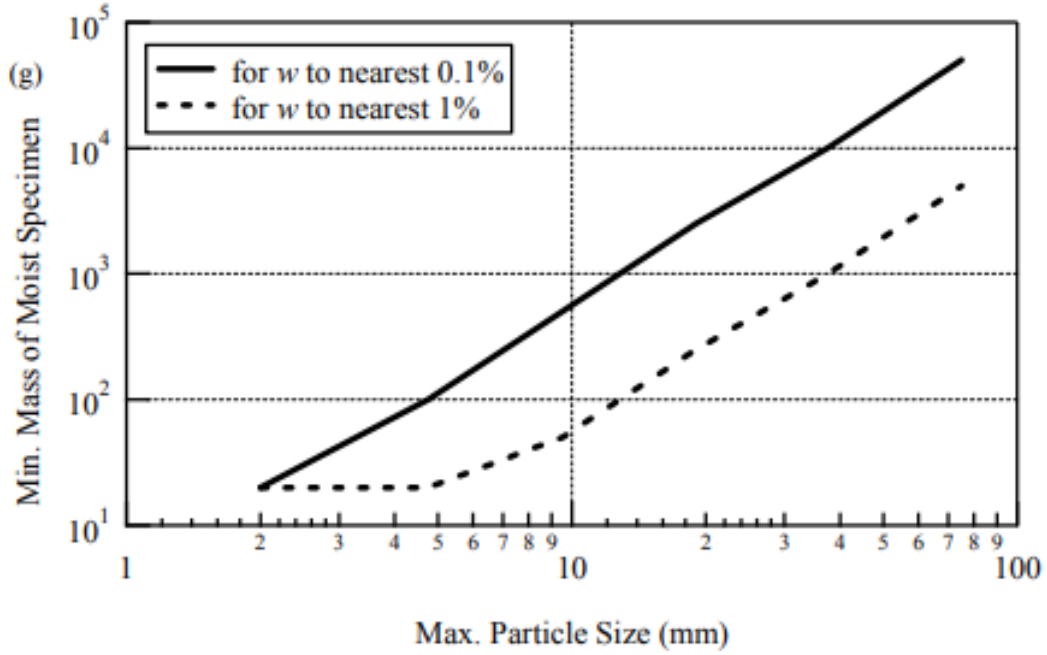

Figure 3.1. Minimum sample mass depending on maximum particle size for moisture content assessment. (Source: Kalinski, Michael E., 2011)

In general, the moisture content test is used with other tests like compaction. Table 3.2 shows the water contain results for the compaction test conducted during this research.

Table 3.2. Moisture content test results for compaction models

GRC	ID	M_c (g)	M_1 (g)	M_2 (g)	w	w_{avg}
0%	MN0001	28.14	83.64	80.51	5.98%	6.47%
		26.58	79.90	76.45	6.92%	
		31.55	125.73	119.96	6.53%	
	MN0002	25.14	77.70	73.24	9.27%	9.02%
		27.48	108.22	101.64	8.88%	
		27.20	102.31	96.16	8.92%	
	MN0003	32.53	125.26	114.44	13.21%	12.16%
		31.44	147.51	135.14	11.93%	
		40.93	115.03	107.48	11.35%	
	MN0004	25.75	102.75	91.61	16.91%	15.27%
		28.96	102.54	92.80	15.26%	
		43.22	126.24	116.27	13.65%	
	MN0005	27.26	68.80	67.55	3.12%	3.27%
		25.00	83.38	81.59	3.16%	
		17.33	63.54	61.97	3.53%	
Fine 10%	MF1001	27.27	63.04	60.93	6.27%	6.11%
		19.77	64.92	62.34	6.06%	
		22.13	81.22	77.88	5.99%	
	MF1002	28.17	92.27	86.55	9.81%	9.64%
		26.68	94.67	88.69	9.65%	
		31.59	100.87	94.89	9.45%	
	MF1003	25.28	90.47	82.93	13.08%	12.42%
		27.72	102.55	94.67	11.77%	
		27.34	90.98	89.90	--	
	MF1004	32.58	121.36	108.67	16.69%	15.03%
		43.91	142.93	130.78	13.99%	
		41.01	207.23	186.29	14.42%	
	MF1005	26.63	91.42	85.70	9.68%	9.15%
		31.57	123.56	115.78	9.24%	
		27.28	93.48	88.28	8.52%	
	MF1006	25.22	72.10	70.65	3.19%	3.25%
		27.54	102.27	100.04	3.08%	
		43.90	127.95	125.12	3.48%	

(cont. on next page)

Table 3.2 (cont.)

coarse 10%	MC1001	28.19	89.97	88.04	3.22%	3.26%
		26.58	92.09	90.13	3.09%	
		31.56	102.76	100.37	3.47%	
	MC1002	25.13	96.25	92.01	6.34%	6.19%
		27.30	105.68	101.31	5.91%	
		27.21	97.88	93.68	6.31%	
	MC1003	32.51	103.52	97.63	9.04%	9.15%
		43.84	159.71	150.12	9.02%	
		24.99	85.67	80.46	9.38%	
	MC1004	17.32	63.52	58.29	12.78%	12.13%
		27.23	98.73	91.38	11.46%	
		19.76	69.93	64.50	12.15%	
	MC1005	25.68	114.69	101.76	17.00%	15.40%
		28.93	131.76	118.11	15.31%	
		43.23	155.69	141.96	13.91%	
coarse 8%	MC0801	28.09	85.86	82.48	6.20%	6.09%
		25.77	80.82	77.56	6.29%	
		28.80	92.31	88.84	5.77%	
	MC0802	17.28	72.62	68.57	7.91%	7.97%
		22.09	92.53	87.35	7.94%	
		19.71	79.44	74.98	8.06%	
	MC0803	15.88	54.74	51.15	10.19%	9.78%
		18.26	85.83	80.00	9.44%	
		26.55	115.94	108.02	9.71%	
	MC0804	27.48	101.60	92.83	13.43%	12.28%
		27.14	126.47	116.24	11.48%	
		27.18	72.05	67.27	11.92%	
	MC0805	-	-	-	--	13.70%
		29.92	102.85	93.14	15.36%	
		21.84	93.46	85.76	12.05%	

Note: GRC: Granulated rubber content, M: modified compaction N: clean sand, F: fine granulated rubber, C: coarse granulated rubber, w :water content, and w_{avg} : average water content.

These tests are purposely done to quantify how the grain size soil has spread (i.e., grain size as a proportion of total weight) and also indicate the percentage of fines. This data is needed to categorize the soil using the Unified Soil Classification System (USCS). Individual particles, or grains, make up soil. The term "grain size" can be taken as the hole size in a square mesh through which a grain pass. Due to the fact that grains in a

mass of soil are not of the same size, hence it becomes simpler to measure grain size using a gradation curve.

A gradation curve comprises points matching to specific particles size and a percentage of soil grains smaller than that grain size (by weight).

Mechanical sieving is used to determine the grain size of dry granular soil. The material is pushed through a stack of sieves. While any number of sieves may be employed, the stack should generally not exceed six sieves. The coarsest sieve is stacked on top, followed by progressively finer sieves. A pan is positioned beneath the lowest sieve to collect the particles that will size smaller than 75 μm that goes through the finest sieve. Calculate the points on the gradation curve by weighing the proportion retained by each filter. Sieve analysis was conducted for the sand that used in the research that shows well-graded silty sand (SM) presented in Figure 3.2 and Table 3.3.

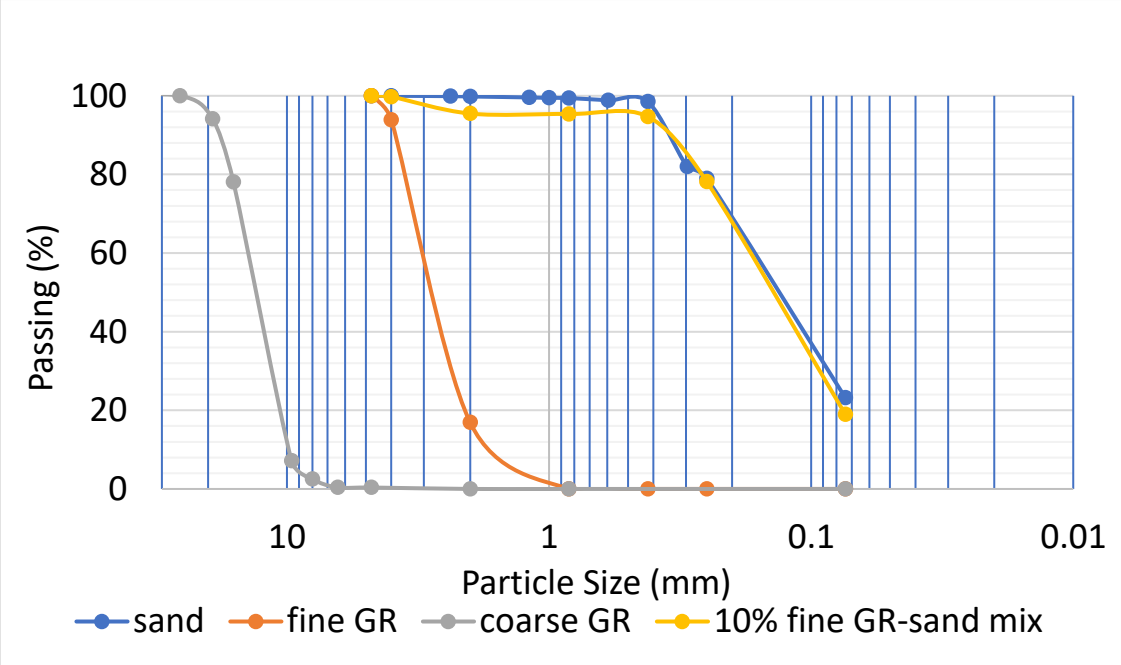

Figure 3.2. Sieve analysis results.

Table 3.3. Soil properties

Property	Value	Unit
Coefficient of gradation	2.68	---
Coefficient of uniformity	2.3	---
USCS soil type	SM	---

3.4. Hydrometer Test

On some occasions, the gradation curve may fail to consistently measure at smaller grain sizes using sieves because the tiny clay particles in soil aggregate and do not pass through the screens independently. However, a hydrometer study can be used to characterize this section of the gradation curve. A hydrometer is a bulb with a graded neck at the top and a strongly weighted base, as shown in Figure 3.3(a).

Figure 3.3. An equipment used for the hydrometer test; (a) hydrometer, and (b) sample mixer

When submerged in a liquid, the hydrometer floats similar to a fishing bobber. The fluid density has an effect on the hydrometer's buoyancy. Heavy fluids enable the hydrometer to float higher. Hydrometer analysis requires mixing soil with water and sodium hexametaphosphate (a dispersion agent) to generate a mix of scattered soil particles. Initially floating in the liquid mixture, the particles settle with time. Larger particles settle more quickly since Stokes' Law says that the spherical particle diameter is

related to the square root of its settling velocity. With the passage of time, as smaller and smaller particles settle below the hydrometer's center of mass, the density of the slurry drops, reducing the hydrometer's buoyancy, and the hydrometer floats lower and lower in the slurry. The hydrometer's position in the mix is recorded as time-dependent, and this data is utilized to construct the gradation curve's points of particle size.

Dry sieving is the more often used and practical test for soil classification utilizing the Unified Soil Classification System (USCS). The USCS soil classification system does not differentiate between particle sizes smaller than 75 μm, but the hydrometer test primarily provides information on the gradation of soil with particle sizes less than 75 m. Hydrometer test findings have a particular application in the assessment of soil activity. The more activity in the soil, the more sensitive it is to shrinking and swelling. Geotechnical engineers in the United States, on the other hand.

3.5. Measurement of Specific Gravity of Soil Solids and Granulated Rubber

The specific gravity of soil solids, Gs, is defined as the bulk density of mineral solids in soil corrected for the presence of water. Otherwise, it may be conceived of as the mass of a volume of soil solids normalized to the mass of a volume of corresponding water. Generally, three significant digits are used to denote specific gravity. Gs is usually specified 2.65 for sands since quartz has a specific gravity of 2.65. Gs for clay is more variable because of the more diverse mineralogy and is commonly estimated to be between 2.70 and 2.80 depending on the mineralogy.

Soil mineralogy determines the specific gravity of soil solids. Gs is generally approximately 2.65 in coarse soils, for example, sands and gravels, where quartz and feldspar dominate the mineralogy. Due to the presence of clay minerals in fine-grained soils, Gs may vary between 2.70 and 2.85. Soil mineralogy determines the specific gravity of soil solids. Gs is generally approximately 2.65 in coarse soils like gravel and sand, where quartz and feldspar dominate the mineralogy. Due to the presence of clay minerals in fine-grained soils, Gs, on the other hand, is more variable, ranging between 2.70 and 2.85.

When determining specific gravity, the most common source of mistake is insufficient de-airing of the soil mixture, resulting in an underestimate of Gs. ASTM

D854 specifies that oven-dried clay specimens may require 2-4 hours of applied suction to de-air adequately. However, for demonstration reasons in this lab and to allow the average three-hour laboratory class time, a 30-minute de-airing period is advised. Additionally, given the brief de-airing interval, it is advised that coarse soil can be used to increase the measurement's precision. The test equipment is a 100ml flask, de-airing device, scale, and distilled water, as illustrated in figure (3.4).

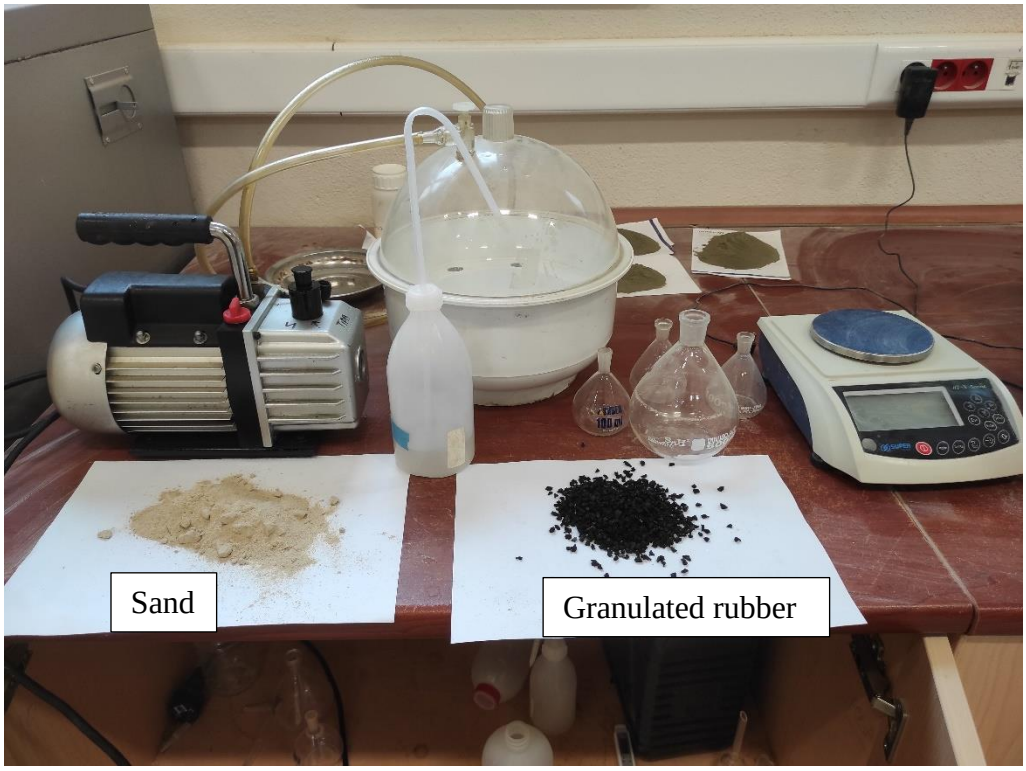

Figure 3.4. Specific gravity test equipment

In the lack of laboratory testing, Gs is frequently presumed based on soil mineralogy. However, some soils, such as organic soils, gypsum, and fly ash, have Gs values much lower than the commonly assumed range of 2.65-2.85. When working with such soils, it is important to measure Gs instead of assuming a value.

Additionally, ASTM standards give criteria for determining whether test findings obtained using this approach are acceptable. Assuming that all tests are conducted by the same laboratory technician, Gs for two independent tests on the same material should be within 0.06 of one another to be regarded as acceptable. Finally, the specific gravity calculated for tire granulated rubber and sand the results presented in table 3.4. For granular rubber, the same steps are followed due to the small specific gravity of granular

rubber, which is very close to water. The sample is left in the water until all particles stabilize.

Table 3.4. Specific gravity values of sand and GR

Sand				
M_a	M_b	M_o	G_s	$(G_s)_{avg}$
130.97	168.4	60.1	2.65	
125.98	163.64	60.1	2.68	2.67
125.975	163.685	60.155	2.68	
Granulated rubber (GR)				
124.78	126.38	14.99	1.12	1.12

3.6. Compaction Test

Compact, fine-grained soil to enhance engineering qualities. Soil properties, including shear strength, compressibility, and hydraulic conductivity, are affected by compaction processes. It is widely utilized in geotechnical constructions such as earth dams, landfill linings, road foundation courses and subgrades, and embankments. Compaction is carried out in the laboratory to forecast compacted soil's performance and create building requirements. The dry unit weight of soil, γ, is defined as:

$$\gamma_d = \frac{M_s}{V} g \tag{3.2}$$

That Ms is the mass of soil solids, V is the volume of soil, and g is the gravitational acceleration constant.

moisture content, w, is defined as:

$$w = \frac{M_w}{M_s} \tag{3.3}$$

M_w is the soil water mass.

Dry unit weight can also be calculated as follows:

$$\gamma_d = \frac{G_s \gamma_w}{1+\frac{wG_s}{S}} \tag{3.4}$$

In term G_s: the specific gravity, γ_w: unit weight of water, and the degree of saturation S. This test was conducted by the modified method using mechanical compacter and C type mold, as shown in Figure 3.5.

Figure 3.5. Mechanical compacter and C type mold

For coarse, fine granulated rubber sand mix with different percentages, the results are presented in Table 3.5.

Table 3.5. Compaction test results

Sample ID	Mold-ID	Mold-W	Mold-V	Soil + Mold	W_{avg}	Dry unit weight
-	-	(kg)	(m^3)	(kg)	%	(kN/m^3)
Clean sand						
MN0005	C1	5.875	0.00211	9.52	3.27	16.38
MN0001	C1	5.875	0.00211	9.64	6.47	16.43
MN0002	C1	5.875	0.00211	9.79	9.02	16.66
MN0003	C1	5.875	0.00211	10.04	12.16	17.23
MN0004	C1	5.875	0.00211	10.01	15.27	16.66
10% fine granulated rubber-sand mix						
MF1006	C1	5.875	0.00211	9.38	3.25	15.76
MF1001	C1	5.875	0.00211	9.50	6.11	15.88
MF1005	C1	5.875	0.00211	9.70	9.15	16.28
MF1003	C1	5.875	0.00211	9.92	12.42	16.69
MF1004	C1	5.875	0.00211	9.87	15.03	16.11
10% coarse granulated rubber-sand mix						
MC1001	C1	5.875	0.00211	9.37	3.26	15.74
MC1002	C2	5.247	0.00212	8.96	6.19	16.18
MC1003	C1	5.875	0.00211	9.75	9.15	16.50
MC1004	C1	5.875	0.00211	9.94	12.13	16.83
MC1005	C2	5.247	0.00212	9.36	15.40	16.51
8% coarse granulated rubber-sand mix						
MC0801	C2	5.380	0.00212	8.99	6.09	15.76
MC0802	C2	5.248	0.00212	8.98	7.97	16.01
MC0803	C2	5.380	0.00212	9.32	9.78	16.60
MC0804	C2	5.380	0.00212	9.45	12.28	16.77
MC0805	C2	5.380	0.00212	9.41	13.70	16.42

3.7. Direct Shear Test

Determines soils shear strength subjected to draining loading conditions, which is required to determine the stability of earth slopes.

Due to the inherent challenges in testing cohesionless soil in triaxial tests, it is frequently employed to evaluate cohesionless soils like sand and gravel. Additionally, the direct shear test can be used to test cohesive soils subjected to drained loading situations in order to measure drained shear strength characteristics. Nevertheless, it is rarely conducted to evaluate cohesive soils and is normally reserved for cohesionless testing soils. Triaxial shear strength testing is more frequently used to determine the drained shear strength of cohesive soils (ASTM D4767).

Figure 3.6 is a schematic representation of the direct shear machine. Typically, cylindrical soil specimens were enclosed in a square shear box. The diameter of the specimen is 59.7 mm. However, the diameter is required to be at least 10 times larger than the largest particle size. The specimen's height must be at least 12.7 mm., and the diameter-to-thickness ratio must not be less than 2:1.

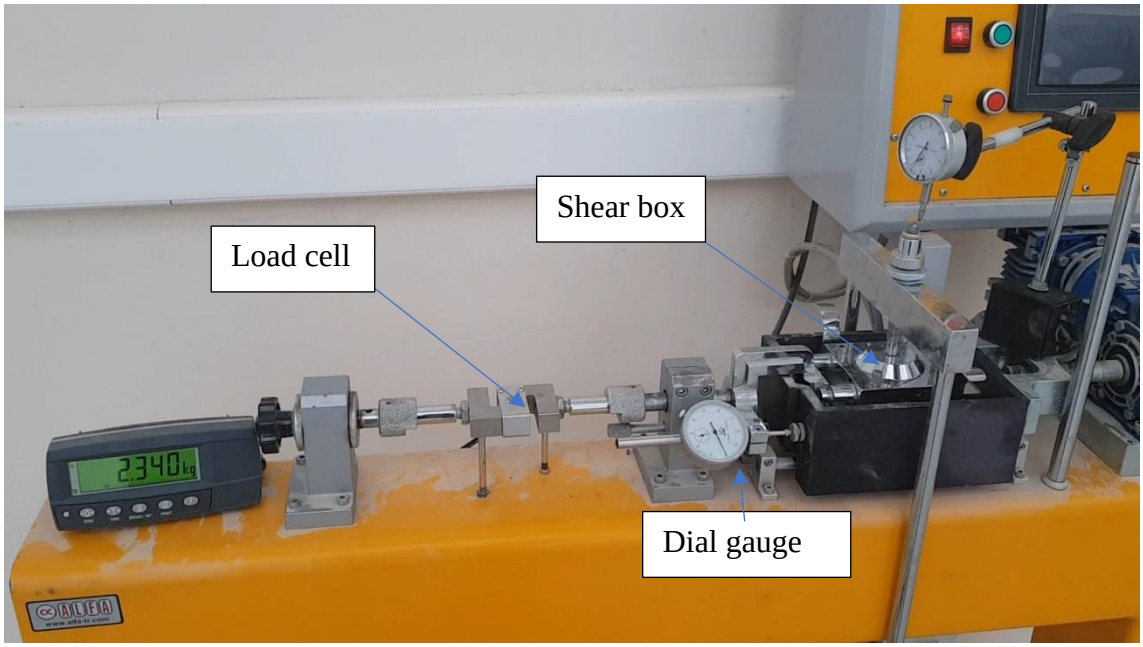

Figure 3.6. Direct shear test device

The shear box in Figure 3.7 is divided into an upper and bottom parts. Two locking pins secure the shear box's top and bottom parts together when the soil sample is being positioned inside, and they must be released for testing. If the locking pins are not removed during testing, the shear box will be damaged. The four separation screws travel through the shear box's upper half, with their points resting on the lower half. During testing, the separation screws are used to split the top and bottom parts of the shear box, minimizing the influence of metal-to-metal interaction on the shear stress.

The shear box is inserted into the shear test machine, and the failure plane is the plane matching the shear box's upper-lower boundary. The shear box's top portion is secured to a load cell, while the lower portion is mounted on roller bearings. The normal load (N) is applied to the specimen through a loading cap on top. Shear force is applied to the sample by driving a screw against the box's bottom half at a rate of 1.24 mm/min.

The failure plane's sheer force is immediately measured as it is moved from the bottom to the top half of the box.

During the test, deformation indicators monitor H and V displacement. Horizontal displacement must be 0.01 mm, while vertical displacement must be 0.01 mm. New machines can use proximeters to find the deformation, LVDTs, and digital dial gauges. These gadgets are easy to use and may be calibrated to output in length units. Figure 3.7 shows the dimension and the failure plane for the tested sample.

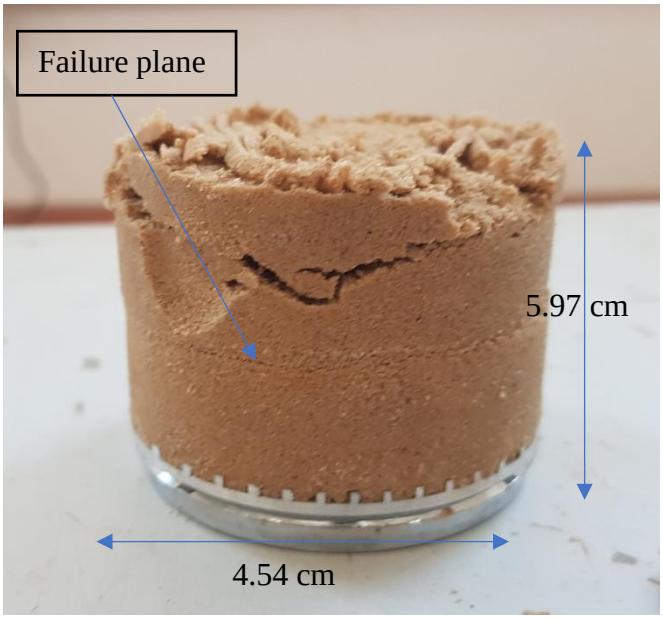

Figure 3.7. Tested sample in the direct shear test device

3.8. Soil Types Under Consideration

The soil utilized in the model experiments is silty sand. The sand's physical characteristics are listed in table 3.6.

Table 3.6. Physical properties of sand used in the model tests

Property	Value	Unit
Max dry unit weight γ_{dmax}	17.2	kN/m^3
Minimum dry unit weight γ_{dmin}	16.4	kN/m^3
The angle of internal friction (Ǿ)	35	Degree
Cohesion (c)	5	kN/m^2

CHAPTER 4

MODEL TESTS

4.1. Introduction

Physical modeling of intriguing geotechnical issues has aided in the clarification of many civil engineering systems' behavior and failure causes. Physical modeling in the laboratory may be used to investigate the mechanics of a variety of natural problems that are directly related to geotechnical issues, as well as the processes that cause these difficulties. Physical models with tight control over material characteristics and well-defined boundary conditions enable parametric investigations to be handled (Davies et al., 2010).

The purpose of this chapter is to demonstrate how a small-scale model can be used to replicate a physical model of a sheet pile foundation implanted in either dry or saturated soil medium under static loading. This chapter describes the model test specimens, materials, measured data, and the steps of the experiment.

The chapter starts with a discussion of the soil tests conducted, the soil model utilized, the technique used to prepare the sand, and the calibration of the equipment used in this research. The static test method is described in detail, as is the equipment used to measure the reaction within the soil media.

4.2 Testing Equipment

Figure 4.1 depicts the testing equipment, which consists of a steel box with walls made of Plexiglas (10 mm thick) and a base that serves as a soil container, as well as a hydraulic jack for applying the load with a circler base bearing plate. The steel box is divided into two parts, the first of which has the following dimensions: length:146 cm, width:70 cm, and height:50 cm. The second part of the steel box is used to hold water and has the following dimensions: length:20 cm, width:70 cm, and height:60 cm.

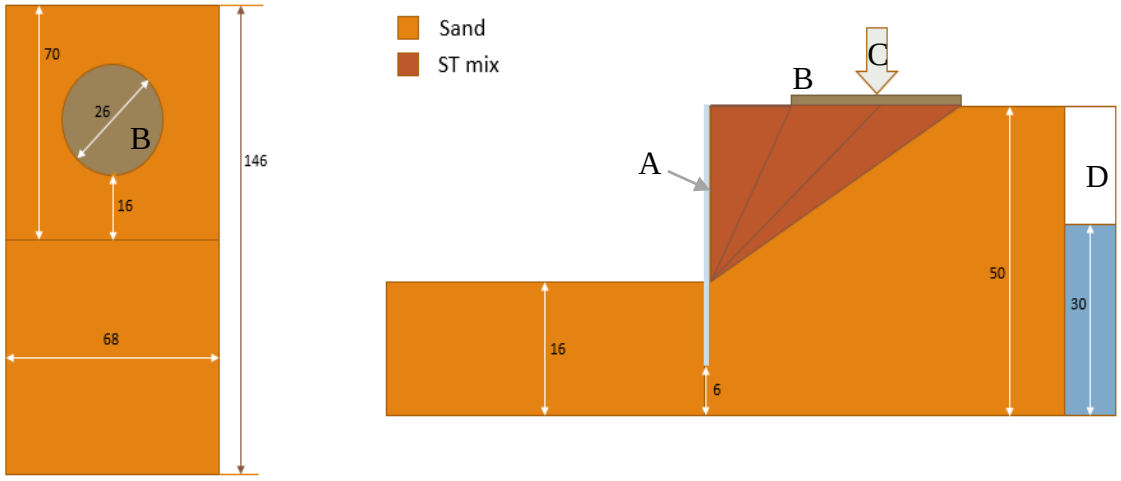

(a) (b)

Note: A: Sheet pile, B: Loading plate, C: Hydraulic jack, D: Water container

Figure 4.1. Experimental model layout a) Top view, b) Side view

4.2. Instruments and Data Acquisition System (DAQ)

The soil and sheet pile responses to load were determined by installing two pressure cells on the sheet pile at 170 mm and 340 mm below the surface, as shown in Figure 4.2. Five pore water pressure transducers evenly spaced inside the backfill at the same level as the pressure cell illustrated in Figure 4.3. A five-ton capacity load cell was used to measure the applied load on a 260 mm diameter loading plate.

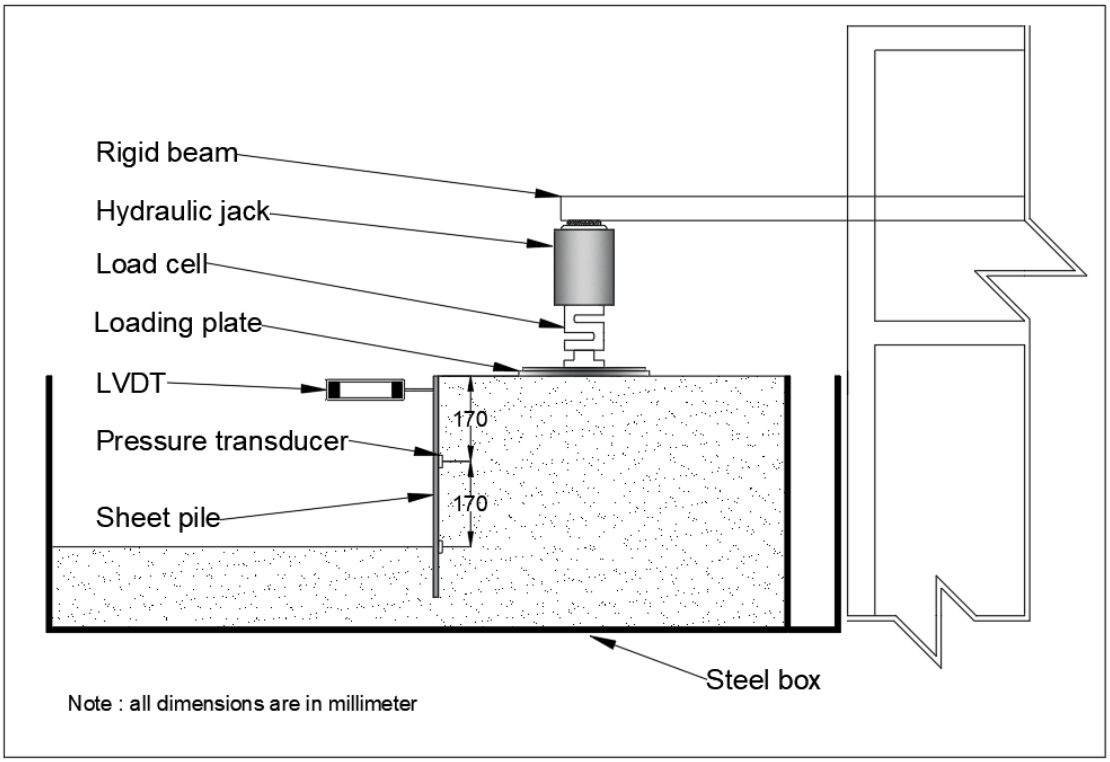

Figure 4.2. Schematic view of the dry model configuration

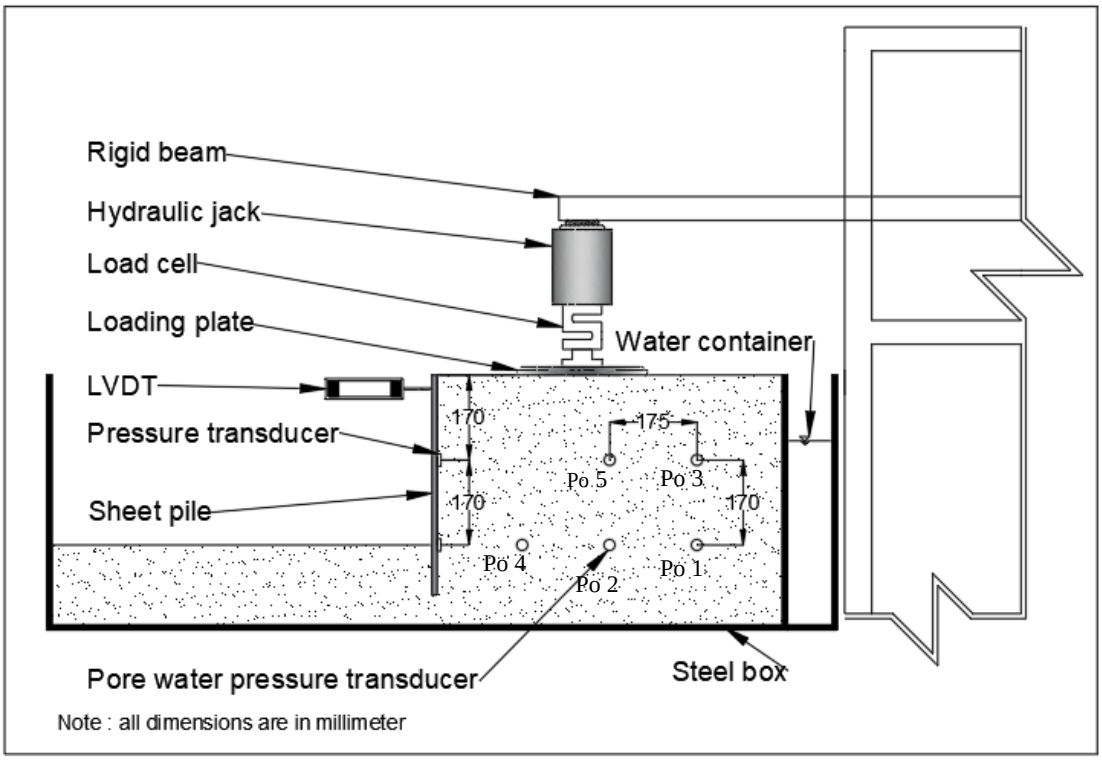

Figure 4.3. Schematic view of the saturated model configuration

The data collection system was designed in such a way that all data could be scanned and captured automatically. Figure 4.4 shows the laptop and data acquisition (DAQ) system used to collect the data.

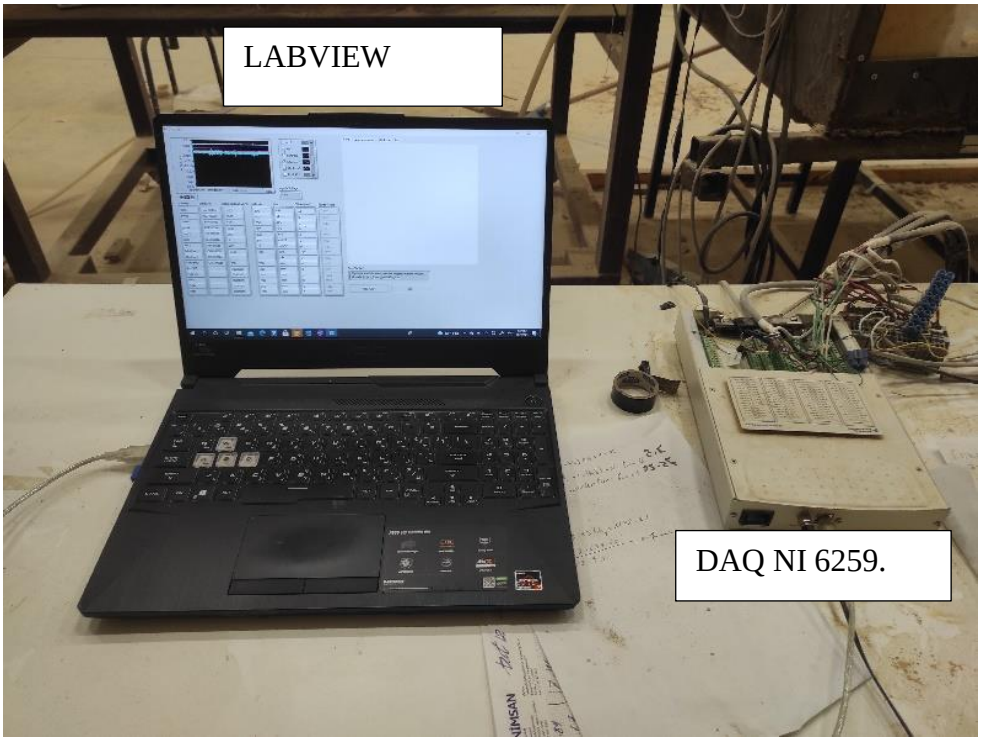

Figure 4.4. Data collecting system

The NI 6259 M Series multi-channel data recording system enables the use of various measuring units depending on the measurement purpose. Analog inputs such as stress, load, pressure, and acceleration were used as testing objects. Figure 4.5 shows the sensors' wires connections to the DAQ device. They employed strain gauges and strain-gauge-based transducers, and others, with a maximum of 16 channels. This Control Unit NI 6259 can read from the sensors every 50 nanoseconds. Figure 4.6 illustrates a representative sample of data from one of the tests.

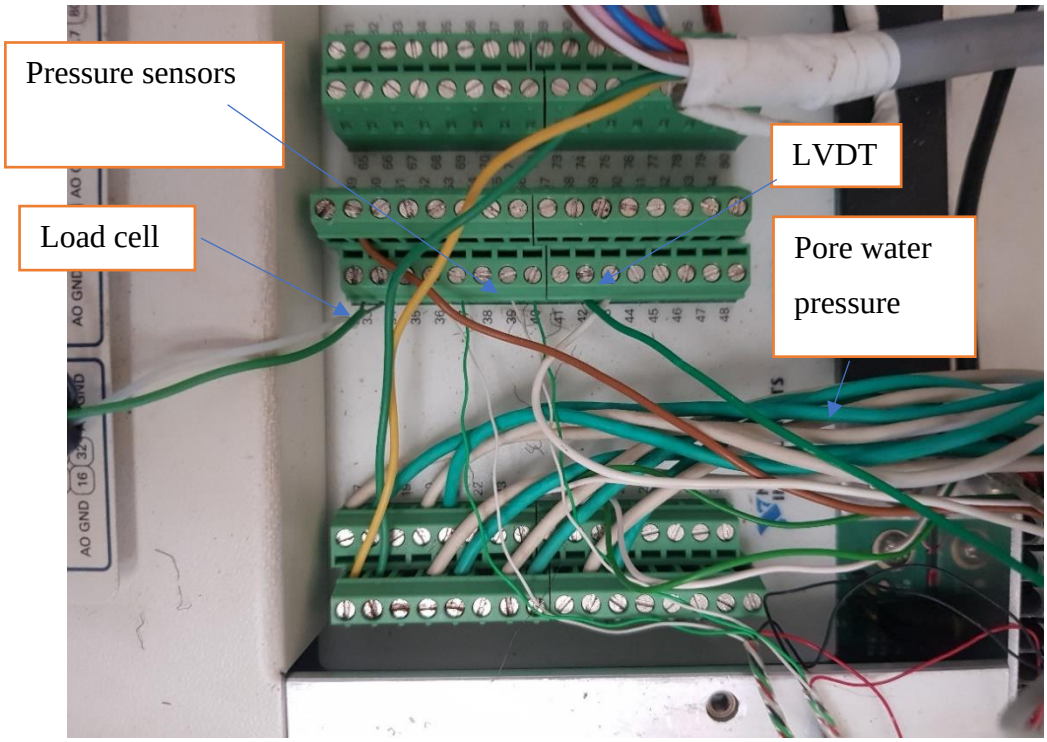

Figure 4.5. Sensors' wires connection in the DAQ device

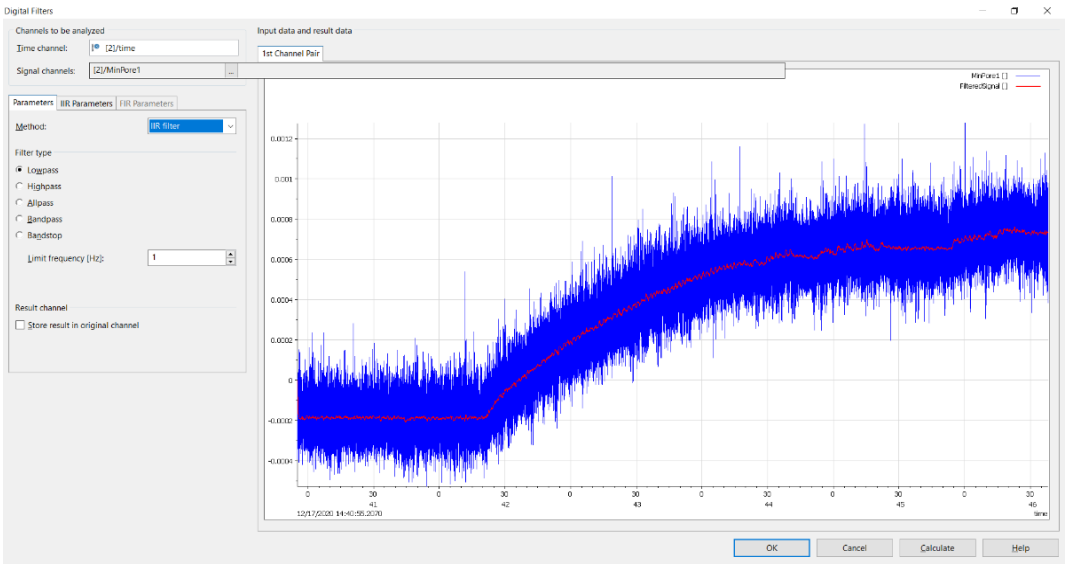

Figure 4.6. Example of received load cell data from test one (Load vs. data index)

4.3. Pressure Measurement

The TML waterproof, 200 kPa pressure transducer (PDA-PB) is shown in Figure 4.7. It is submerged into saturated soil. This transducer's waterproof solid build makes it suited for usage in harsh environments and underwater or outdoors. Appendix A contains information about the (PDA-PB) transducer.

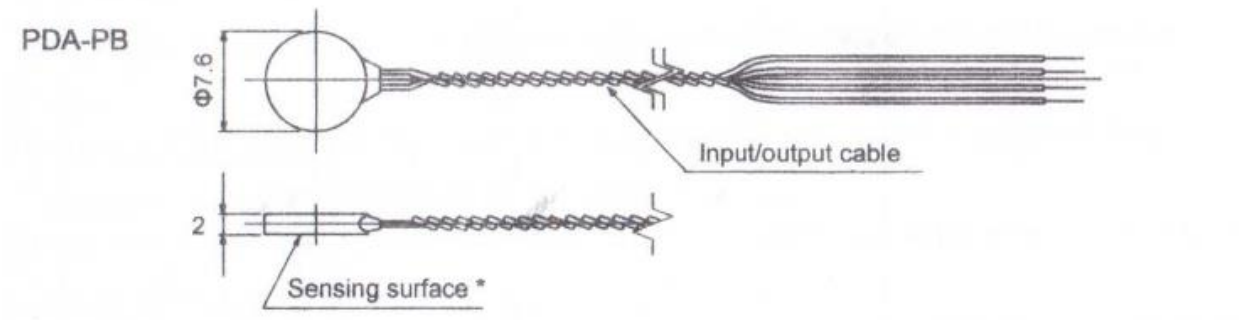

Figure 4.7. Pressure transducer (TML waterproof, PDA-PB)

4.4. Pore Water Pressure Measurement

The KPA-PA pore water pressure transducer utilized in this research is shown in Figure 4.8. This transducer is appropriate for measuring the pore water pressure in the soil. This transducer is used to determine the pore-water pressure within the soil model at various depths throughout the test. This transducer's dual design is unaffected by lateral pressure, ensuring an accurate measurement. Because the mesh in the filter and the space between the pressure-sensing surface and the filter are filled with water, the pore pressure gauge provides highly accurate measurement. The filter must be fitted on the pressure gauge's main body in the following manner.

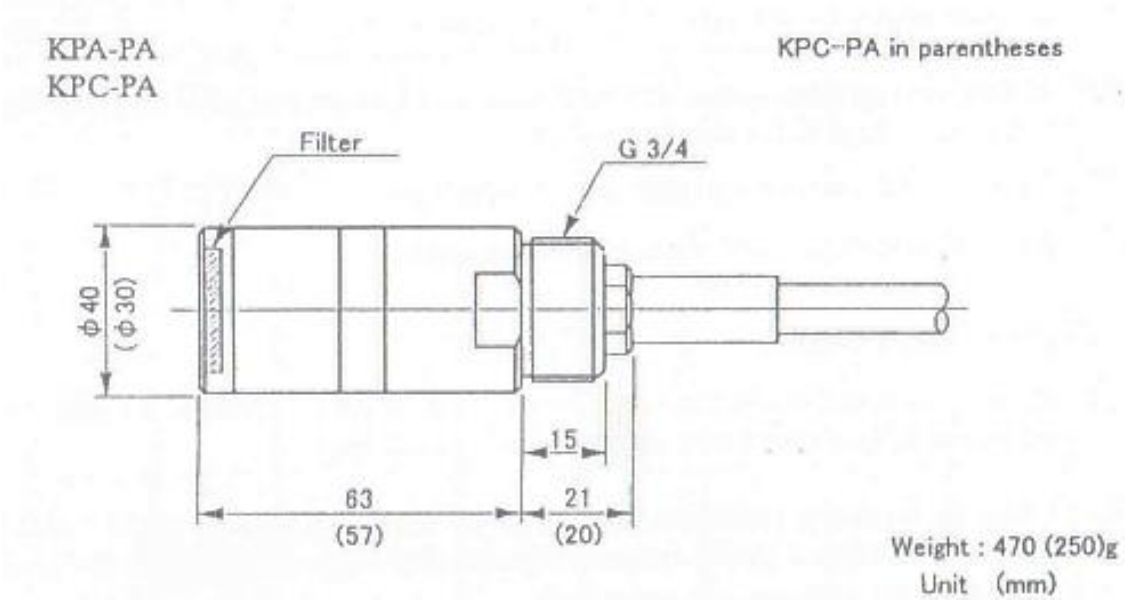

Figure 4.8. Pore water pressure transducer.

4.5. Load Measurement

Figure 4.9 illustrates the DEF-A 5000-ton loadcell mounted between the hydraulic jack and the loading plate to measure the load. The DAQ collected the data as time history data with a time interval of 20 ms.

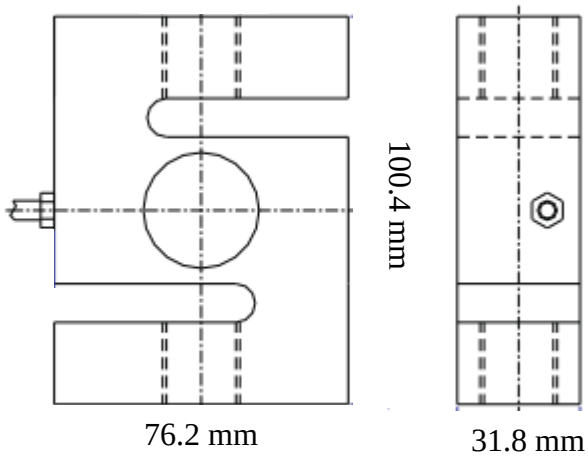

Figure 4.9. Schematic view of the loadcell

4.6. Linear Variable Displacement Transducer (LVDT)

The LVDT translates a position or linear displacement from a mechanical reference (zero or null position) to a proportional electrical signal that contains information about the phase (direction) and amplitude (distance). The operation of the LVDT is not dependent on electrical contact between the moving portion (probe or core assembly) and the coil assembly but electromagnetic coupling.

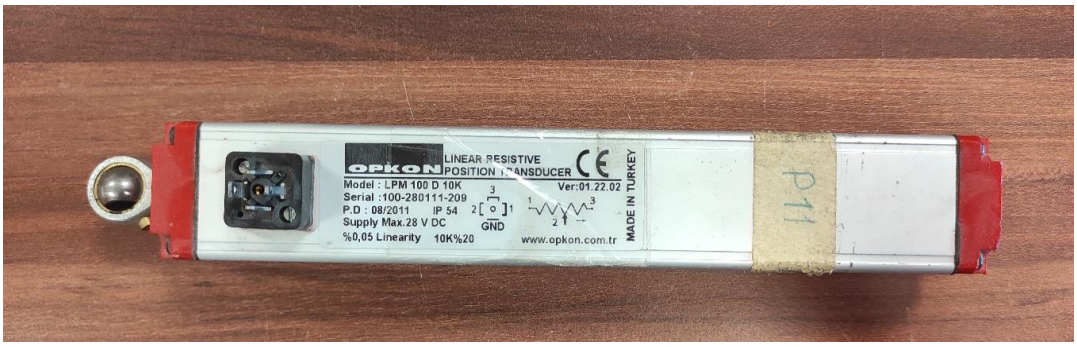

Figure 4.10. Linear variable displacement transducer

4.7. Sand Preparation Method and Calibration

The sand in the test tank was prepared using a tamping and showering procedure. To create a homogenous layer with the necessary density, the sandy soil model was built using the raining approach. The height of the drop and the pace at which the sand is discharged have the greatest effect on the density of the sand layer in the raining technique (Turner and Kulhawy, 1987) to maximize the height of the sand's free fall.

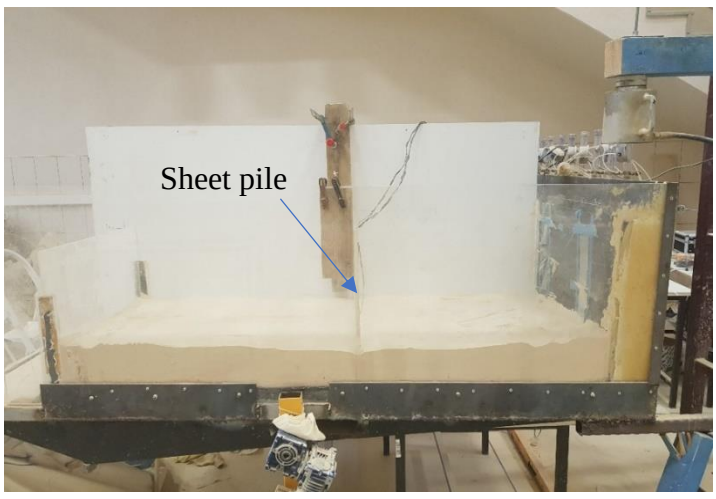

Figure 4.11. Sheet pile and the foundation part.

Several trials with varying fall heights were conducted in order to attain the appropriate density. Figure 4.11 shows the foundation part after completion and inserting the sheet pile. On the other hand, Figure 4.12 shows the backfill and the guiding plates.

Figure 4.12. Preparing the backfill (Top view)

4.8. Velocimetry of Particle Images (PIV) Method

The incremental displacement and strain values were determined by comparing successive pairs of images using image processing software (PIV as implemented in the MATLAB program. Figure 4.13 shows the equipment that was used, a portable64 megapixels camera aided in seeing soil movement during testing and picture processing. The camera was positioned in front of the wall of the text box. All parameters, including focus, gain, and shutter speed, were changed automatically. Two projectors on either side of the camera and lab lights above the camera's optical axis prevented optical impacts from the environment on the viewing window by minimizing errors caused by random pixel intensity variation.

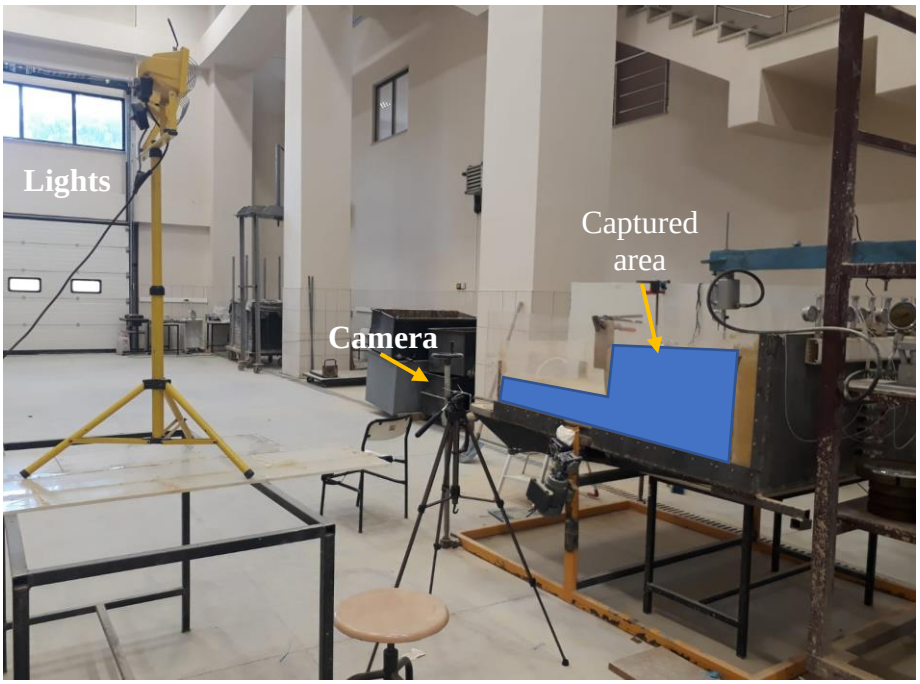

Figure 4.13. The equipment used for the PIV process

As illustrated in Figure 4.14, the digital image was divided into square patches of pixels to create a regular mesh. Because the precision of PIV is reliant on the patch size and grid spacing, an initial study into convergence and stability was undertaken using a range of patch sizes and grid spacings.

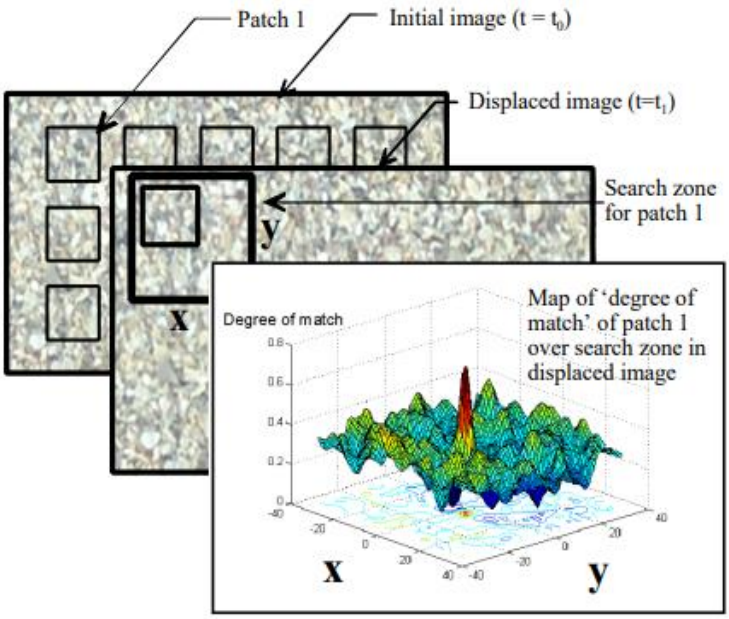

Figure 4.14. PIV algorithm steps

According to Lesniewska and Wood (2011), if the patch is too small, the amount of information provided may prevent the software from confidently recognizing the displaced patch, resulting in the appearance of erroneous displace values, as shown in Figure 4.15.

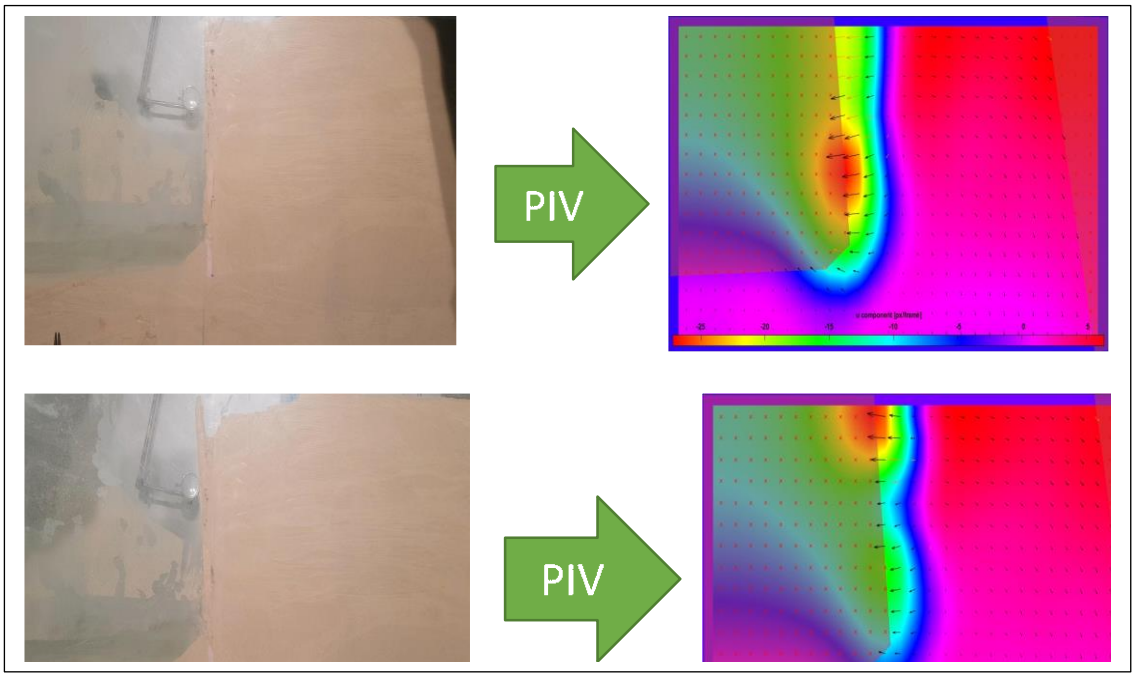

Figure 4.15. PIV analysis results

The second parameter to choose is the grid spacing for subsequent displacement estimations within each image. Strain calculations necessitate the separation of displacement data. A finer grid provides more detail but also increases the likelihood of unpredictable values. Thus, choosing the optimal patch size for the PIV analysis implies striking a balance between two opposing interests. Greater precision is achieved with larger patches, while smaller patches ensure a greater number of measurement points in the image and reveal detail in places with a high strain gradient. The use of somewhat big, overlapping patches is a good compromise that addresses these issues.

4.9. Physical Model - Testing Setup

A hydraulic jack mounted to a 260 mm diameter loading plate is utilized to apply the load on the soil model, which is demonstrated in this study. The M Series Data Acquisition NI 6259 model was used for registering data from the sensors, and the LABVIEW application was utilized to interface with it. As illustrated in Figure 4.16. In addition to monitoring the applied force-time history, this equipment can also measure the displacement-time history at the sheet pile end, the lateral pressure-time history on the sheet pile face, and the pore water pressure-time history, among other things.

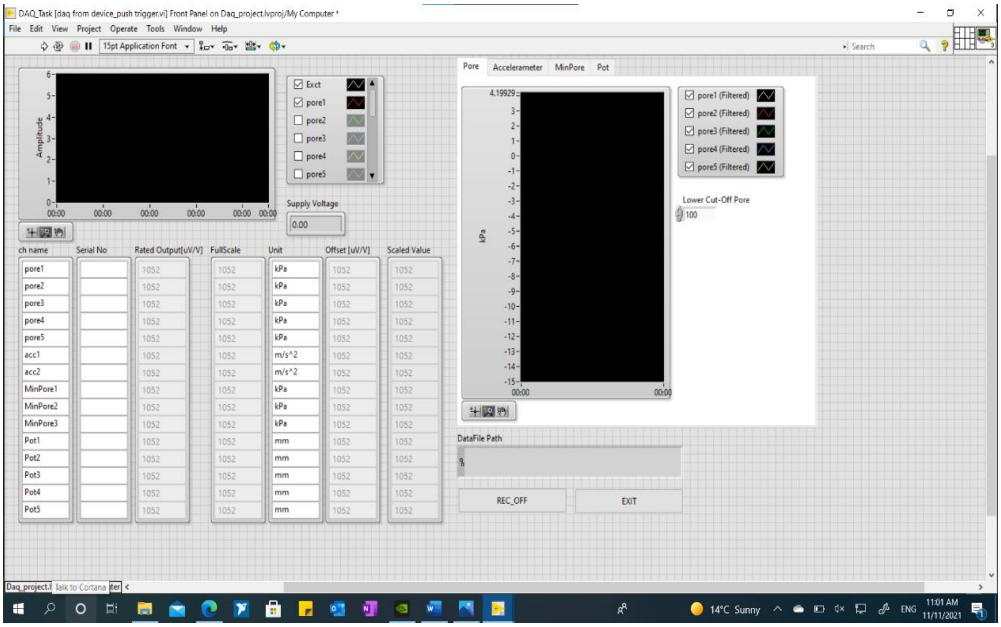

Figure 4.16. Application interface programed by LABVIEW

At various depths throughout each test, pressure-time histories were recorded using pressure transducers, and pore water pressure was monitored using a pressure transducer that measures pore water pressure. The DAQ system's fundamental structure is composed of a central unit capable of transmitting digital trigger signals and receiving analog signals from the ground and sensors. The DAQ system is configured to acquire readings every 20 milliseconds. Additionally, the load, pressure, PWP, displacement waveform, O-P time (time between the start of loading and the maximum value point in the case of load; the time between the start of loading and the maximum value point in

the case of displacement), and time product are stored in the PC as raw data in a text file. The data were filtered and analyzed using the processing software NI DIAdem.

4.10. Measurements of The Lateral Pressure, Pore Pressure, and Displacement

Figure 4.17 illustrates the use of pressure transducers to determine the lateral pressure on the sheet pile. Figure 4.18 shows the small pore water pressure gauges to determine the pore water pressure in saturated conditions.

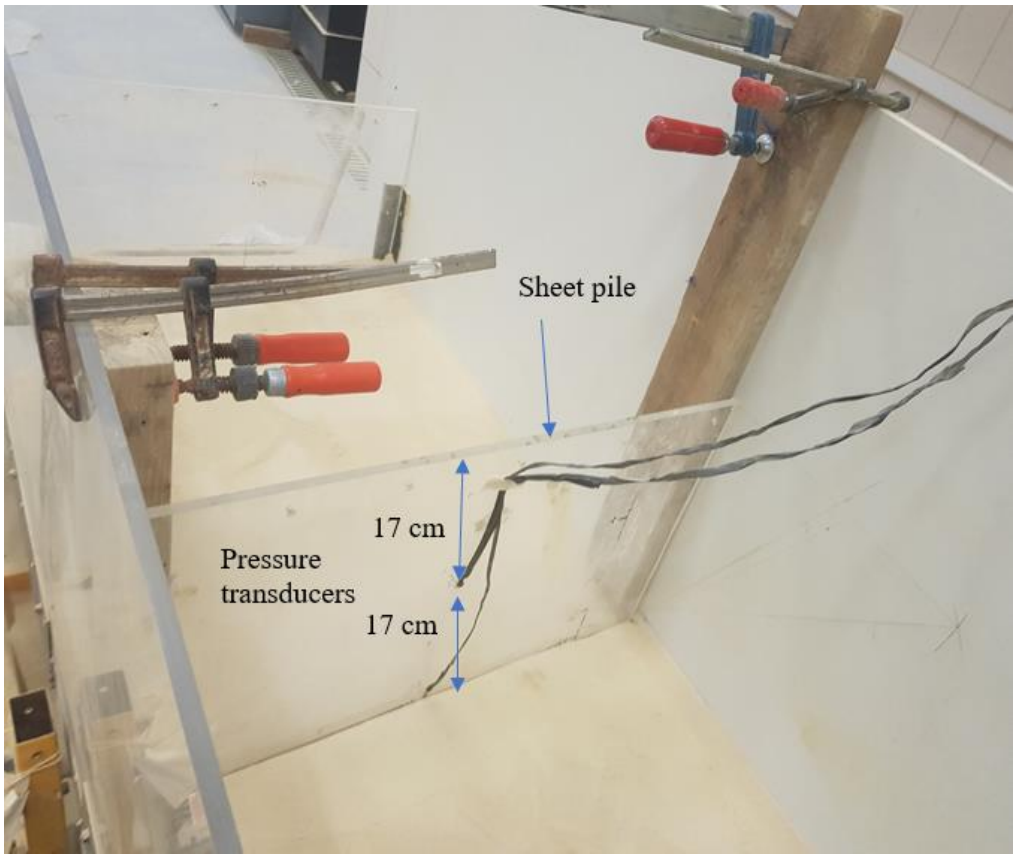

Figure 4.17. Pressure transducers mounted on the sheet pile

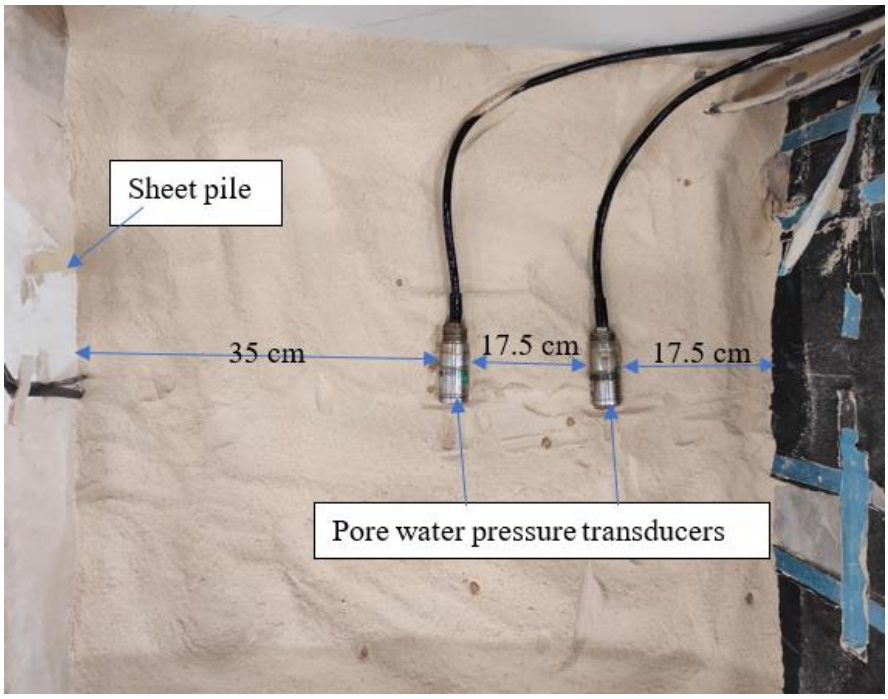

Figure 4.18. Pore water transducers place in the soil model

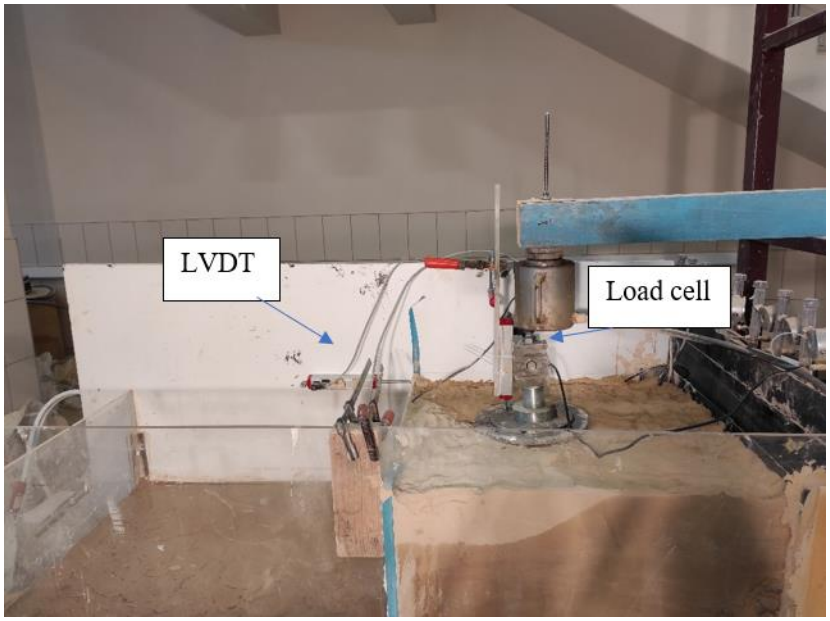

Figure 4.19. Load cell and LVDT placed in the model

All of them were connected to the NI 6259 DAQ in order to collect data from the transducers.

4.11. Testing Program

The testing program consists of two major parts. The first part is devoted to dry sand models with a total of 4 tests. Table 4.1 shows the sand and the GR-sand mix density. The tests were performed in a medium soil state. A bearing plate size was 260 mm. The load is applied by a hydraulic jack and measured by the load cell that was attached to the plate.

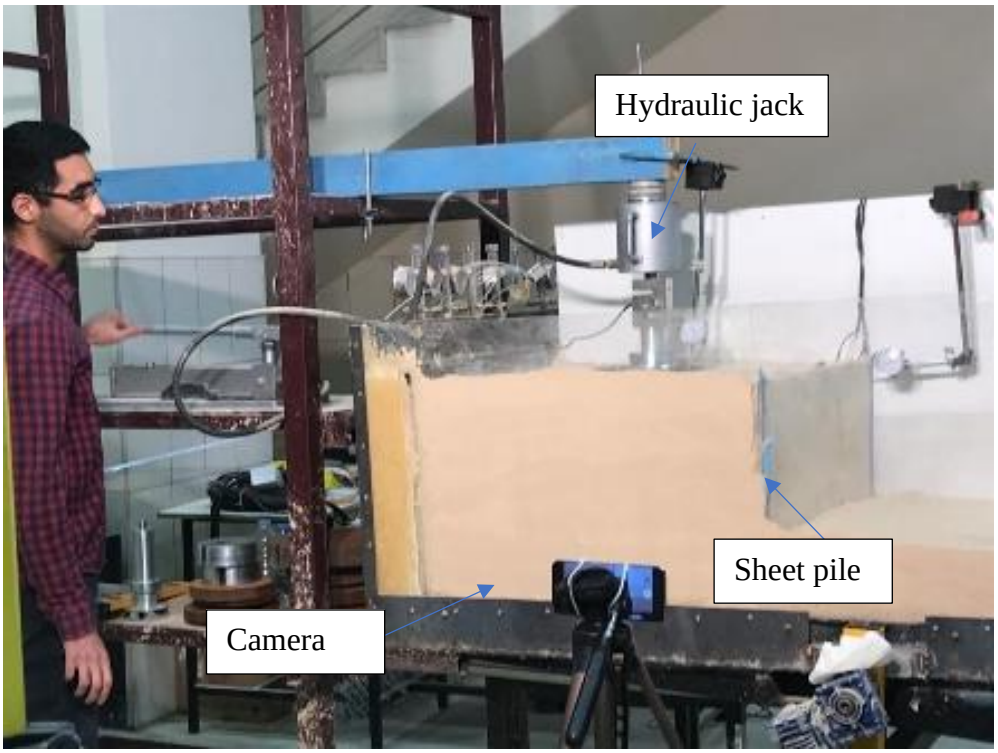

Figure 4.18. Test setup for the dry model

Table 4.1. Dry mode: Sand and granulated rubber-sand mix weight and volume

Test Mode Name	Sand weight	Mixture weight	Sand volume	Mixture volume	Sand unit weight	Mixture unit weight
	(kg)	(kg)	(m^3)	(m^3)	kN/m^3	kN/m^3
DT2	533.9	-	0.32	-	16.33	-
DT4	519.985	25.53	0.30	0.017	16.82	14.39
DT5	466.7	52.34	0.29	0.035	16.02	14.75
DT6	436.45	80.96	0.27	0.052	15.95	15.21

Note: DT: dry test.

The second part consists of 4 models in a saturated condition. The same method was used to prepare the dry sand model used to prepare the models. Table 4.2 contains each model's sand and the GR-sand mix volume and density. In these tests, first, the tank is isolated with silicone lined from inside, then a grid of 6 mm holes made in the backside connected to the water tank. As in dry tests, the raining technique was used to fill the tank with soil. After that, the soil medium was saturated from the back by filling the water container, where water flowed through it. Meanwhile, the flow was maintained uniform and laminar by controlling the head of water in the water tank. After that, saturation was achieved by submerging the sand layer for about 10 hours, as shown in Figure 4.19.

Figure 4.19. Final test setup for the saturated model

Table 4.2. Saturated models' sand and granulated rubber-sand mix weight and volume.

Test Mode Name	Sand weight	Mix weight	Sand vol	Mix vol	Sand unit weight	Mix unit weight
	(kg)	(kg)	(m3)	(m3)	kN/m3	kN/m3
ST 1	510.75	-	0.32	-	15.62	-
ST 2	490.29	26.22	0.30	0.02	15.86	14.78
ST 3	445.16	52.48	0.29	0.03	15.28	14.79
ST 4	425.36	78.45	0.27	0.05	15.54	14.74

Note: ST: saturated test

The following steps describe the testing methodology:

1. Preparing the layers of sand, which have a total depth of 160 mm for foundation and 500 for the backfill.
2. Installing the pressure transducers on the sheet pile at 170 mm and 340 mm depth from the surface.
3. Driving the sheet pile into the foundation sand and fix it with clamps to the model
4. In-state of saturation, the pore water pressure gauge is installed equally spaced at the same levels of the pressure transducers.
5. Installing the liner transducer at the pile head
6. Leveling the surface and installing the loading plate in the center of the backfill, and checking if it is parallel to the surface of the model
7. Connecting the data logger to the LABVIEW program and checking the reading
8. Start applying the load manually through the hydraulic jack

CHAPTER 5

PRESENTATION AND DISCUSSION OF THE TEST RESULTS

5.1. Introduction

The first step was determining the optimal ratio of sand to granulated rubber from the 38 direct shear tests and 4 compaction tests. This chapter discusses the laboratory test results starting with the direct shear tests and the compaction tests.

5.2. Direct Shear Test

To find the best mixing ratio for granulated rubber-sand mix, coarse and fine rubber were used with a different percentage by volume. The granulated rubber was distributed randomly, as shown in Figure 5.1. The percentages of the granulated rubber mixed with sand were 6%, 8%, 10%, 12%, and 15% for each ratio three tests conducted with normal weights of 20 kg, 50 kg, and 100 kg.

5.2.1. Fine Granulated Rubber-Sand mixture:

Figure 5.1. Tested sample shows the fine granulated rubber distribution in the sand-granulated rubber mixture.

For 20 kg normal force, Figure 5.2 shows the shear stress-strain diagram for clean sand and sand mixed with 6%, 8%, 10%, 12%, and 15% granulated rubber. The maximum shear stress of the clean sand sample (DN0001) was 69.66 kPa. 6% GR mixture (DF0601) expressed that initial response weaker than the clean sand sample in the first half then matched it in the second part with the maximum shear stress of 68.19 kPa. 8% GR mixture (DF0801) was the weakest in the tested samples, with a maximum shear stress of 63.52 kPa. 15% GR mixture (DF1501) was similar to the 8% GR mixture with minor initial strength higher than the clean sand sample with the maximum shear strength of 63.67 kPa. 12% GR mixture (DF1201) produced the same performance as the clean sand sample along with the test, but it showed late stronger behavior in the end. Its maximum shear stress was 69.07 kPa; in the end, all the samples that were discussed earlier did not display a peak point. On the other hand, the 10 % GR mixture (DF1001) exhibits a definite peak point and higher response than the other samples. Its maximum shear stress was 72.15 kPa.

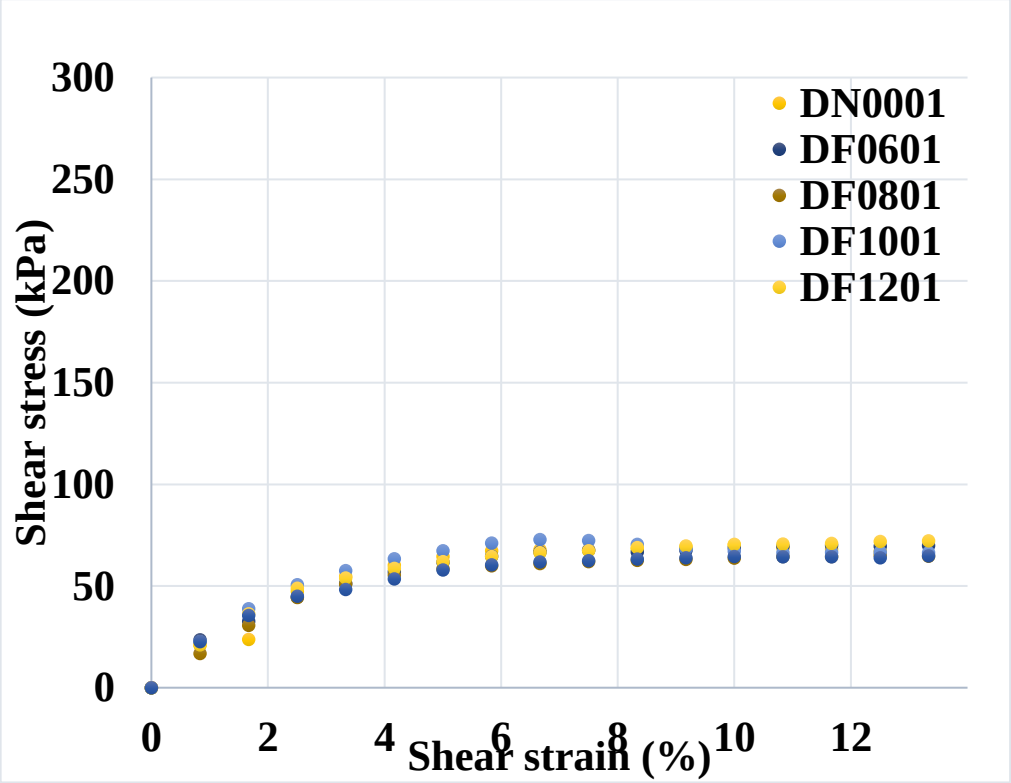

Figure 5.2. Fine granulated rubber-sand mix's direct shear test results with 20 kg normal force.

For 50 kg normal load, Figure 5.3 shows the shear stress-strain diagram for clean sand and sand mixed with 6%, 8%, 10%, 12%, and 15% granulated rubber. The samples that showed peak point is the clean sand (DN0002) and the 10 % GR mixture (DF1002). The maximum shear stress of the clean sand sample was 128.68 kPa. 6% GR mixture (DF0602) with a maximum shear stress of 131.81 kPa showed slightly weaker than the clean sand sample at the beginning, but it continued to gain strength until the end of the test to be the strongest sample without a clear peak point. 15 % GR mixture (DF1502) showed higher initial strength than the clean sand sample. With maximum shear stress of 136.9 kPa. 10 % GR mixture (DF1002) its maximum shear stress of 136.90 kPa, showed higher shear stress than the clean sand sample but weaker initial strength. 8% GR mixture (DF0802) was weaker than the clean sand sample, but its strength was equal to the clean sand sample's peak point. 12% GR mixture (DF1502) followed 8 % GR mixture behavior, but it was initially stronger than the 8 % GR mixture. with a maximum shear stress of 131.12kPa.

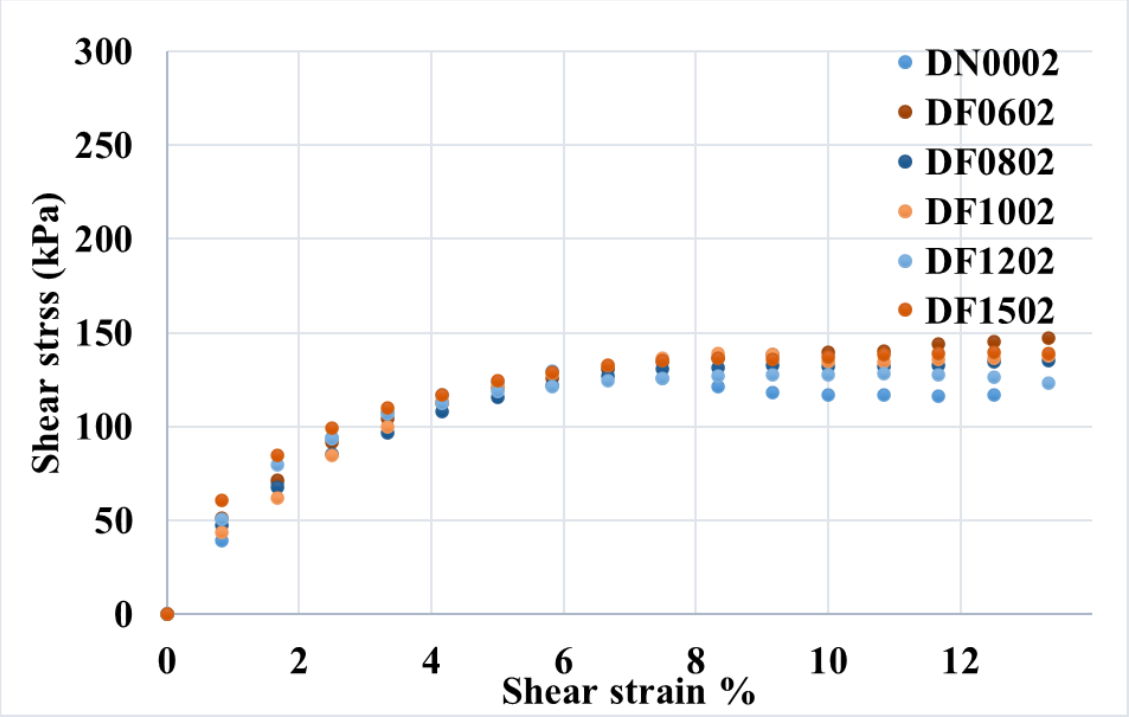

Figure 5.3. Fine granulated rubber-sand mix's direct shear test results with 50 kg normal force.

Finally, 100 kg normal load samples, Figure 5.4 shows the shear stress-strain diagram for clean sand and sand mixed with 6%, 8%, 10%, 12%, and 15% granulated rubber. The clean sand sample (DN0003) showed maximum shear stress of 261.22 kPa. The 6 % GR mixture sample (DF0603) matched the behavior of the clean sand sample until reaching 0.05 shear strain. After that, the shear strength remained constant without gaining any strength when the shear strain exceeded 0.075. It began to lose strength. The maximum shear stress was 234.87 kPa. The 8% GR mixture sample (DF0803) exhibited similar behavior to the clean sand sample but was weaker with 242.29 kPa shear stress. The 12% GR mixture sample (DF1203) did not exhibit a peak but ended stronger than the 6%GR mixture sample after reaching 0.075 shear strain with a maximum shear stress of 234.54 kPa. 15% GR mixture sample (DF1503) had a smooth response with a 242.77 kPa shear stress peak. Finally, the 10% GR mixture sample (DF1003) demonstrated behavior weaker than the clean sand sample with a 258.63 kPa shear stress peak. It should be noted that the clean sand sample was the strongest in this group.

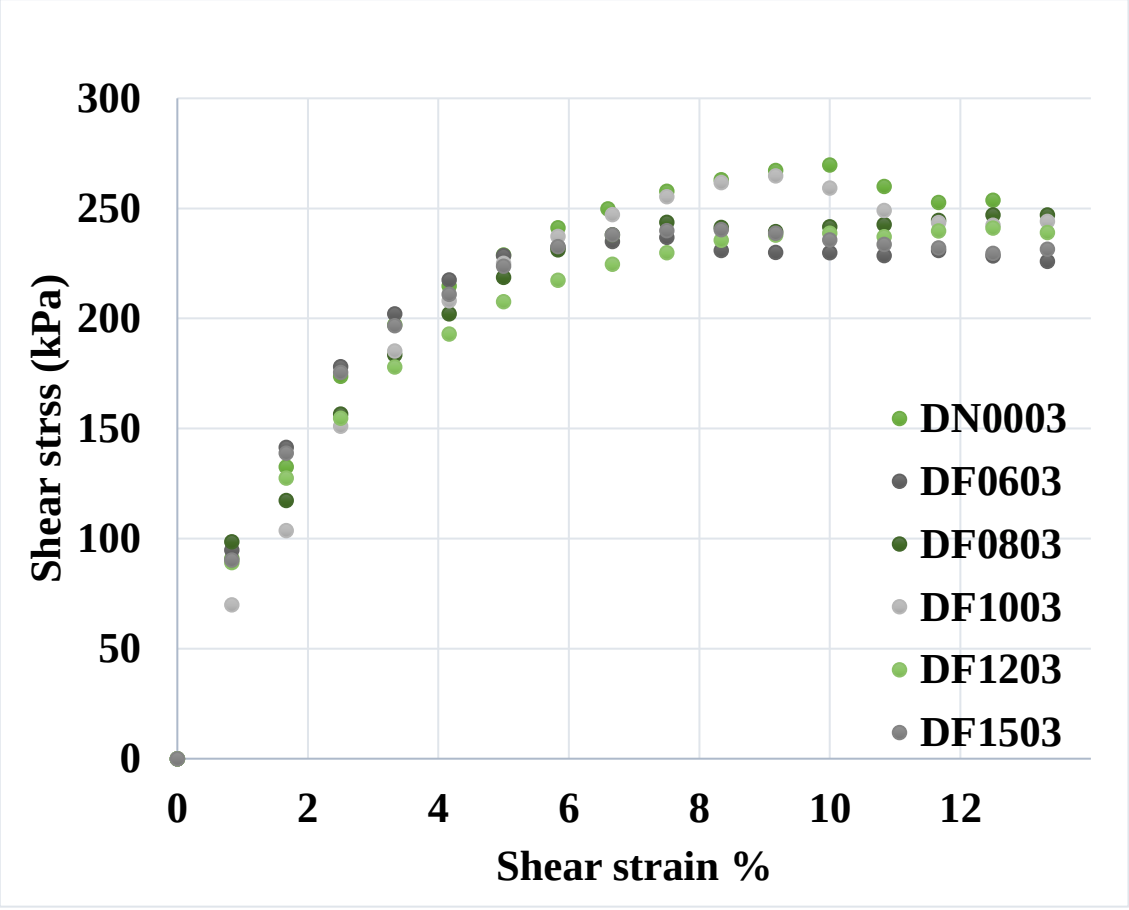

Figure 5.4. Fine granulated rubber-sand mix's direct shear test results with 100 kg normal force.

5.2.2. Coarse Granulated Rubber-Sand mixture:

A series of direct shear tests were conducted on finely granulated rubber to determine the ideal mixing percentage that results in more robust or similar behavior for a clean sample tested initially. The mixture was mixed randomly with a percent by volume Figure 5.4, illustrating the tested sample and the distribution of granulated rubber in the sample.

Figure 5.5. Tested sample shows the coarse granulated rubber distribution in the sand-granulated rubber mixture.

20 kg normal force samples results show in Figure 5.6. The maximum shear stress of the clean sand sample (DN0001) was 69.66 kPa. The 6% GR mixture sample (DC0601) was the weakest group. Its maximum shear stress was 65.21 kPa. The 8% GR mixture sample (DC0801) demonstrated a parallel graph to the clean sand sample until 0.072 shear strain was reached. At this point, the sample demonstrated higher values than the clean sand sample. The maximum shear stress of the 8% GR mixture sample was 70.45 kPa.10% GR mixture sample (DC1001), its maximum shear stress was 71.19 kPa and produced a more potent reaction than the clean sand sample at the start. However, as the test

progressed, the difference between them became smaller. The 12% GR mixture sample (DC1201) demonstrated the strangest behavior in the group with a maximum shear stress of 81.88 kPa. The 15% GR mixture sample (DC1501) demonstrated a similar response to the 8% GR mixture sample, which was slightly weaker initially. Its maximum shear stress was 70.58 kPa.

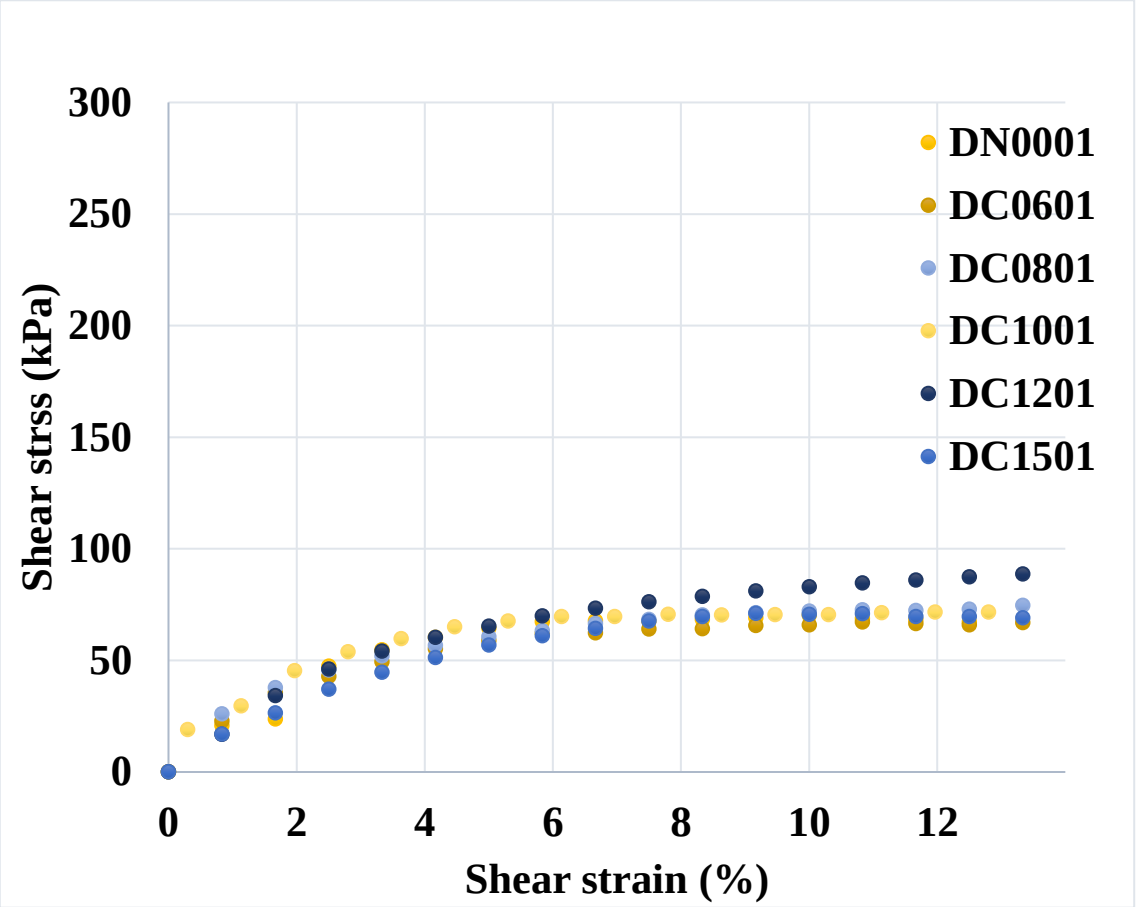

Figure 5.6. Coarse granulated rubber-sand mix's direct shear test results with 20 kg normal force

For the 50 kg samples group shown in Figure 5.7, the clean sand sample (DN0002) reaches its peak of 128.68 kPa at 0.065 shear strain and continues to lose resistance until the shear stress becomes constant at 0.09 shear strain. The 15% GR mixture sample (DC1502) was the weakest without an exact peak value and maximum shear stress of 122.05 kPa.The 8% GR mixture sample (DC0802) behaved similarly to the clean sand sample with a peak of 130.47 kPa. The 12% GR mixture sample (DC1202) initially responded weaker than the clean sand sample. However, it exhibited no peak. Its

maximum shear stress was 139.27 kPa. 6% GR mixture sample (DC0602), its maximum shear stress was 135.05 kPa. 10%GR mixture sample (DC1002) was the strongest sample in the group without a clear peak. Its maximum shear stress was 145.6 kPa.

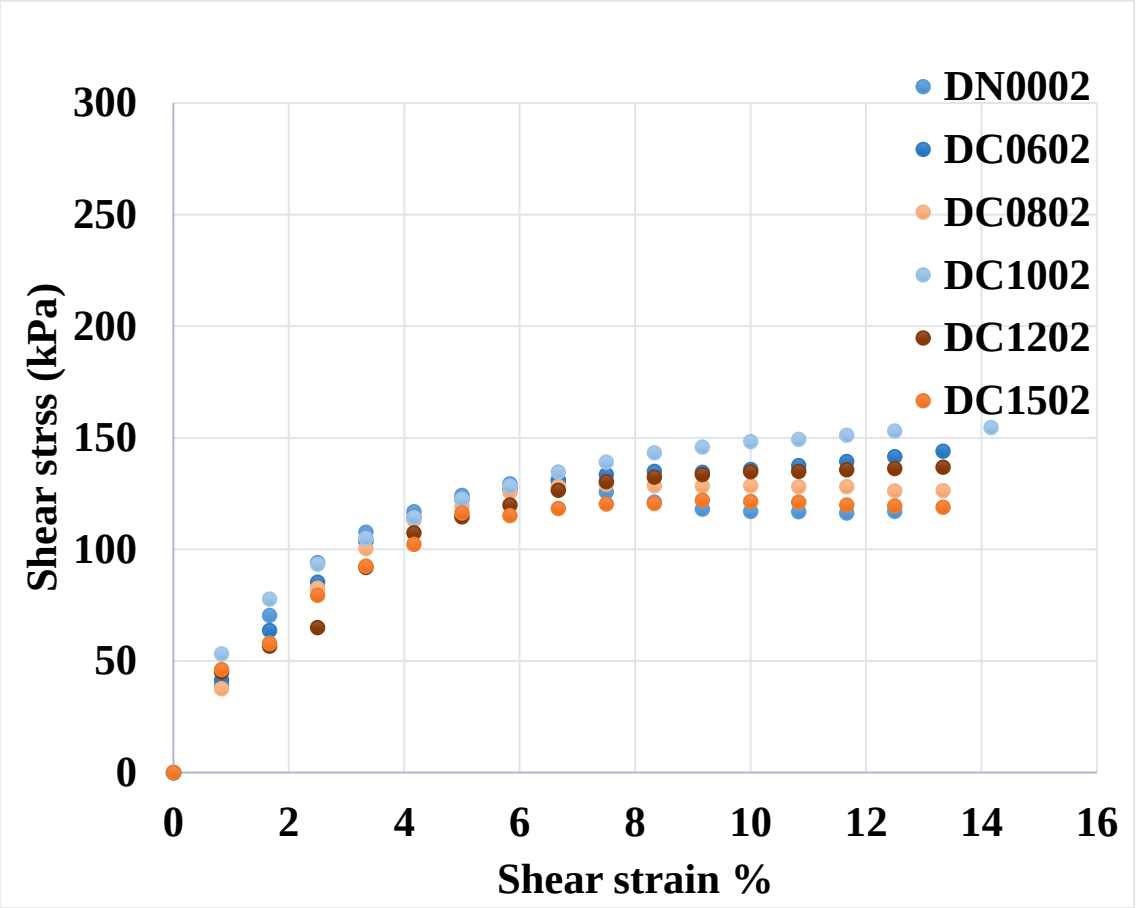

Figure 5.7. Cores granulated rubber-sand mix's direct shear test results with 50 kg normal force.

The samples behaved more consistently in the 100 kg normal force group, as shown in Figure 5.8.The clean sand sample (DN0003) was the strongest, with a clear peak of 261.22 kPa.8% GR mixture sample (DC0803) was the weakest, with a peak of 232.29 kPa.15% (DC1503),12% (DC1203), and 6% (DC0603) GR mixture samples showed the same behavior with a maximum shear stress of 236.43 kPa,242.06 kPa, and 242.92 kPa, respectively.10% GR mixture sample (DC1003) was the strongest with maximum shear stress 251.47 kPa among GR mixture samples and the closest to the clean sand sample.

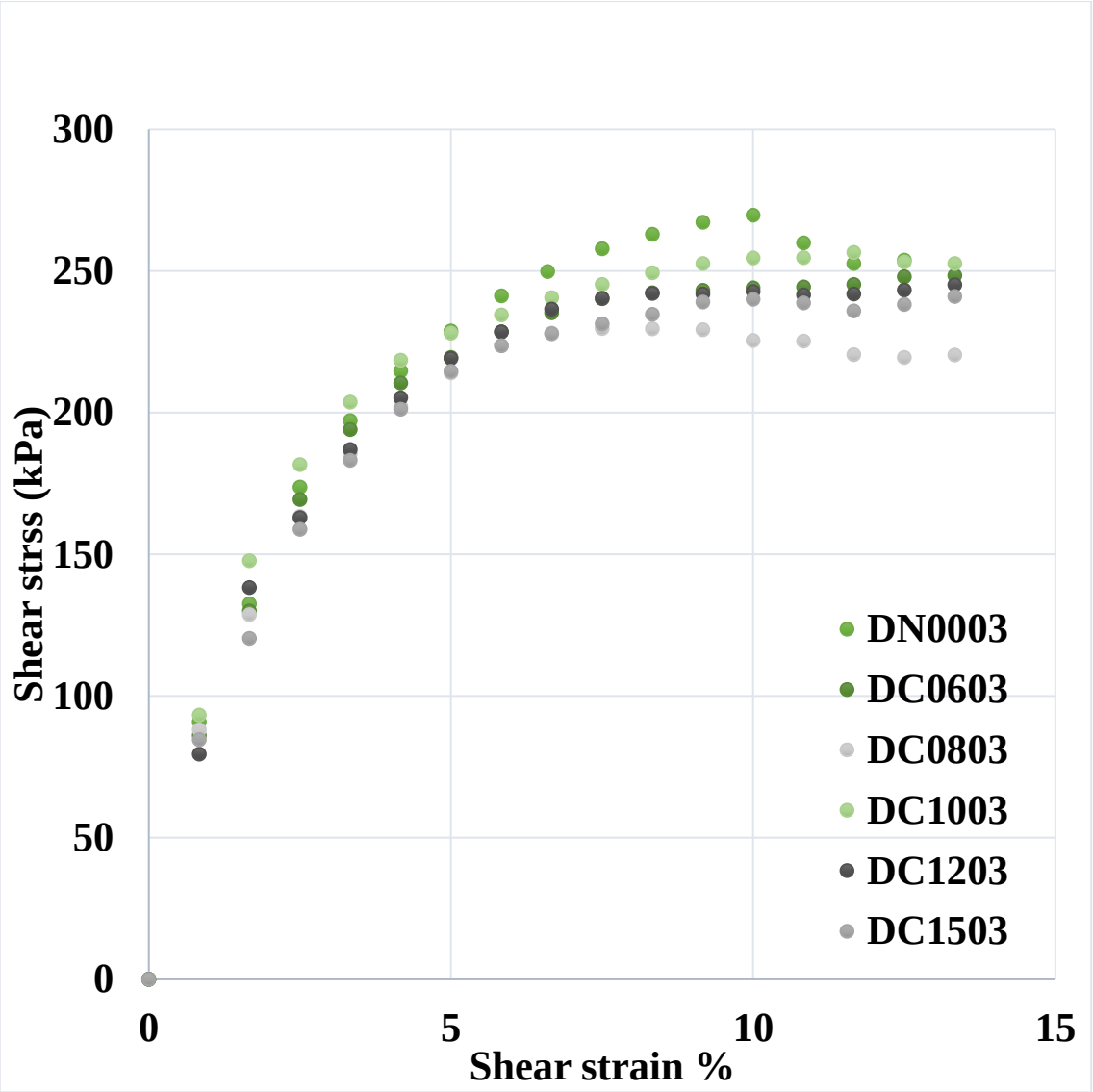

Figure 5.8. Cores granulated rubber-sand mix's direct shear test results with 100 kg normal force.

5.3. Compaction Test Results

Each modified Proctor test consisted of five molds and was conducted using a mechanical compacter and a type C mold; the results are shown in Figure 5.8. Only clean sand was tested at an optimal moisture content of 12.16 % and a maximum dry density of 17.22 kN/m^3, followed by a 10% coarse granulated rubber-mix test at an optimal moisture content of 12.13 % and a maximum dry density of 16.83 kN/m^3. On the other hand, when sand containing 10% fine granulated rubber was tested, the optimal water content was 12.2%, and the highest dry density was 16.77 kN/m^3. Finally, sand containing 8% coarse

granulated rubber didn't show a noticeable difference in the optimum water content, and maximum dry density was tested, as illustrated in Figure 5.8.

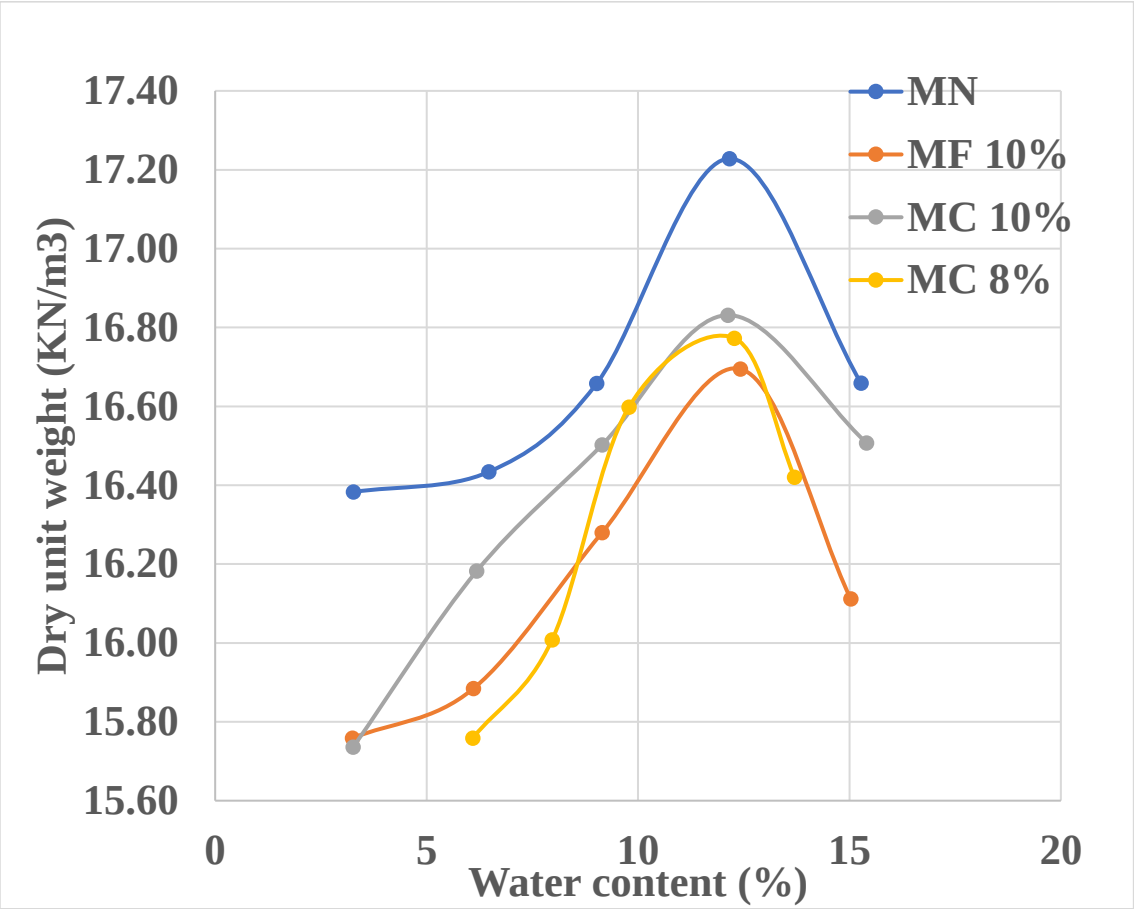

Figure 5.9. Compaction test results

5.4. Summary

Direct shear test results:

- Fine granulated rubber
    - For 20 kg, the 10% mixing ratio increased the shear strength by 3.6%, but 8% and 15% mixing percentages decreased the shear strength by 8.8% and 8.6%, while 12% and 6% mixing ratios showed a minor effect on the average the shear strength.
    - For 50 kg, all mixing ratios increased the shear strength,10%, and 15% mixing percentages increased the shear strength by 6.3% and 6.1%, while the others were less than 2.4%.

- For 100 kg, all mixing ratios decreased the shear strength. 10% mixing ratio was the minimum that decreased the shear strength with only 0.9% on the other hand 12% mixing ratio decreased the shear strength with 10.2% followed by 10% shear strength redaction with 6% mixing ratio and for 8% and 15 percent mixes the were nearly equal that they decreased the shear strength by 7.2% and 7%.

- Coarse granulated rubber
  - For 20 kg, the 12% mixing ratio showed the highest increase in shear strength by 17.5%, followed by a 10% mixing ratio that increased the shear strength by 2.2%, while 8% and 15% mixing ratios showed significant increases in shear strength by 1.14%and 1.3%. On the other hand, the 6% mixing ratio decreased the shear strength by 6.3%.
  - For 50 kg, 10 % mix showed the highest increase in shear strength by 13%, while 12%, 8%, and 6% mixing ratios increased the shear strength by 8.2%, 1.38 %, and 4.9 %, while 15 % mixed the shear strength decreased by 5.15 %.
  - For 100 kg, all the samples showed a decrease in the shear strength, and the weaker mix was an 8% mixing ratio that shear strength for it decreased by 11.1% while the minimum shear strength decrease is 3.7% for 10% mix.

Compaction test results:

For clean sand, the maximum dry density (MDD) was 17.23 $kN/m^{3,}$ and the optimum moisture continent (OMC)was 12.16%, for 10% fine granulated rubber-sand mix, the MDD decreased by 3.1%, and the OMC increased by 2.1% compared with10% coarse granulated rubber-sand mix the MDD decreased by 2.3% and the OMC increased by 0.2% on the other hand 8% coarse granulated rubber-sand mix was tested too the MDD decreased by 2.6%, and it did not show any change in the OMC.

CHAPTER 6

PHYSICAL MODEL TESTS RESULTS

6.1. Introduction

The previous chapter showed the improvement of the sand when it is mixed with granulated rubber. Based on the laboratory test results, 10% finely granulated rubber mixing percentage with sand was selected. This chapter presents the experimental model results in dry and saturated conditions with a 10% granulated rubber-sand mix backfill.

6.2. Dry Soil Models

This group contains four experimental models. The first one was only clean sand that worked as a control model test. The rest had triangle shape backfill areas with different angles that had the granulated rubber-sand mix. All of the models were prepared in the same way. The density was uniform along with the models, as shown in Table 4.1.

6.2.1. First Model – Clean Sand Backfill Model (Control Model):

The control model was performed by the clean sand, and the model setup is shown in Figure 6.1.

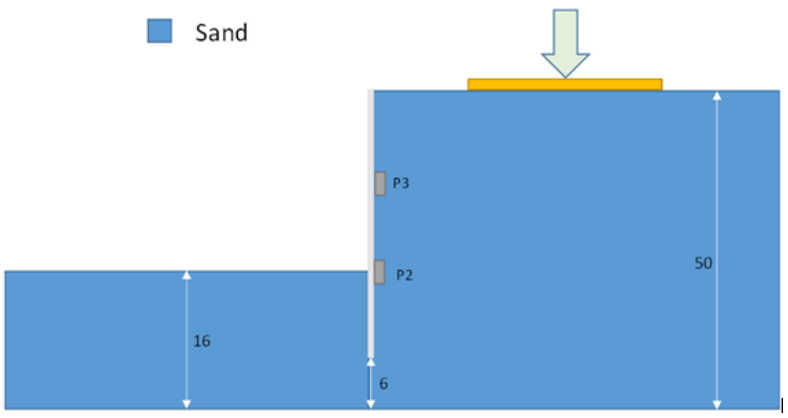

Figure 6.1. Clean sand backfill model (Control model).

Figure 6.2 presents the load cell data recorded during the test. The x-axis gives the data index, while the y-axis presents the applied load. As shown in the graph, there are three peak points that indicate a failure in the soil until reaching the maximum applied load of 133.66 kg.

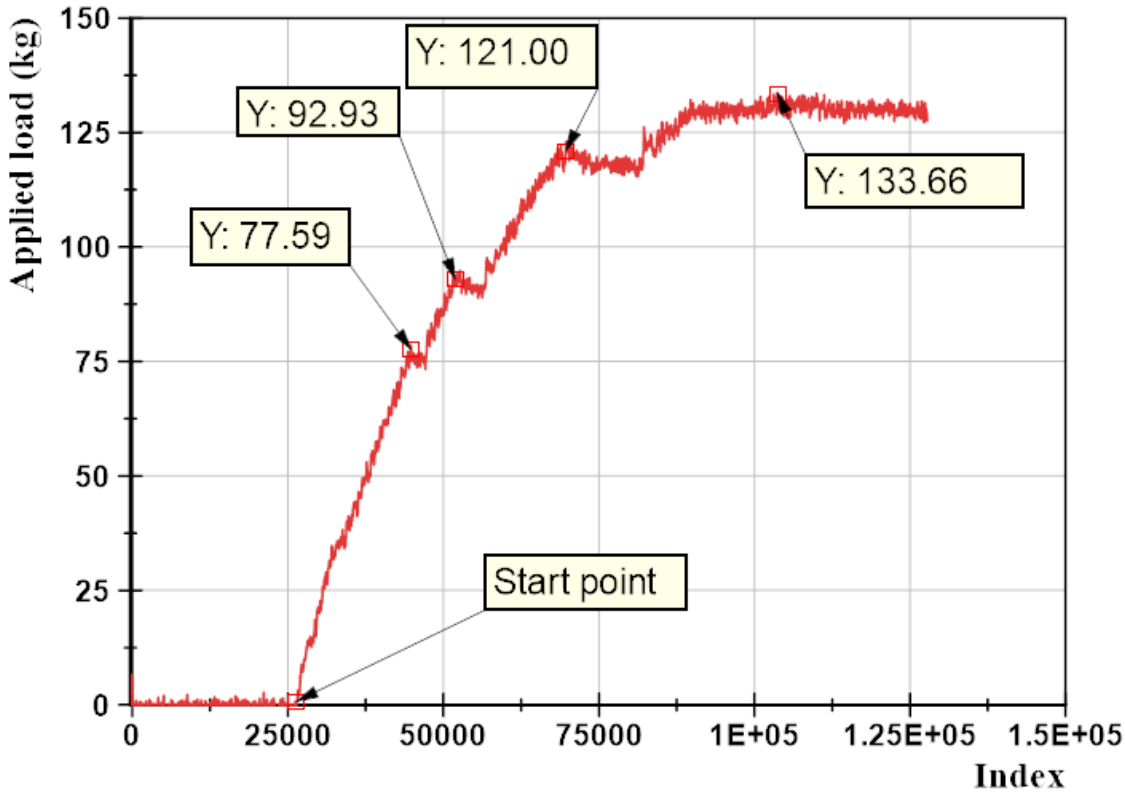

Figure 6.2. Load cell data recorded from the first dry model condition.

Figure 6.3 represents the lateral pressure recorded by the (P2) sensor at 340 mm depth. The initial lateral pressure was 0.3 kPa. The pressure increased with the applied load. The maximum pressure was 2.39 kPa, followed by a sudden decrease to 2.08 kPa, and stayed constant to the end of the test.

Figure 6.4 illustrates the lateral pressure acting on the sheet pile at a depth of 170 mm. This figure shows steep increases in pressure until reaching 2.24 kPa, which is the maximum pressure. There was two minor pressure relief before reaching the maximum point. After reaching the maximum point, the pressure decreased to 1.34 kPa and stayed constant to the end of the test.

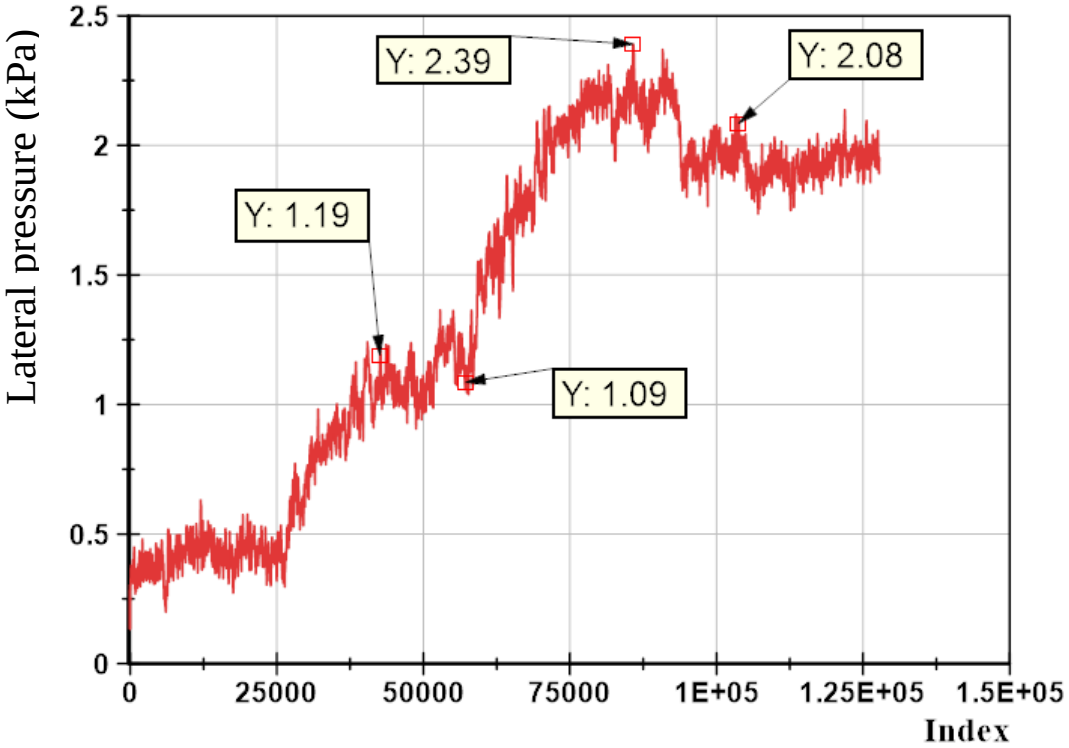

Figure 6.3. Lateral pressure data (P2) recorded from the first model dry condition.

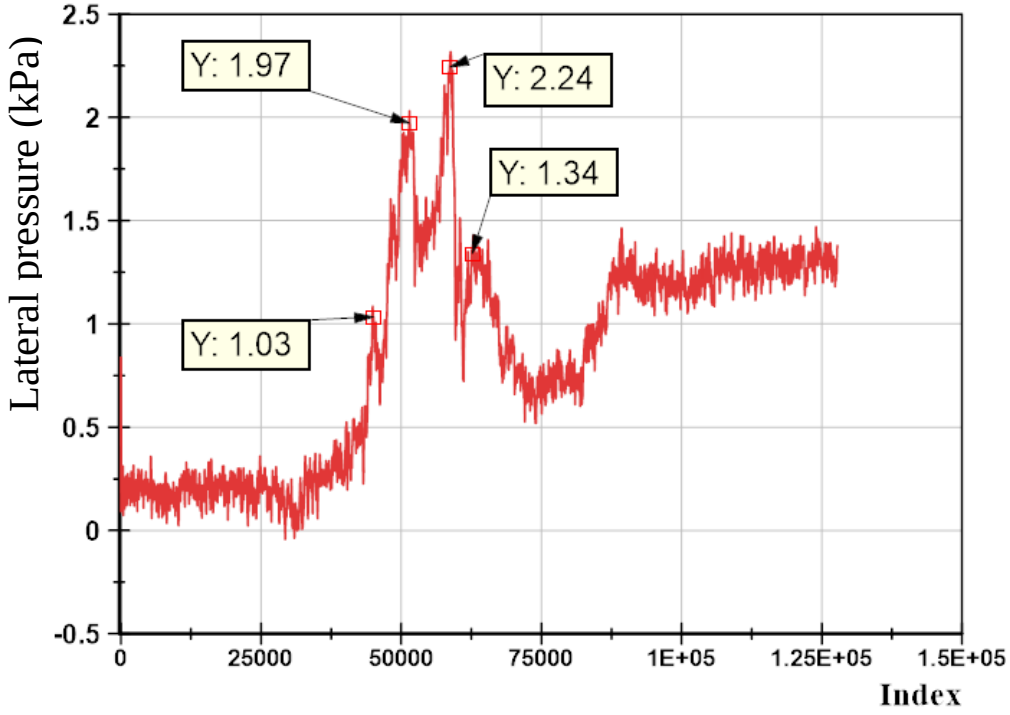

Figure 6.4. Lateral pressure data (P3) recorded from the first model dry condition.

By plotting the lateral pressure and applied load against the sheet pile lateral displacement, we can get a clear understanding of the model behavior.

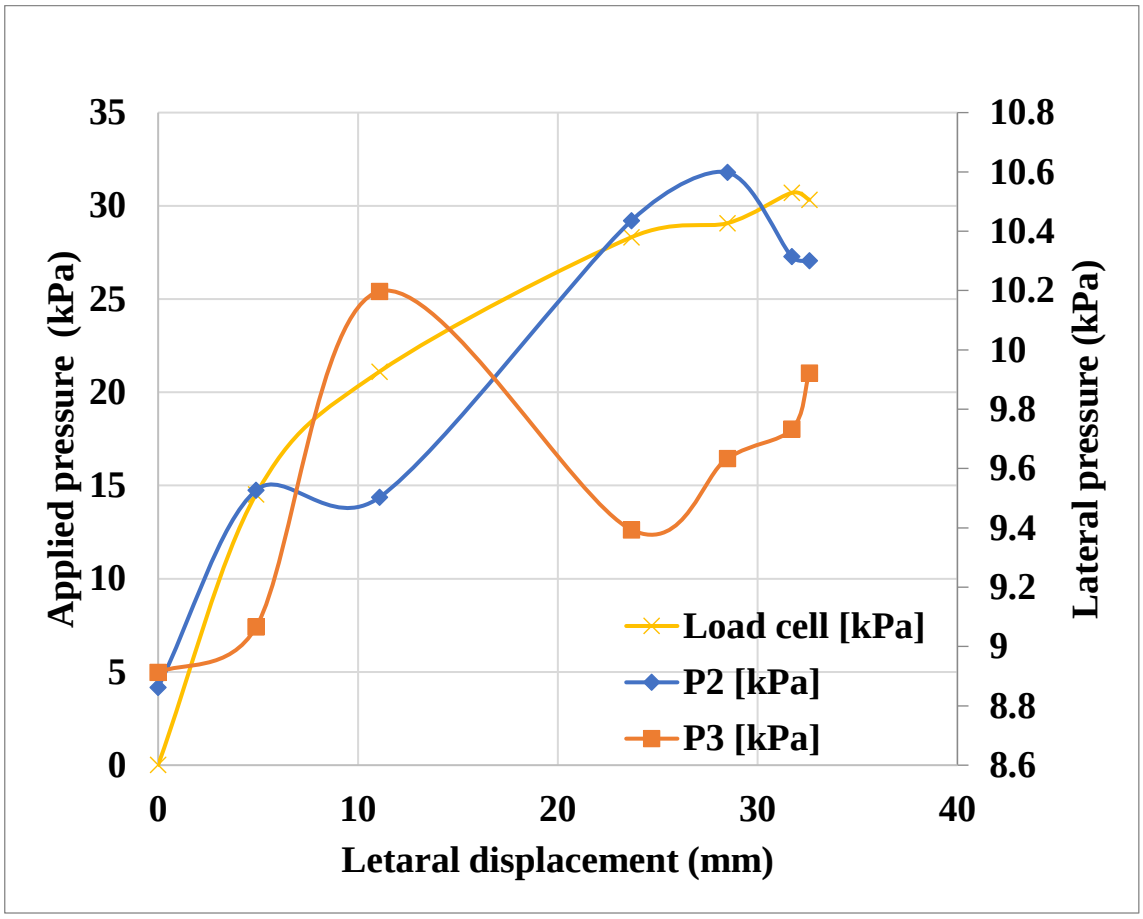

Figure 6.5. Applied load and pressure development with the lateral displacement first model dry condition.

According to Figure 6.5, the rate of displacement initially increased steeply for the first 5mm displacement, then decreased but remained constant throughout the test. At (P2) level, the lateral pressure increased more than the lateral pressure at (P3) level for the first 5mm lateral displacement. Then lateral pressure began to decrease at the same time that (P3) level began to increase. This indicates that the majority of the pressure causing the movement acted on (P2) level. This was caused due to the continued rearrangement of the soil mass during the test due to the small collapses.

6.2.2. Second model

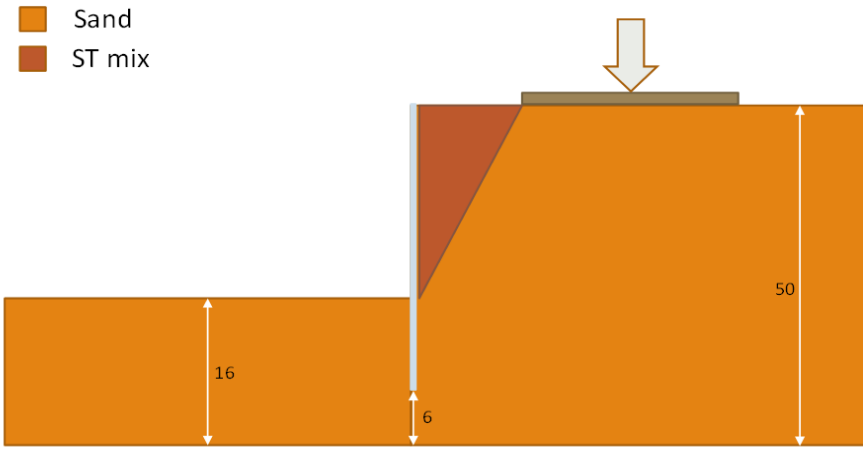

Figure 6.6. Second model dry condition.

After testing the clean sand model, the second model, which is the backfill reinforced with fine granulated rubber, is shown in Figure 6.6. The reinforced area mixture is represented by ST in the figure. The backfill had a triangle area with a 16 cm base and 34 cm height.

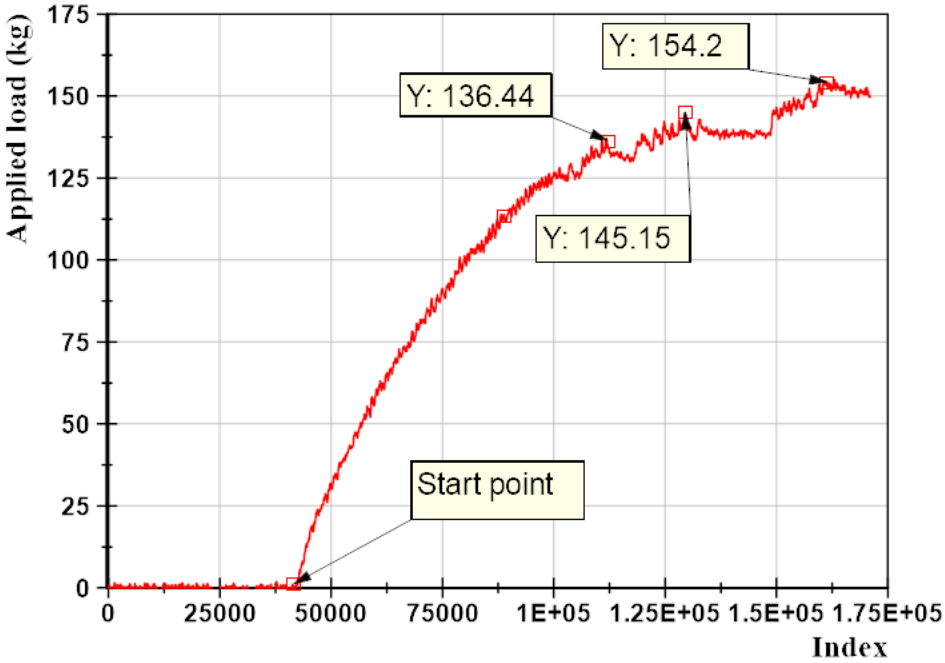

Figure 6.7. Load cell data recorded from the second dry model condition

Figure 6.7 shows the applied load history through the test with a maximum load of 154.2 kg. Before reaching the maximum loading level, three load reliefs at 125, 136.44, and 145.15 kg indicate the minor failure in the soil.

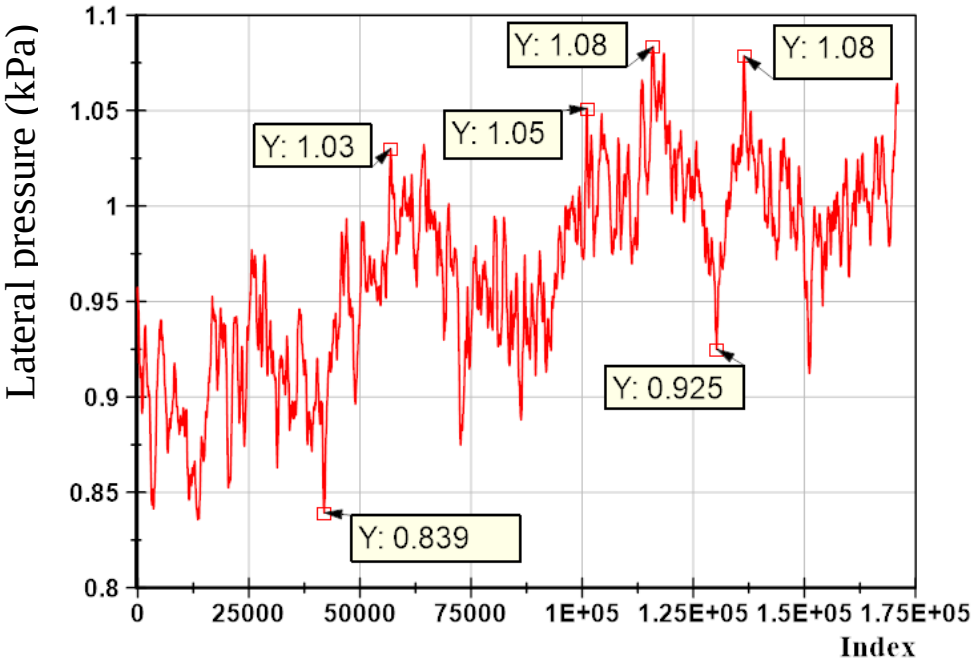

Figure 6.8. Lateral pressure data (P2) recorded from the second model dry condition.

Figure 6.8 illustrates the recorded data of the pressure transducer (P2). As shown in the figure, the pressure at the beginning of the test was 0.839 kPa. The maximum pressure was 1.08 kPa. The pressure faulted before reaching the maximum made two local peaks, as shown in the figure.

Figure 6.9 shows the recorded pressure transducer (P3) data. The maximum pressure is 0.6 kPa, and the minimum is 0.32 kPa. It shows that the pressure suddenly increased at the beginning of the test, then the pressure stays steady for a little time and starts dropping following a downtrend to the end of the test.

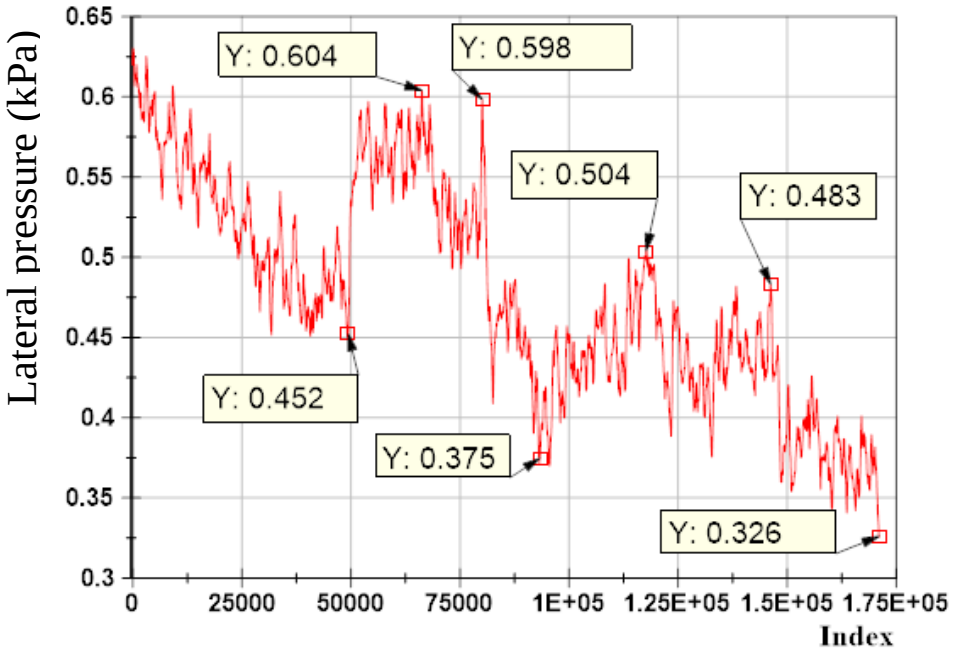

Figure 6.9. Lateral pressure data (P3) recorded from the second model dry condition.

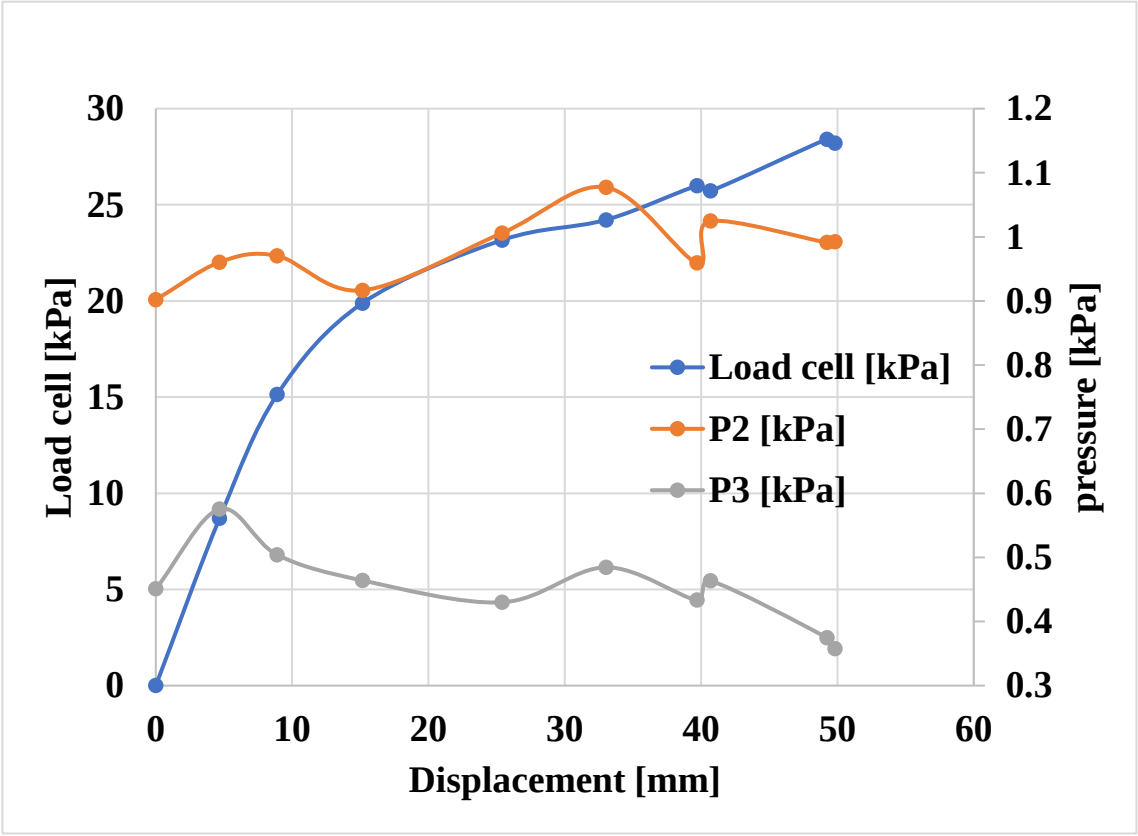

Figure 6.10. Applied load and pressure development with the lateral displacement second model dry condition.

Figure 6.10 illustrates the applied load and lateral pressure with lateral displacement. The pressure at (P3) level was the most affected by the load initially, then started a downtrend when the applied load reached 47 kg. On the other hand, the pressure at (P2) level shows a continuous uptrend after the applied load reached 107.6. The pressure spiked when the applied load reached 140 kg, representing the major failure.

6.2.3. Third Model

Figure 6.11 shows the granulated rubber-sand mix for this test. The mix had a triangle area with a 32 cm base and 30 cm height.

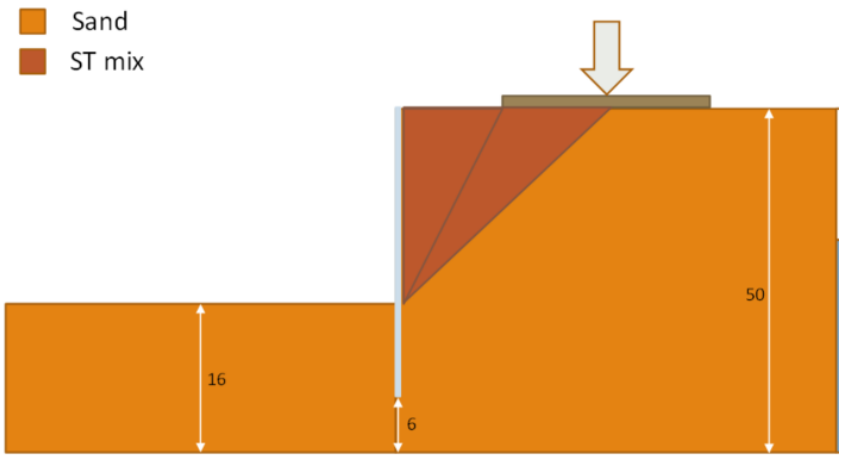

Figure 6.11. Third model setup dry condition.

The third model, which is the backfill reinforced with fine granulated rubber, is shown in Figure 6.11. The reinforced area mixture is represented by ST in the figure. The backfill had a triangle area with a 32 cm base and 34 cm height

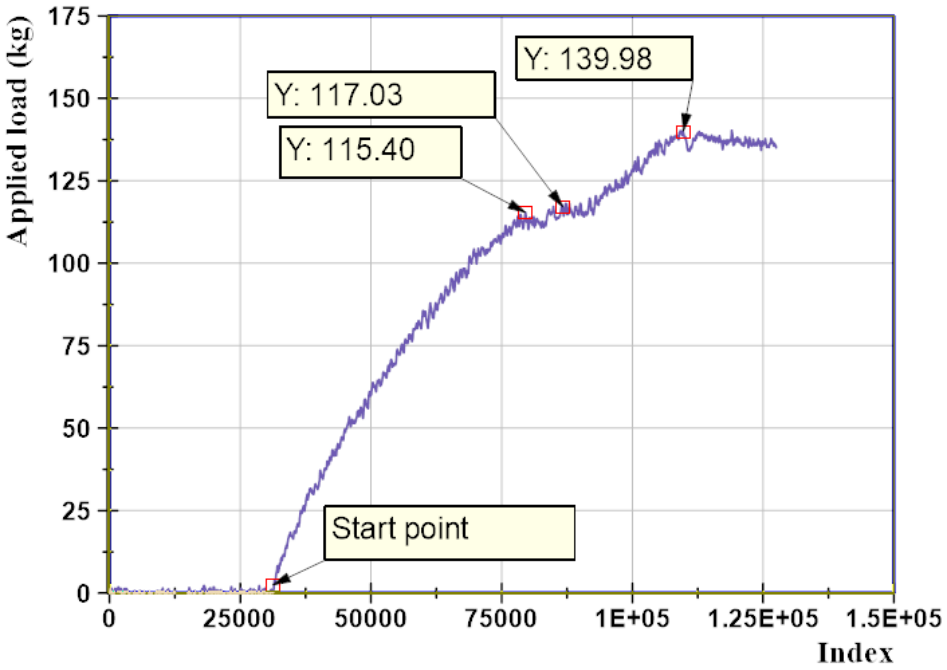

Figure 6.12. Load cell data recorded from the third dry model condition.

Figure 6.12 shows the applied load history. The test starting point is shown in the figure. The maximum applied load was 139.98 kg. The loading rate changed after reaching 115.4 kg due to minor failures in the soil.

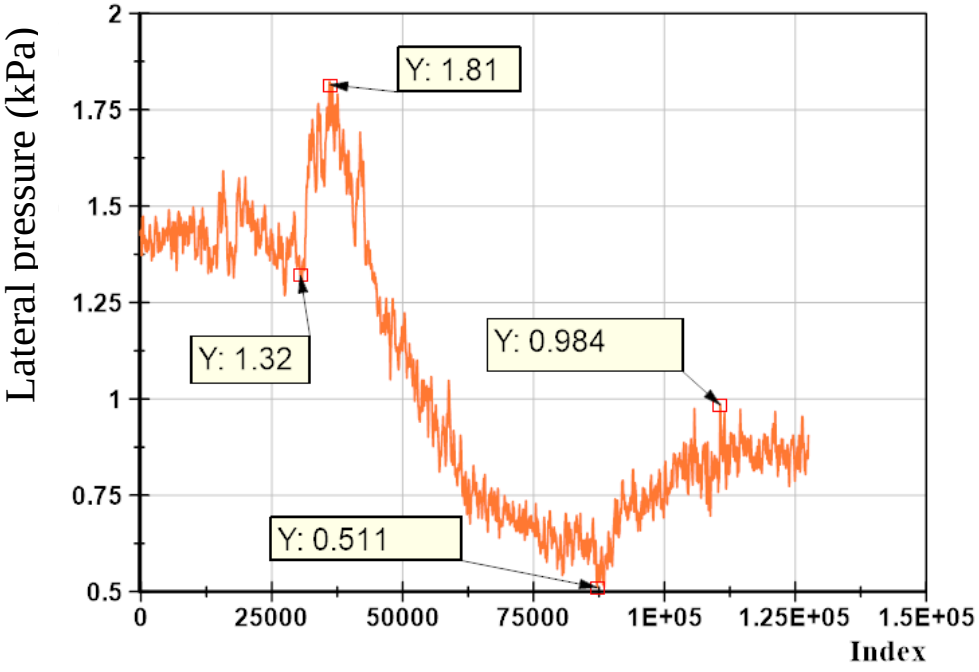

Figure 6.13. Lateral pressure data (P2) recorded from the third model dry condition.

Figure 6.13 shows the pressure-time history on the sheet pile at 340 mm depth from the surface. The lateral pressure shows an instant increase when starting loading, giving the highest pressure 1.81 kPa. After that forming a downtrend until it reaches the first failure shown in the load history. The soil reformed, causing the pressure to rise again until the second load relief happened, as shown in Figure 6.12. The behavior shows that the sheet pile moved, causing the pressure to fall in at the start. Then, the soil re-arraigned and conveyed the pressure to the P2 level when the first failure happened.

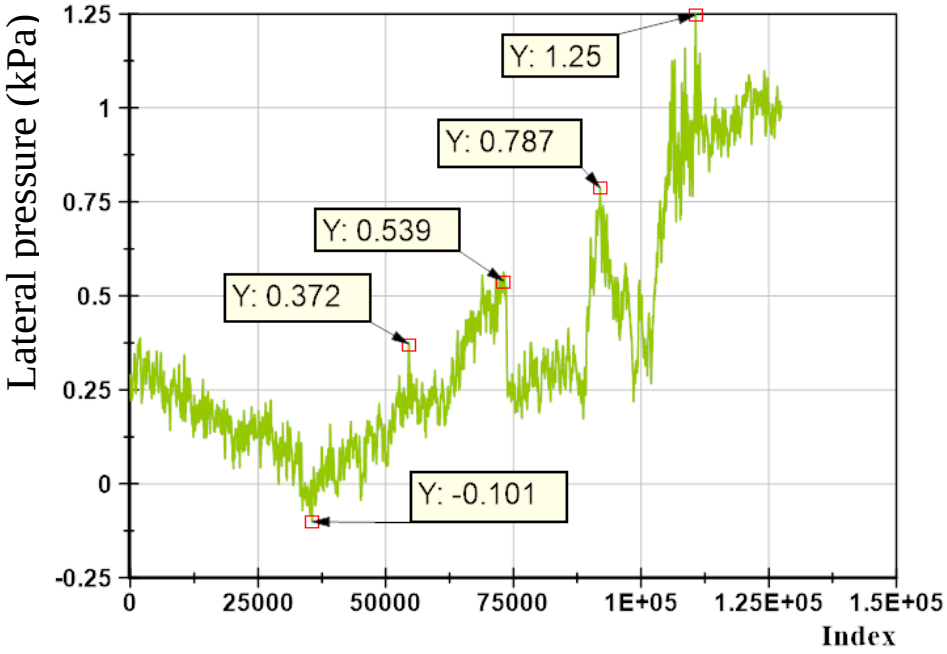

Figure 6.14. Lateral pressure data (P3) recorded from the third model dry condition.

Figure 6.14 shows the pressure history for the (P3) sensor mounted at 170mm depth from the surface. The start points were taken from the applied load history. The maximum pressure was 1.25 kPa. It shows an instant decrease in the pressure at the beginning of the test, reaching -0.101 kPa, followed by a pressure increase. Three pressure peaks that were noticed indicated the minor failure.

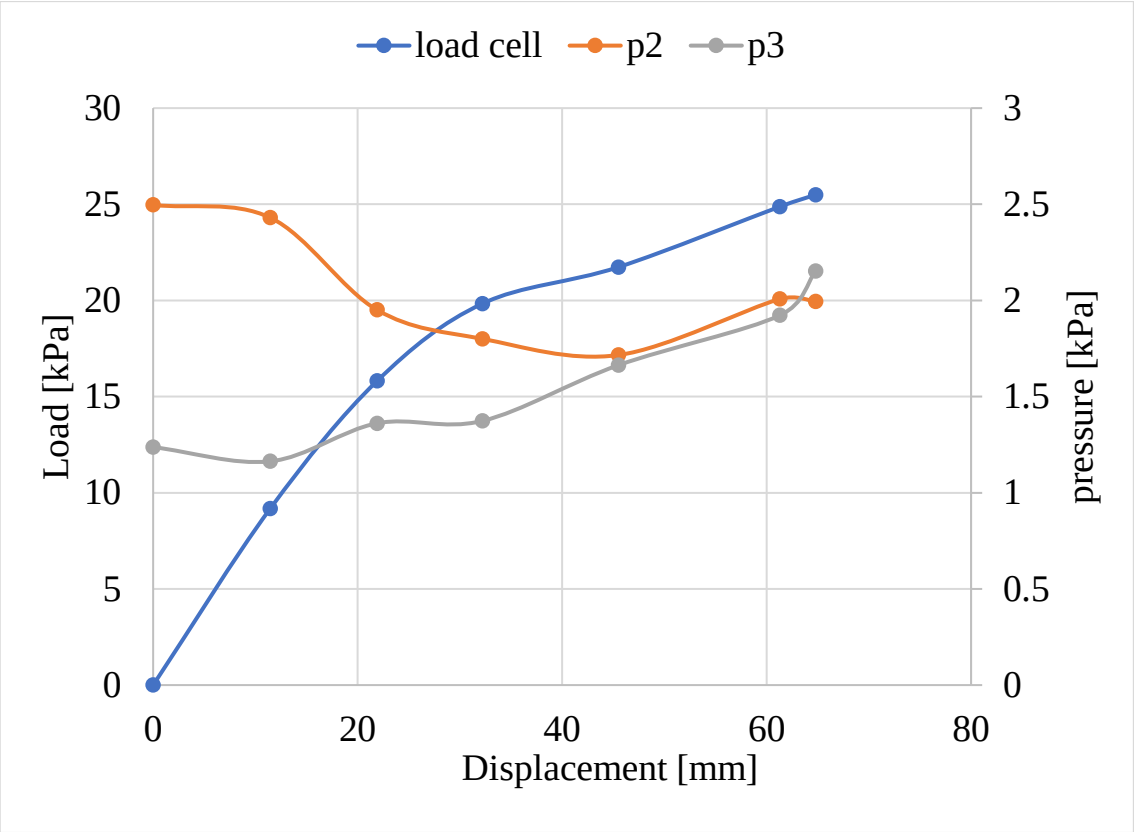

Figure 6.15. Applied load and pressure development with the lateral displacement third model dry condition.

Figure 6.15 shows the lateral displacement against the load and its pressure. At first, the pressure was increased in the (P3) sensor and decreased in (P2) they acted against each other until the applied load reached 119 kg. Later, they showed the same behavior. It shows that the first 45mm, the pressure in (P3) was rising at the same time the pressure in (P2) was falling.

6.2.4. The Fourth Model

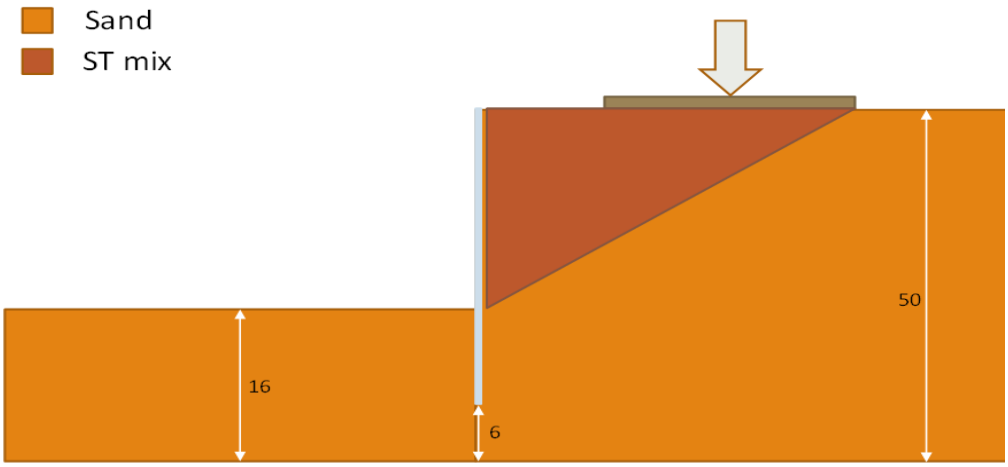

Figure 6.16. Fourth model setup dry condition.

The fourth model, which is the backfill reinforced with fine granulated rubber, is shown in Figure 6.11. The reinforced area mixture is represented by ST in the figure. The backfill had a triangle area with a 48 cm base and 34 cm height. The time history for the load cell and the pressure cell is shown below.

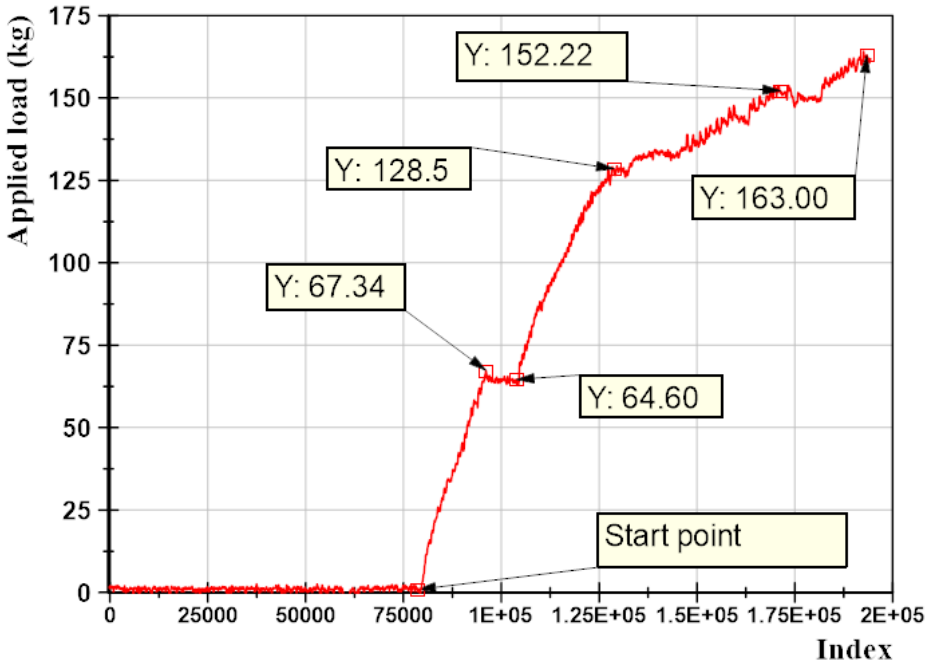

Figure 6.17. Load cell data recorded from the fourth dry model condition

As shown in Figure 6.17, the maximum applied load was 163 kg. The first minor failure happened when the applied load reached 67.34 kg. At 128.5 kg applied to load, the rate of the load changed.

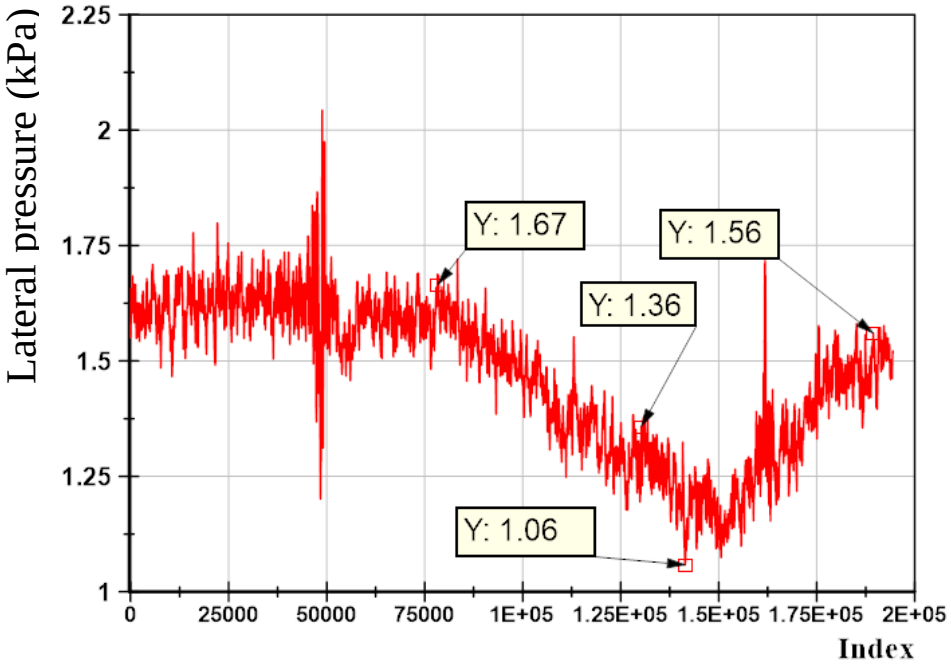

Figure 6.18. Lateral pressure data (P2) recorded from the fourth model dry condition.

Figure 6.18 shows the pressure at the beginning of the test was 1.67 kPa, the decreased to reach 1.06 kPa. The pressure at the end of the test was 1.56 kPa

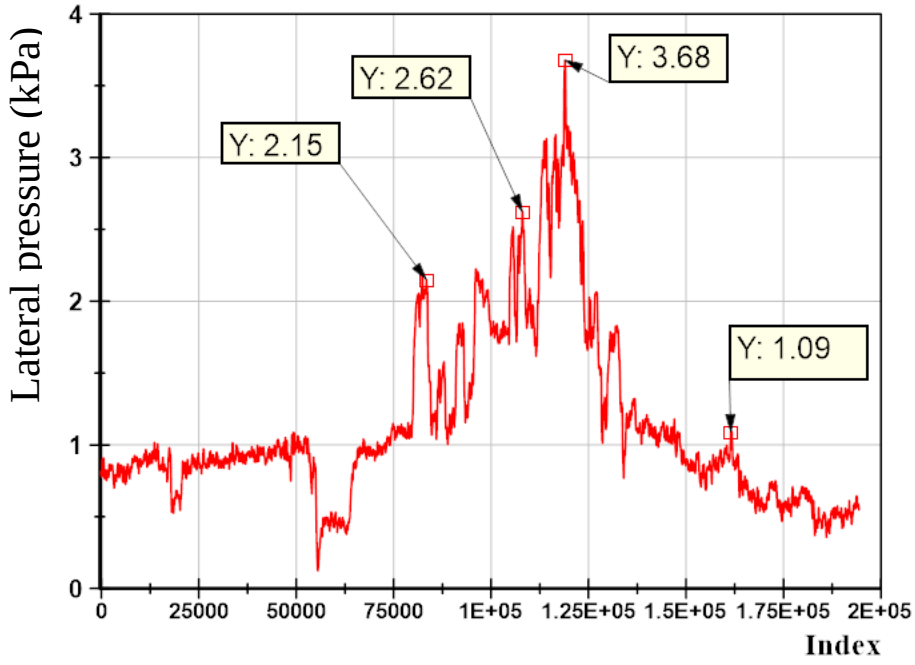

Figure 6.19. Lateral pressure data (P3) recorded from the fourth model dry condition.

Figure 6.19 shows the lateral pressure on the sheet pile at 170 mm depth. A sudden drop, then the pressure build was observed by passing through minor failures until the applied load reached 68 kg. The maximum pressure was 3.52 kPa when the applied load reached 119 kg. After that, the pressure started to decrease until it reached 0.5 kPa at the end of the test.

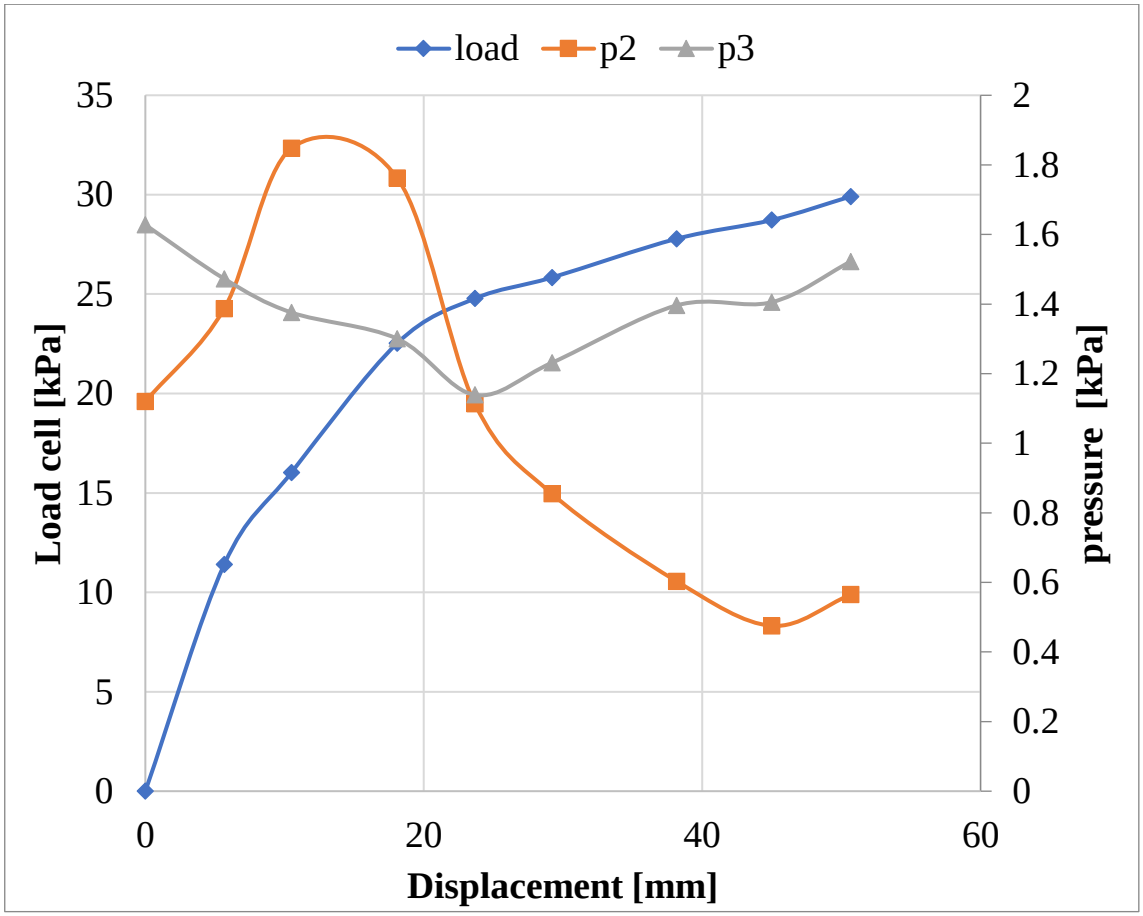

Figure 6.20. Applied load and pressure development with the lateral displacement fourth model dry condition.

Figure 6.20 shows the lateral displacement against the load and the pressure. It shows that at first, the pressure was increased in the (P2) and reduced in (P3). (P2) and (P3) acted against each other until the load reached 117 kg. Then, (P2) started to decrease when the applied load reached 135 kg, and the pressure in (P3) started to increase.

6.3. Saturated Models

This section presents the results of the pressure on the sheet pile, pore water pressure, and the applied load on the saturated models.

6.3.1. First Model - Clean Sand Backfill (Control Model):

Clean sand model in the saturated condition the model setup shows in Figure 6.21.

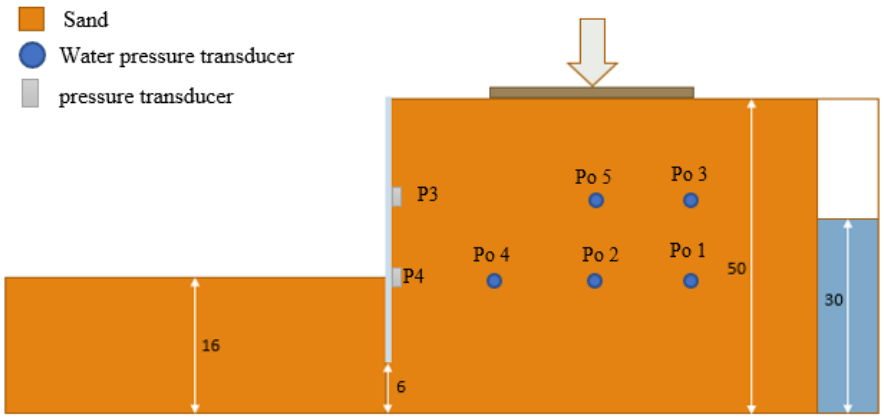

Figure 6.21 First model setup with clean sand backfill saturated condition (control model).

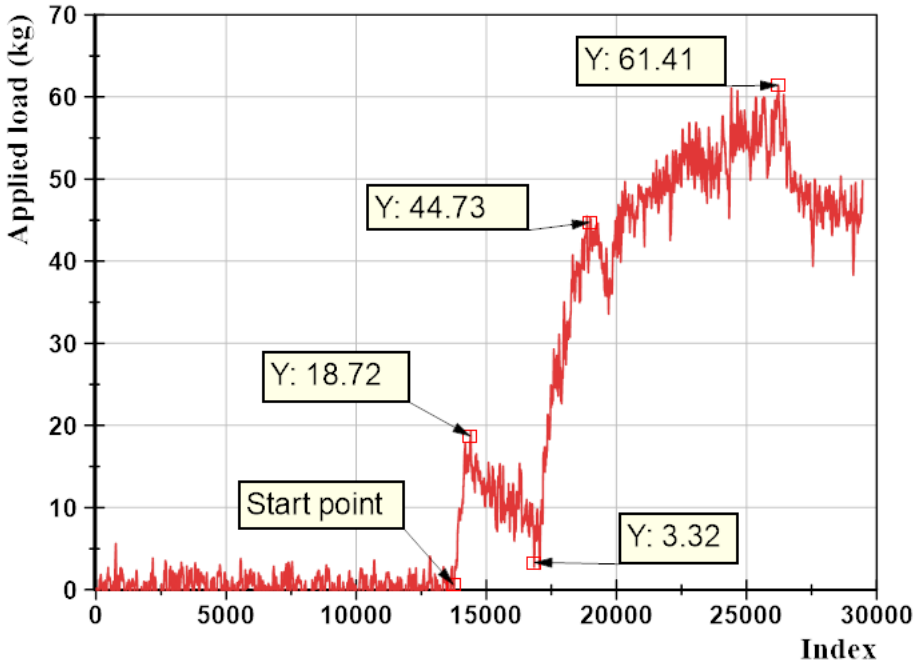

Figure 6.22. Load cell data recorded from the first saturated model condition

The applied load history shown in Figure 6.22 indicates that two pressure reliefs developed at 18.72 kg and 44.73 kg loads, respectively, before reaching the maximum load of 61.41 kg.

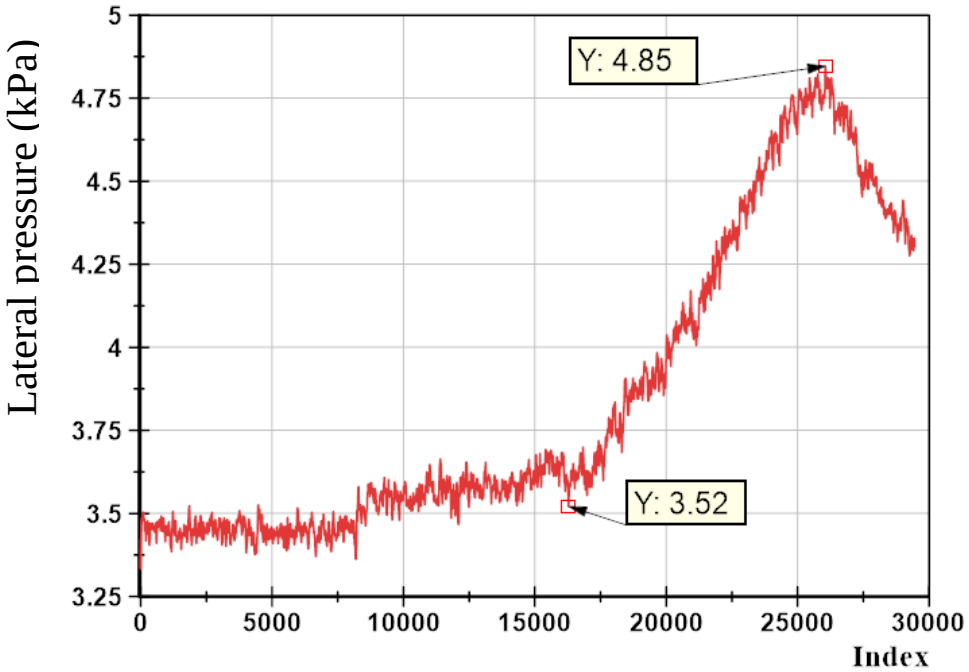

Figure 6.23. Lateral pressure data (P2) recorded from the first model saturated condition.

Figure 6.23 illustrates the lateral pressure acting on the sheet pile at a depth of 340 mm. The pressure increased steadily until it reached a peak of 4.85 kPa, and then decreased to 4.32 kPa at the end of the test.

The pressure-time history on the sheet pile at a depth of 170 mm from the surface depicted in Figure 6.24 indicated an early increase to reach the maximum pressure of 2.43 kPa, followed by a period of steady pressure then sudden multidrop in pressure.

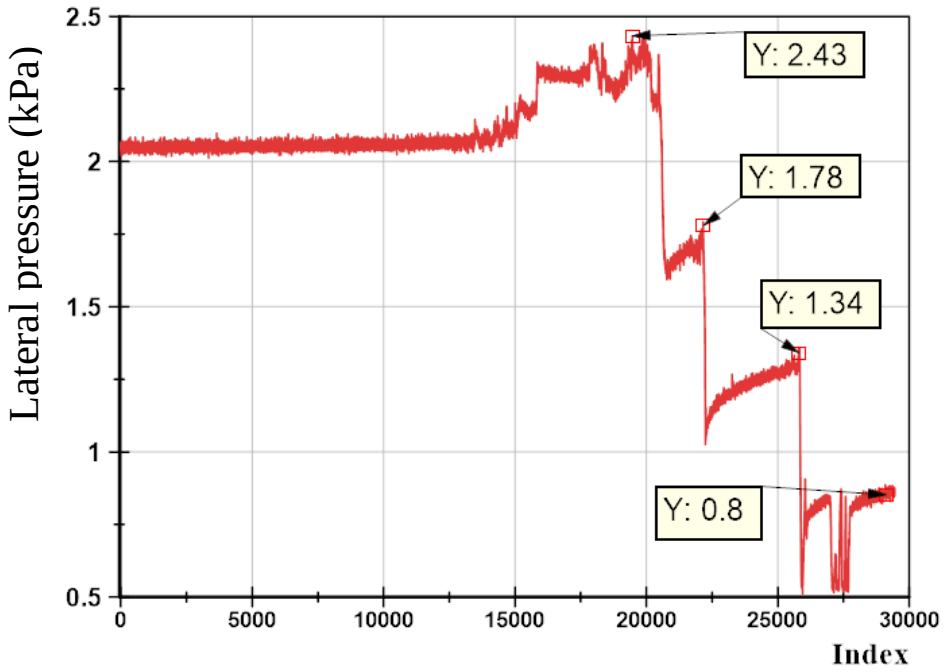

Figure 6.24. Lateral pressure data (P3) recorded from the first model saturated condition.

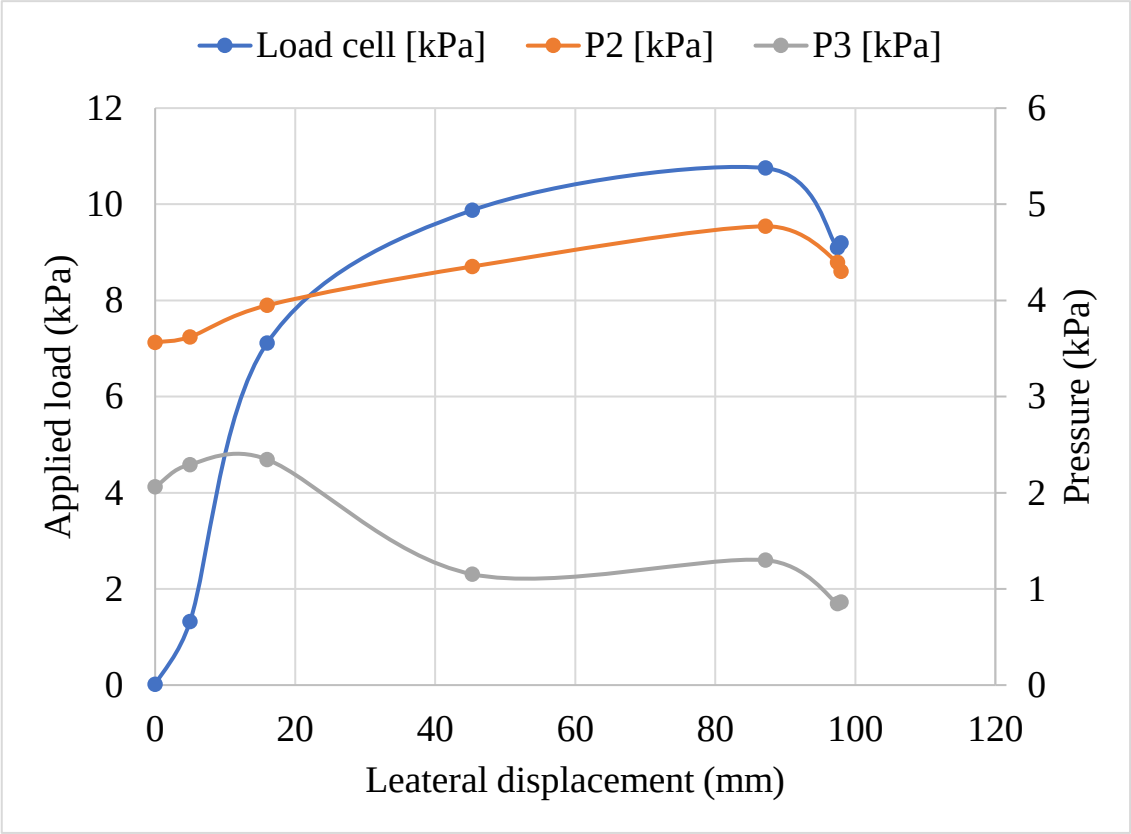

Figure 6.25. Applied load and pressure development with the lateral for first test saturated condition.

As illustrated in Figure 6.25, the pressure on the sheet pile grew throughout the test at 340 mm depth. At the same time, the pressure began to decrease at 170 mm depth when the applied weight reached 5 kPa.

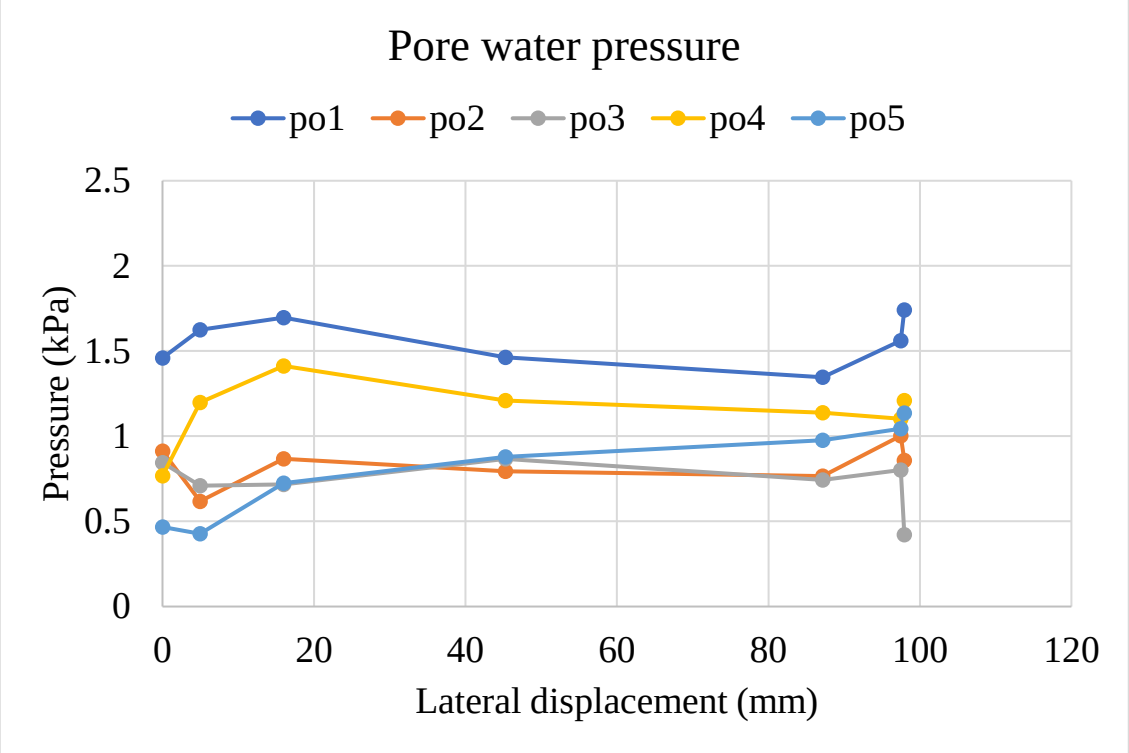

Figure 6.26. pore water pressure changes with lateral displacement for the first model.

Figure 6.26 shows the pore water pressure (PWP) in five points during the test. In the beginning of the test, the pressure increased after the displacement exceeded 17 mm the pressure started to decrease in all points from the beginning to the end of the test except the pressure in PO5 point was increasing,

6.3.2. Second Model

The model setup shows in Figure 6.27 shows the model setup. The reinforced area mixture is represented by ST in the figure. The backfill had a triangle area with a 16 cm base and 34 cm height.

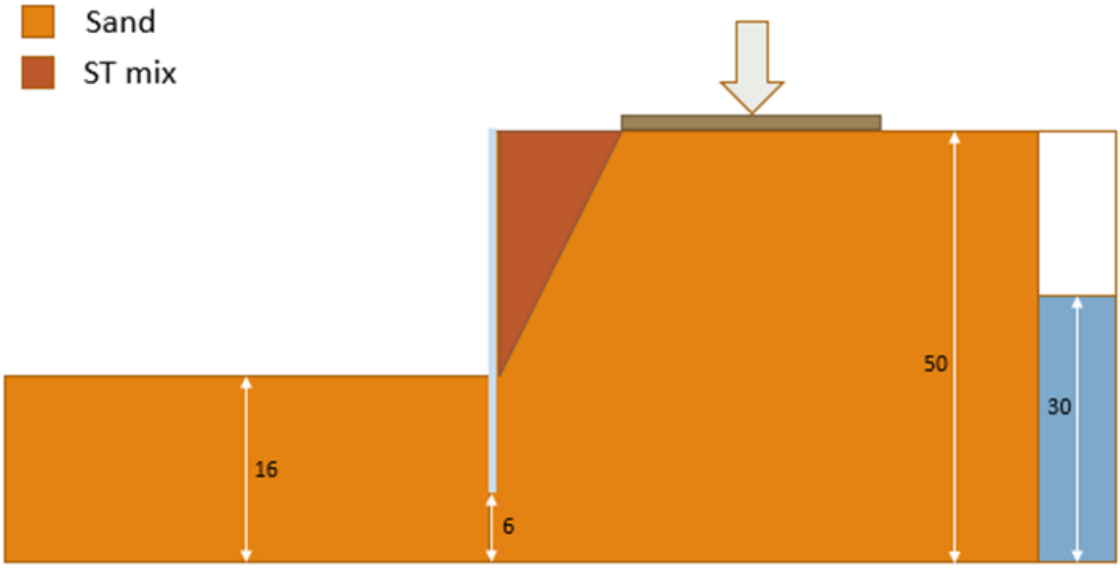

Figure 6.27. second model setup saturated condition.

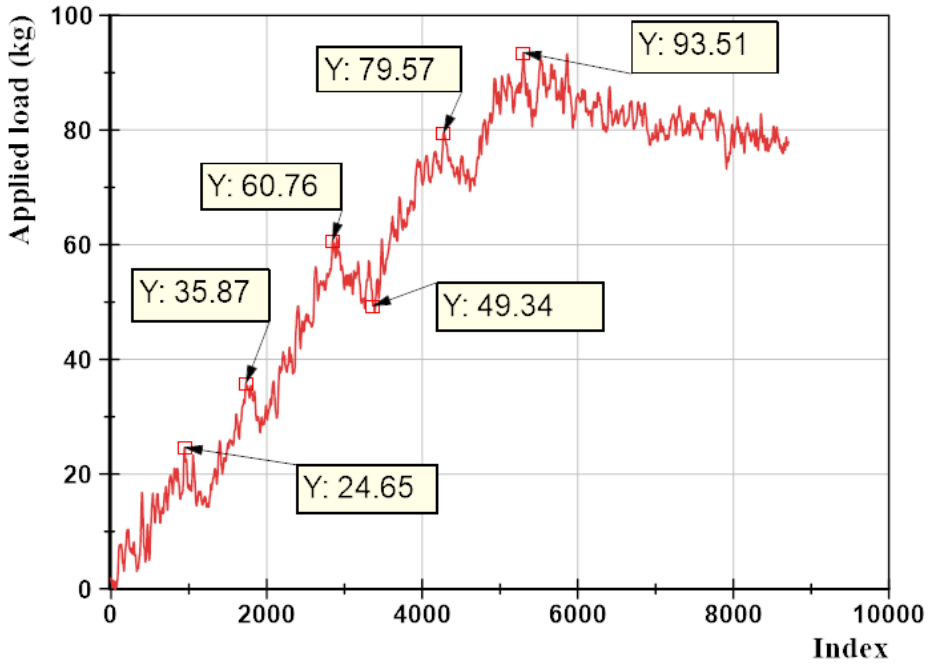

Figure 6.28. Load cell data recorded from the second saturated model condition.

According to Figure 6.28, the highest applied load was 93.51 kg, with multiple load relief points visible prior to reaching the maximum point. At the end of the test, the applied load was 77.5 kg.

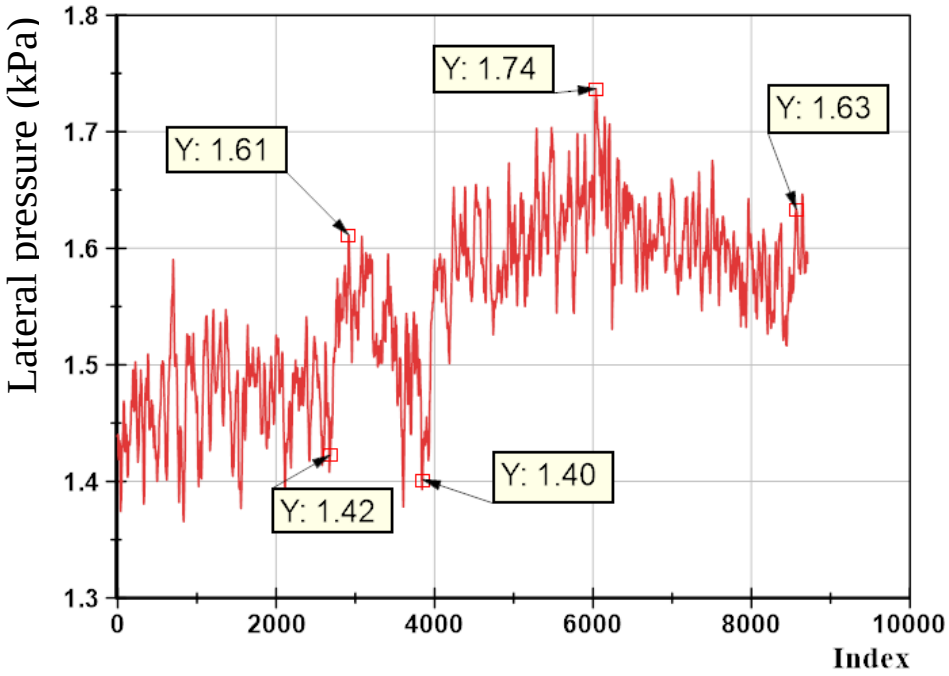

Figure 6.29. Lateral pressure data (P2) recorded from the second model saturated condition.

According to Figure 6.29, the maximum lateral pressure measured was 1.74 kPa. Pressure drops before reaching the maximum pressure, as shown in the figure. At the end of the test, the pressure was 1.58 kPa.

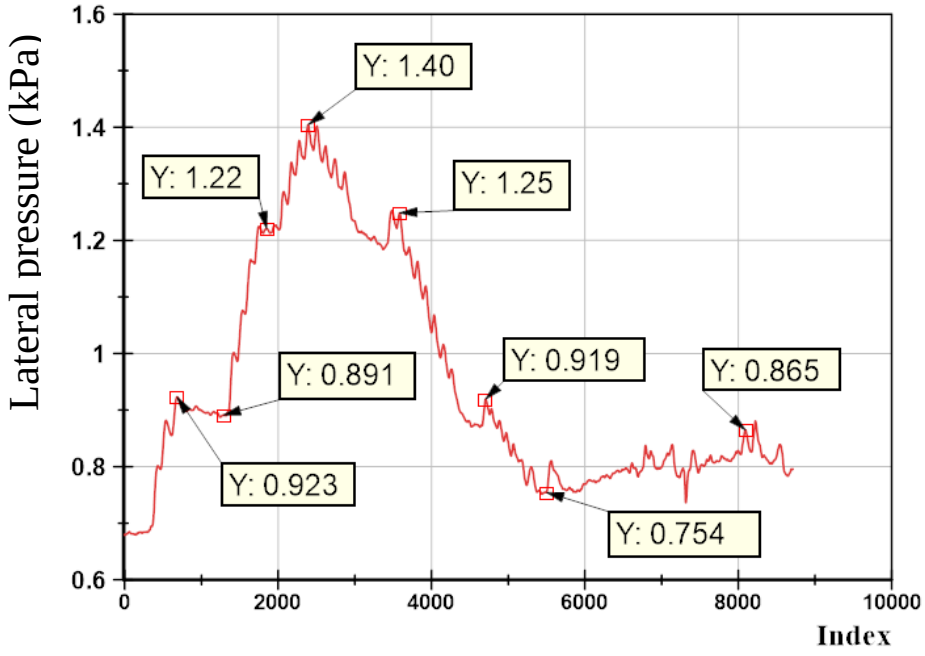

Figure 6.30. Lateral pressure data (P3) recorded from the second model saturated condition.

As shown in Figure 6.30., the highest measured pressure was 1.4 kPa, and the applied load was 48.7 kg. Two pressure decreases are observed before reaching the maximum pressure point, the first at 0.923 kPa and the second at 1.22 kPa. After reaching its maximum, the pressure begins a downward trend. It does, however, increase when the applied load reaches its maximum value.

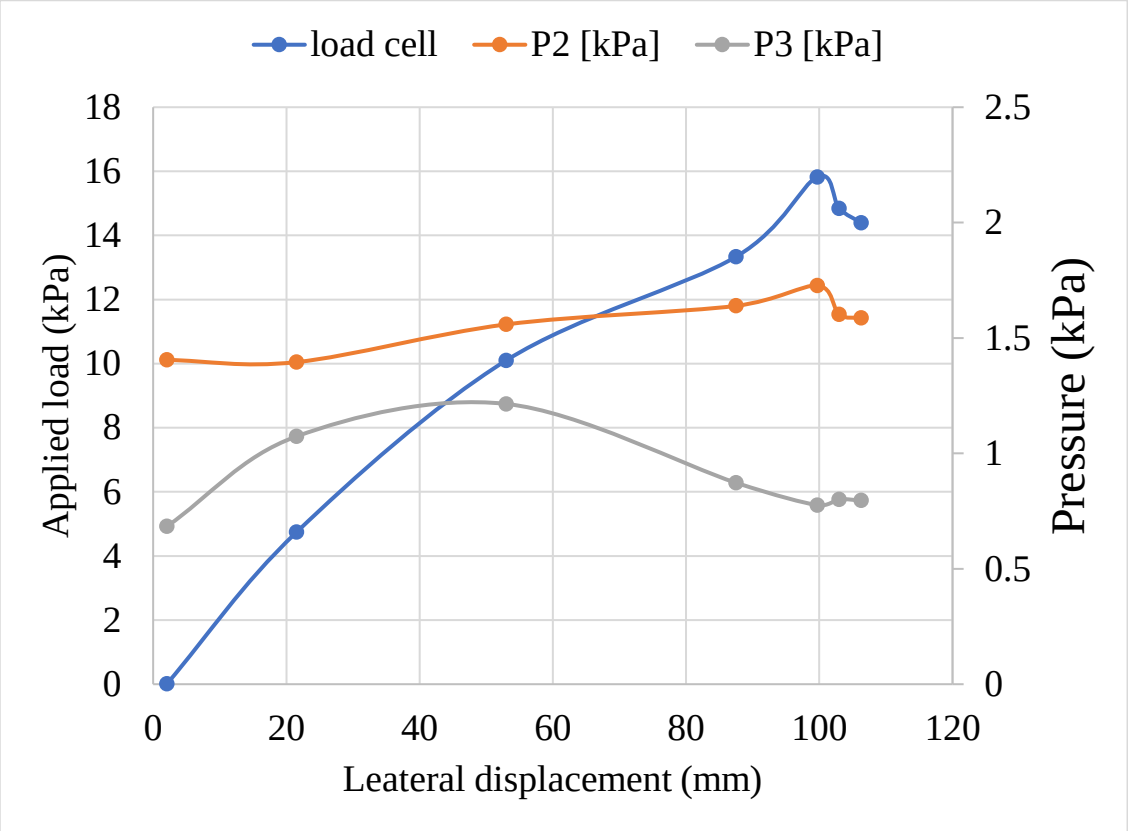

Figure 6.31. Applied load and pressure development with the lateral for second test saturated condition.

As illustrated in Figure 6.31, the maximum displacement is 100mm. The majority of displacement occurred prior to the applied load achieving its maximum value. The lateral pressure was increasing at (P3) level at the same time decreasing at (P2) level until the lateral displacement reached 20mm. After the lateral displacement reaches 40mm, the pressure starts dropping at (P3) level while the pressure in (P2) was started increasing before that. The maximum applied pressure was 15.8 kPa.

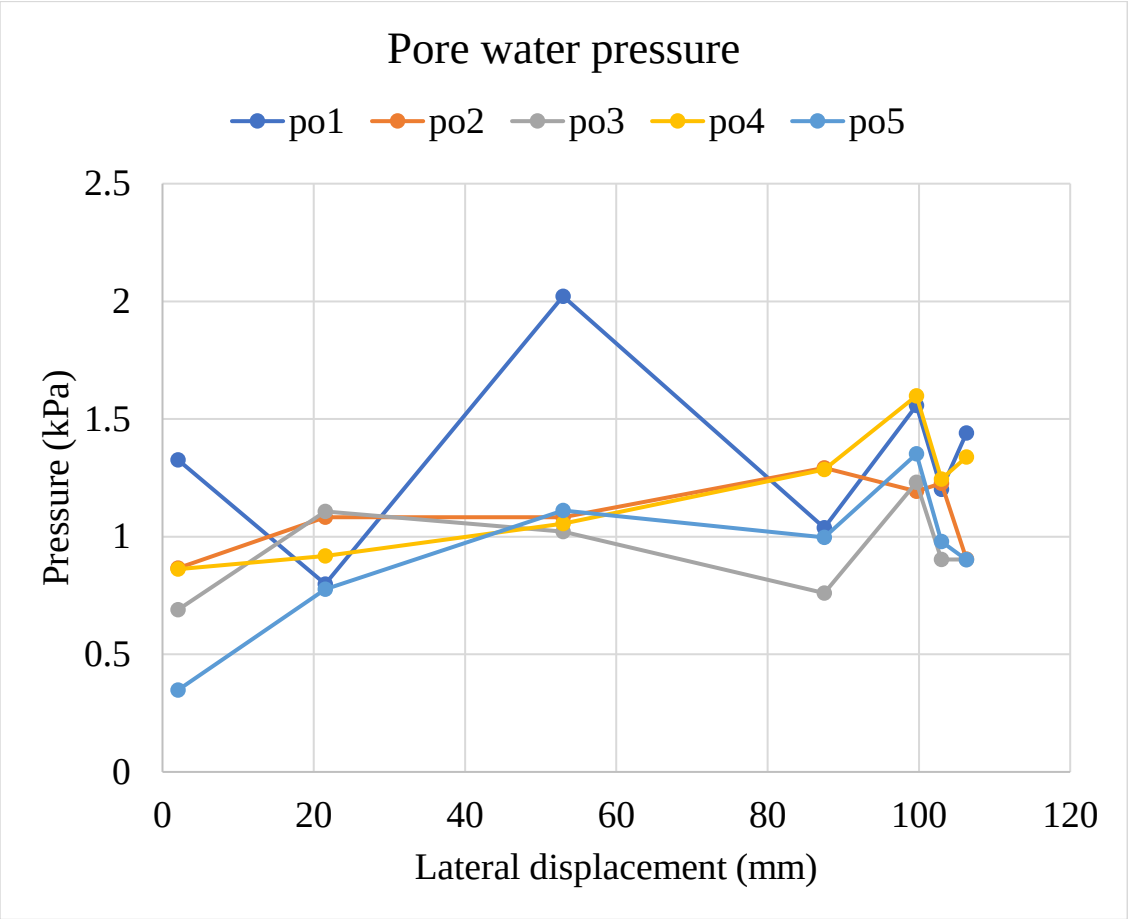

Figure 6.32. pore water pressure changes with lateral displacement for the second model.

Figure 6.32 shows the pore water pressure (PWP) in five points during the test. The pressure increases in all points from the beginning until the lateral displacement reaches 55 mm, where the pressure readings were very close to each other, ranging between 1 kPa and 1.2 kPa. The PWP at PO5, PO3, and PO1 start to decrease after that.

6.3.3. Third Model

The model setup shows in Figure 6.33 shows the model setup. The reinforced area mixture is represented by ST in the figure. The backfill had a triangle area with a 32 cm base and 34 cm height.

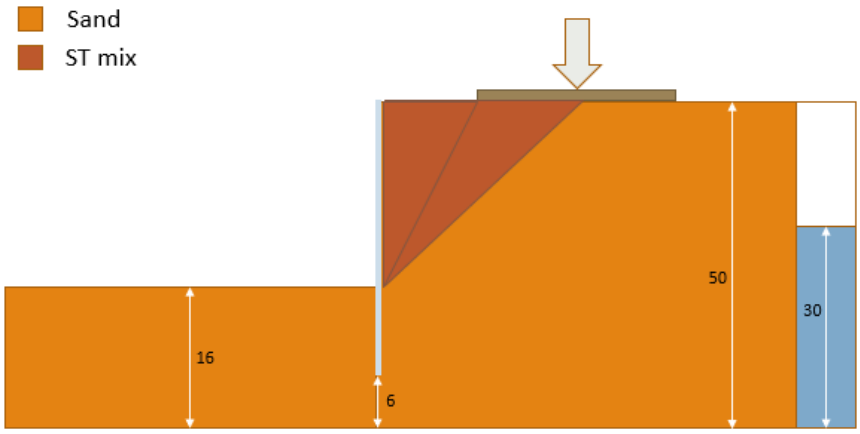

Figure 6.33. Third model setup saturated condition

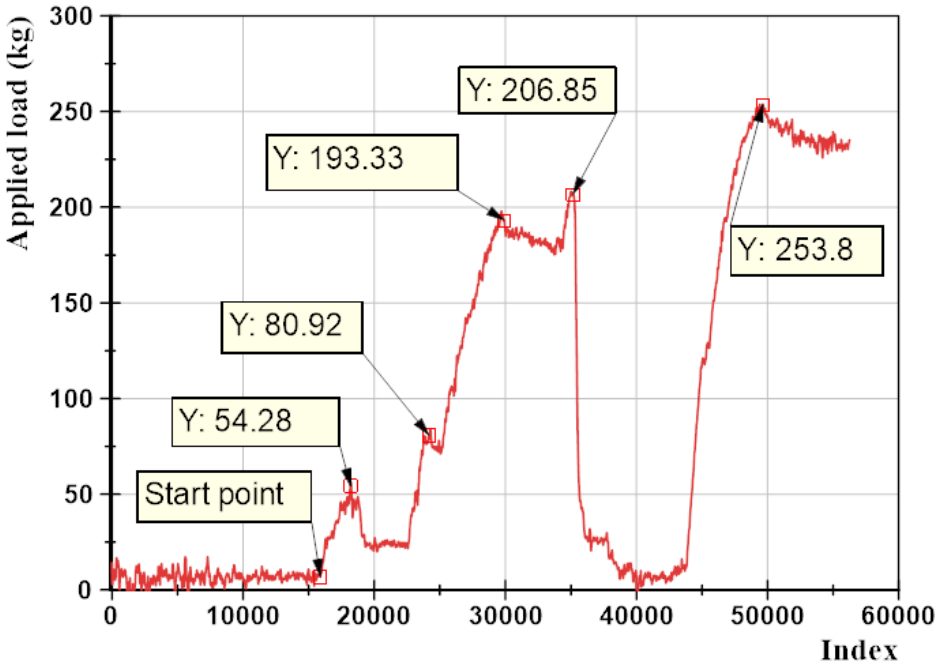

Figure 6.34. Load cell data recorded from the third saturated model condition.

According to Figure 6.34, the highest applied load was 253.8 kg. Before that, a significant load relief occurred when the applied load exceeded 206.84 kg. There was also some load relief at 54.28 kg. The biggest load drop was at 206.85 kg, which indicates the major failure.

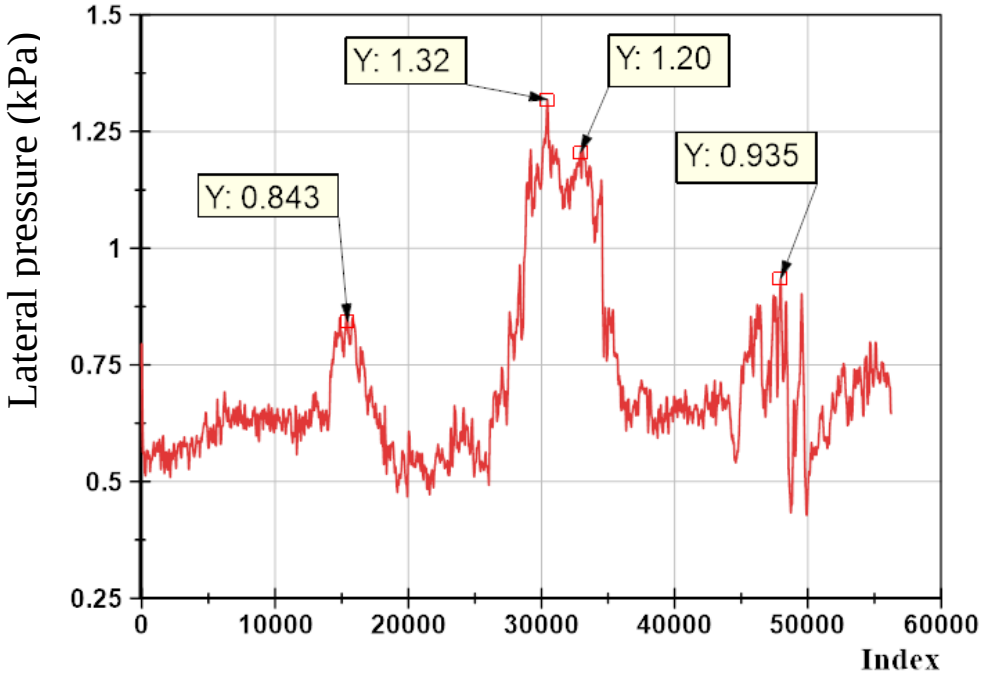

Figure 6.35. Lateral pressure data (P2) recorded from the third model saturated condition.

From Figure 6.35, the maximum pressure was 1.32 kPa. There was one local peak point before reaching the maximum pressure, as shown in the figure.

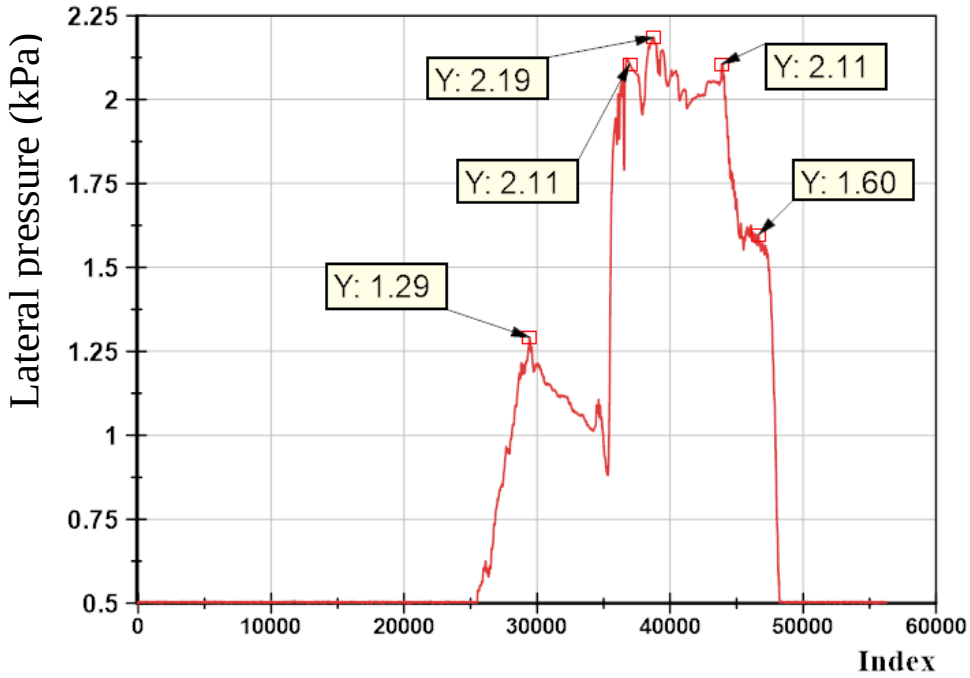

Figure 6.36. Lateral pressure data (P3) recorded from the third model saturated condition.

According to Figure 6.36, the greatest pressure before reaching the maximum peak point was 2.11 kPa. A local peak with a pressure of 1.29 kPa was observed. The maximum measured pressure was 2.19 kPa.

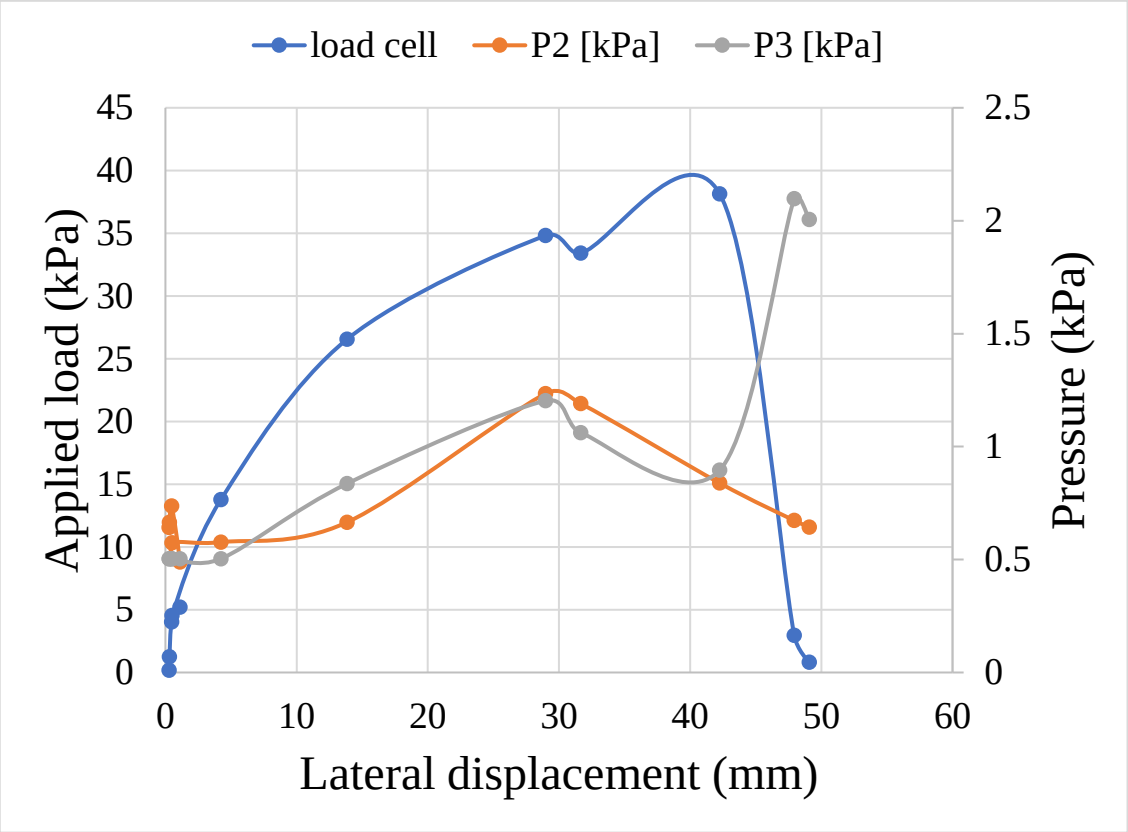

Figure 6.37. Applied load and pressure development with the lateral for third test saturated condition.

Figure 6.37 shows the lateral pressure and the applied pressure against the lateral displacement. The lateral pressure was increasing in both levels on the sheet pile until the applied pressure reached 35 kPa. After reaching the applied load 35kPa, the lateral pressure starts to decrease to the end of the test. The maximum applied pressure was 39 kPa. The failure point was the first peak when the applied pressure reached 35 kPa and displacement 30 mm.

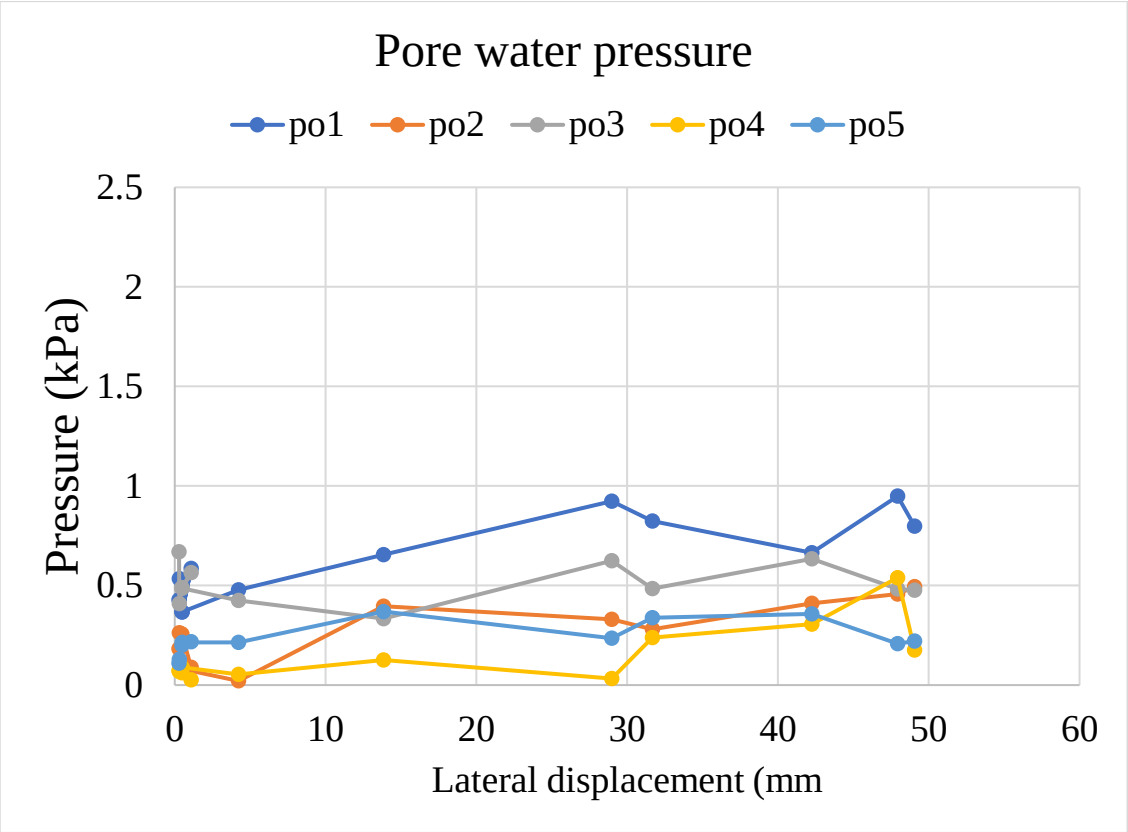

Figure 6.38. Pore water pressure with lateral displacement for the third model.

Figure 6.38 shows the water pressure at different points. PO1 was the highest-pressure point. The pressure in points PO2, PO4, and PO5 were close to each other at the end of the test. Before the failure happened in the soil, the pressure in points PO1 and PO3 increased then started to decrease after the failure. The pressure in points PO2, PO4, and PO5 started to increase after the failure.

6.3.4. Fourth model

The model setup shows in Figure 6.39 shows the model setup. The reinforced area mixture is represented by ST in the figure. The backfill had a triangle area with a 48 cm base and 34 cm height.

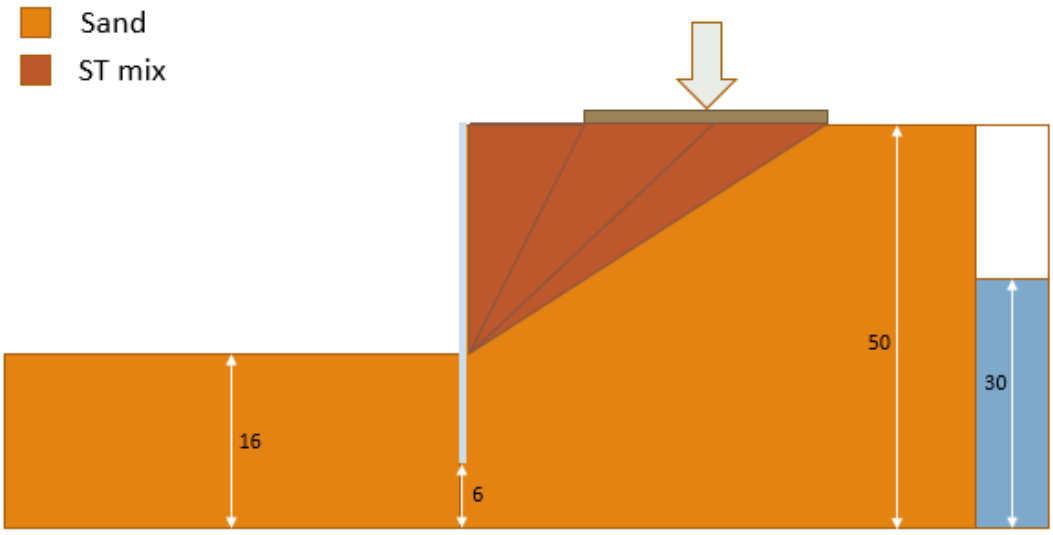

Figure 6.39. Fourth model setup saturated condition.

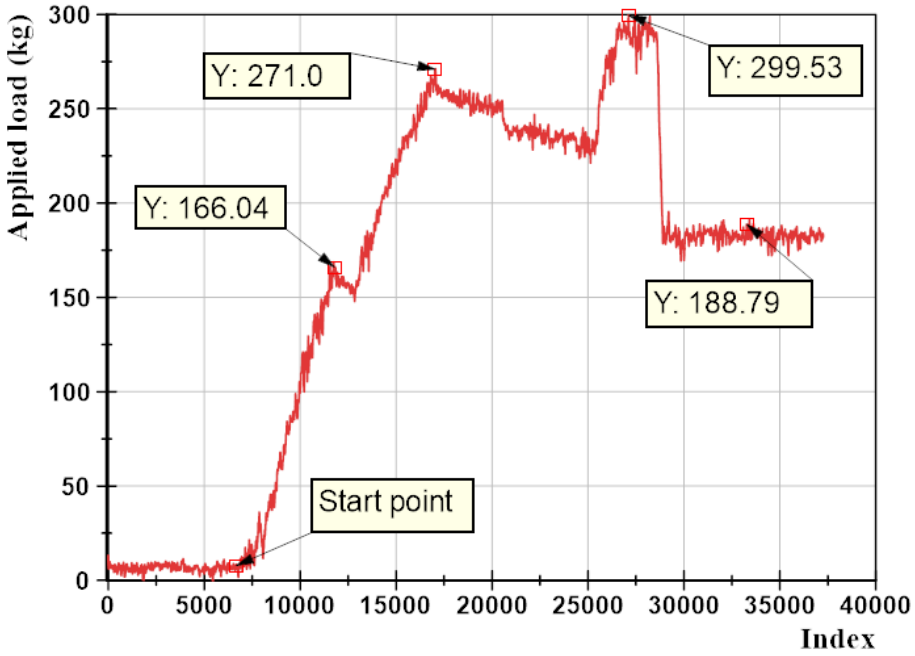

Figure 6.40. Load cell data recorded from the fourth saturated model condition.

According to Figure 6.40, the maximum applied load was 299.53 kg. Two pressure drops happened, as shown in the figure. The first drop happened when the applied load reached 166.04 kg, and the second happened when the applied load reached 271 kg.

According to Figure 6.41, the maximum pressure is 0.866 kPa prior to a peak shown with a pressure of 0.826 kPa. Following that, the pressure was reduced and then increased to its maximum value.

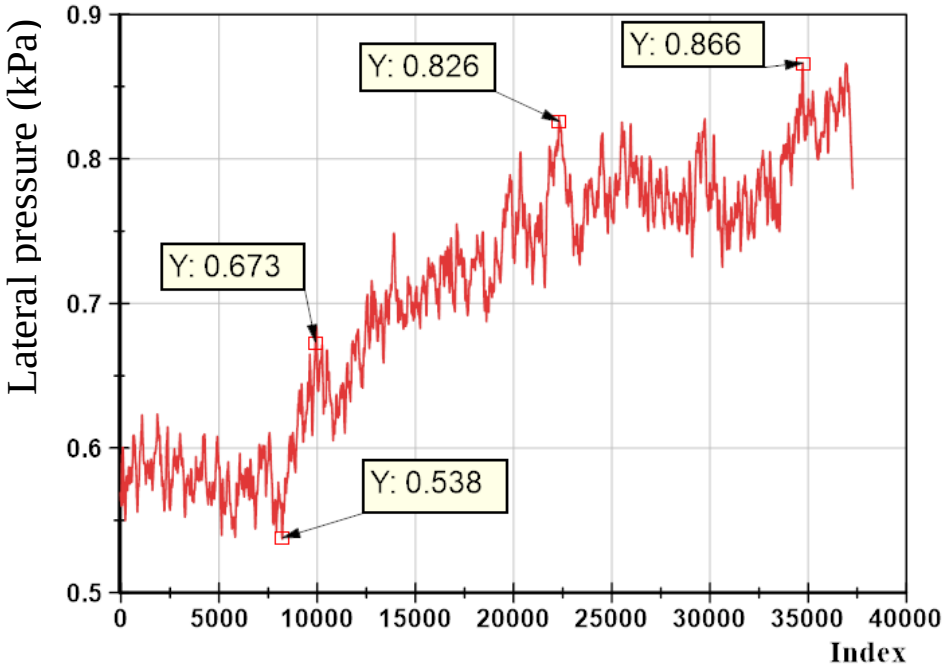

Figure 6.41. Lateral pressure data (P2) recorded from the fourth model saturated condition.

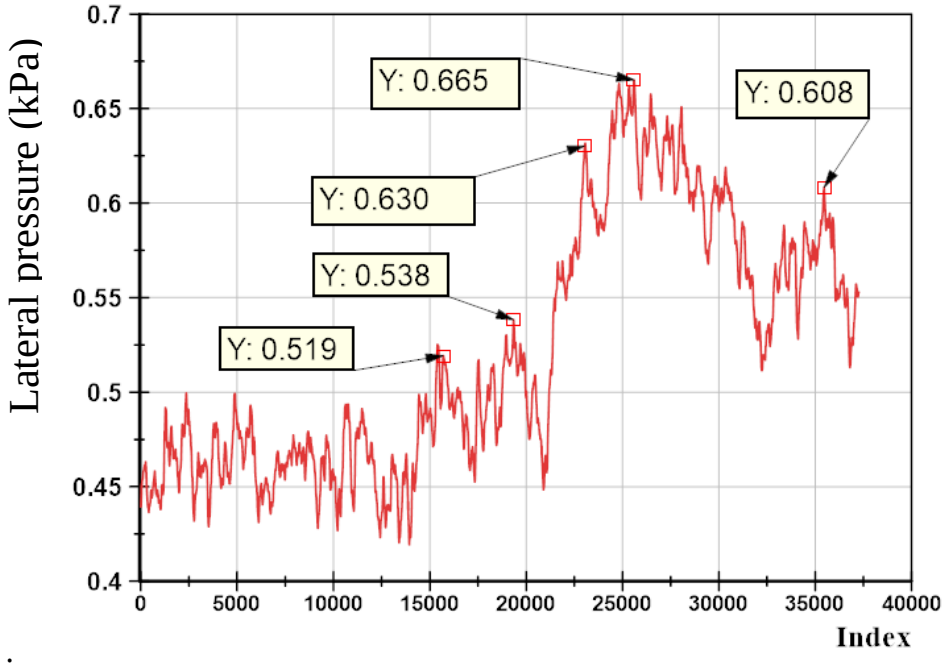

.

Figure 6.42. Lateral pressure data (P3) recorded from the fourth model saturated condition.

From Figure 6.42, the maximum pressure is 0.665 kPa. Before reaching the maximum pressure, several pressures drop happened, as shown in the figure.

From Figure 6.43, the first peak is considered to be the failure point when the stress reaches 47 kPa. The lateral pressure showed an increase before the applied stress reached 47 kPa. In spite of the applied stress, the lateral pressure decreased.

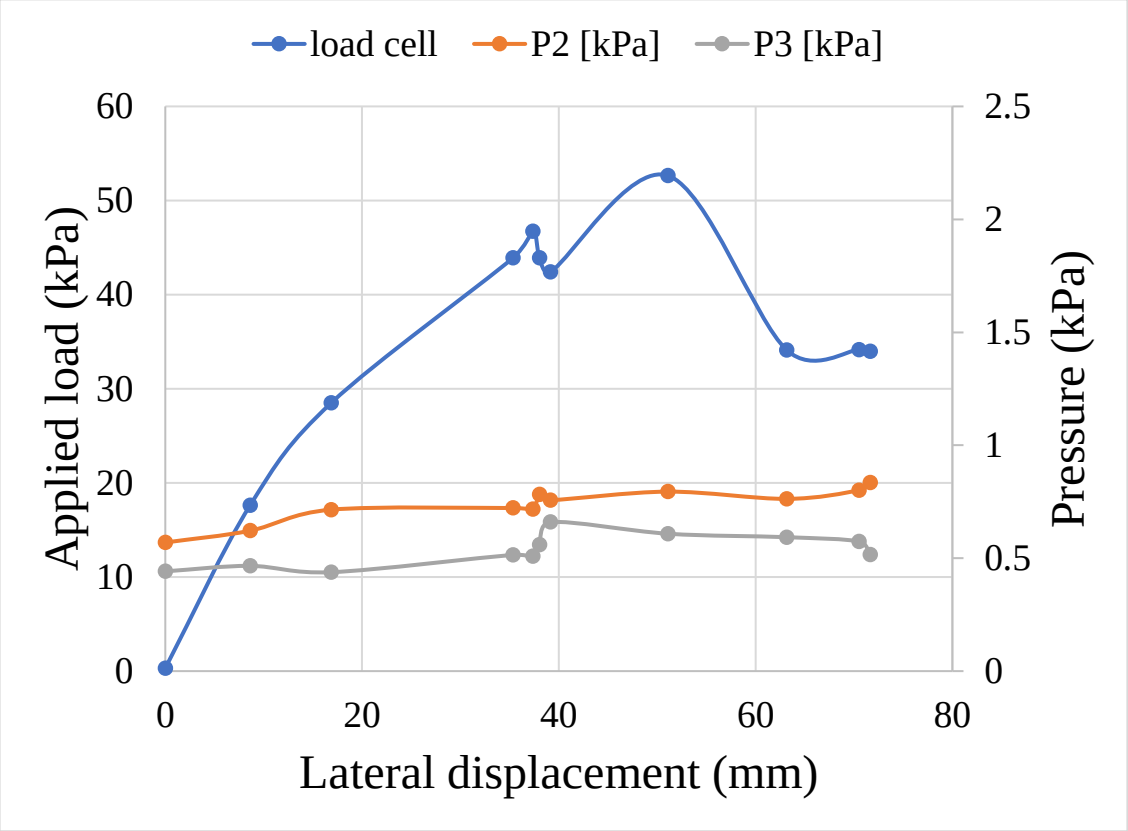

Figure 6.43. Applied load and pressure development with the lateral for fourth test saturated condition.

Figure 6.44 shows the water pressure in five points. The sudden change in water pressure in the middle of the graph corresponds to the failure. The pressure at PO5 and PO4 was higher than the other points during the test.

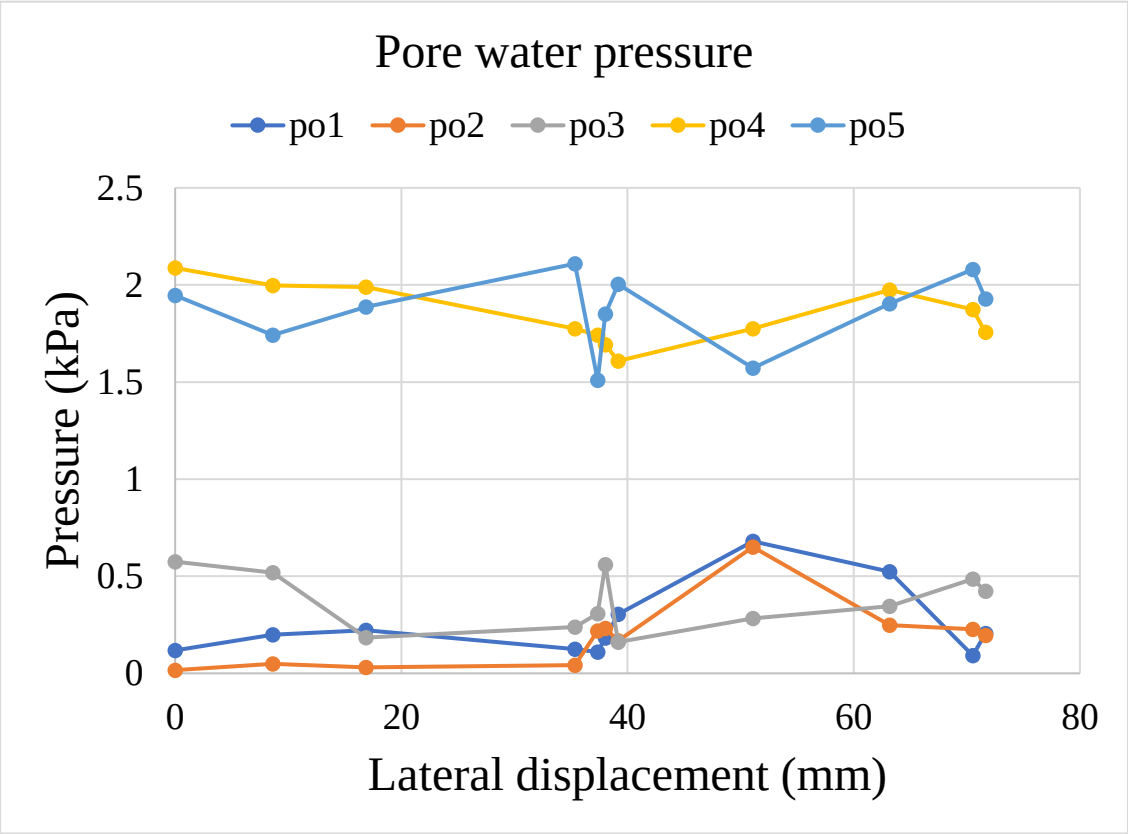

Figure 6.44. Pore water pressure with lateral displacement for the fourth model.

6.4. Summary

Table 6.1. Dry model results

Model	Maximum applied load	P2 pressure		P3 pressure		Lateral displacement
	kg	kPa		kPa		mm
		Max	Min	Max	Min	
DT1	133	2.25	0.45	2.31	0.1	32.59
DT2	155	1.08	0.83	0.63	0.32	49.81
DT3	140	1.8	0.5	1.2	0.1	64.8
DT4	164	3.67	0.12	2.04	1.05	50.67

Table 6.2. Saturated model results

Model	Maximum applied load	P2 pressure		P3 pressure		Lateral displacement
	Kg	kPa		kPa		mm
		Max	Min	Max	Min	
ST1	61.4	4.84	3.41	2.40	0.58	79.94
ST2	93.5	1.73	1.44	1.4	0.67	106.28
ST3	250	1.31	0.5	2.10	0.55	49.06
ST4	299.5	0.86	0.55	0.66	0.41	71.64

CHAPTER 7

CONCLUSION

The aim of this study was to examine the ability to use granulated rubber as lightweight backfill behind the sheet pile wall. Hence, the sheet pile and sand-granulated rubber mixture as a backfill material were modeled in this research program. The following conclusions were found from this study:

- Direct shear tests and compaction tests were conducted to find the optimum granulated rubber mixing ratio and its effect on the physical and mechanical properties. Fine granulated rubber-sand mix was tested with different mixing zthe shear strength with a mixing ratio of 10%.
- The 10% fine granulated rubber-sand mix showed enhancement in shear strength by 3.6%, and with 150% higher normal stress, the shear strength increased by 6.3%, but when the normal increased farther more, the shear decreased by 0.9%.
- For coarse granulated rubber-sand mix, due to the large size of the granulated rubber particles, the shear strength is enhanced by 17.5% in the 12% mix, but it drops with higher normal stress. Hence, the best mixing ratio was 10 %.
- This sudden change in shear strength for mixes was caused by the effect of rubber particles distribution inside the sample, and relatively the small size of the testing sample made this effect on the results.
- Compaction test results when 10% coarse and fine granulated rubber mixes tested show the maximum dry density dropped by 3.1 % when finely granulated rubber used and 2.1% for coarse granulated rubber for 10% mixing ratio. This is caused by the number of rubber particles inside the mix because the mixing ratio is by volume. The course is less than fine particles in the mix.
- Granulated rubber showed a promising result that reduced stiffness and density, on the other hand, increased the shear resistance and permeability that made it suitable to be a good soil improvement when lightweight backfill wanted.

The 10% fine granulated rubber mix was tested in the experimental model in dry and saturated conditions. The dry soil model results are shown in Figure 7.1. DT1 in the figure represents the sand model that worked as a control model. By comparing the results of the other models with the control model, we can reach the following conclusions:

- DT4 represents the fourth model showing that increasing the mix volume gave higher lateral displacement with lower applied force. Because the soil under the loading plate was the mix, only the led to the majority of the applied pressure to pass through the mix part.
- DT 3, representing the third model, showed the weakest behavior among the tested soil models. This weak behavior shows that the weakest area is between the backfill and the original soil. Because in this model, the applied load acted directly on the area between the backfill and the original soil.
- DT2 represents the second model. The results show that the second model showed a response similar to the sand model that shows the type of soil under the loading plate is very important in stress distribution. In the second model, the backfill was extending from the sheet pile to the edge of the loading plate, reducing the lateral pressure on the sheet pile.

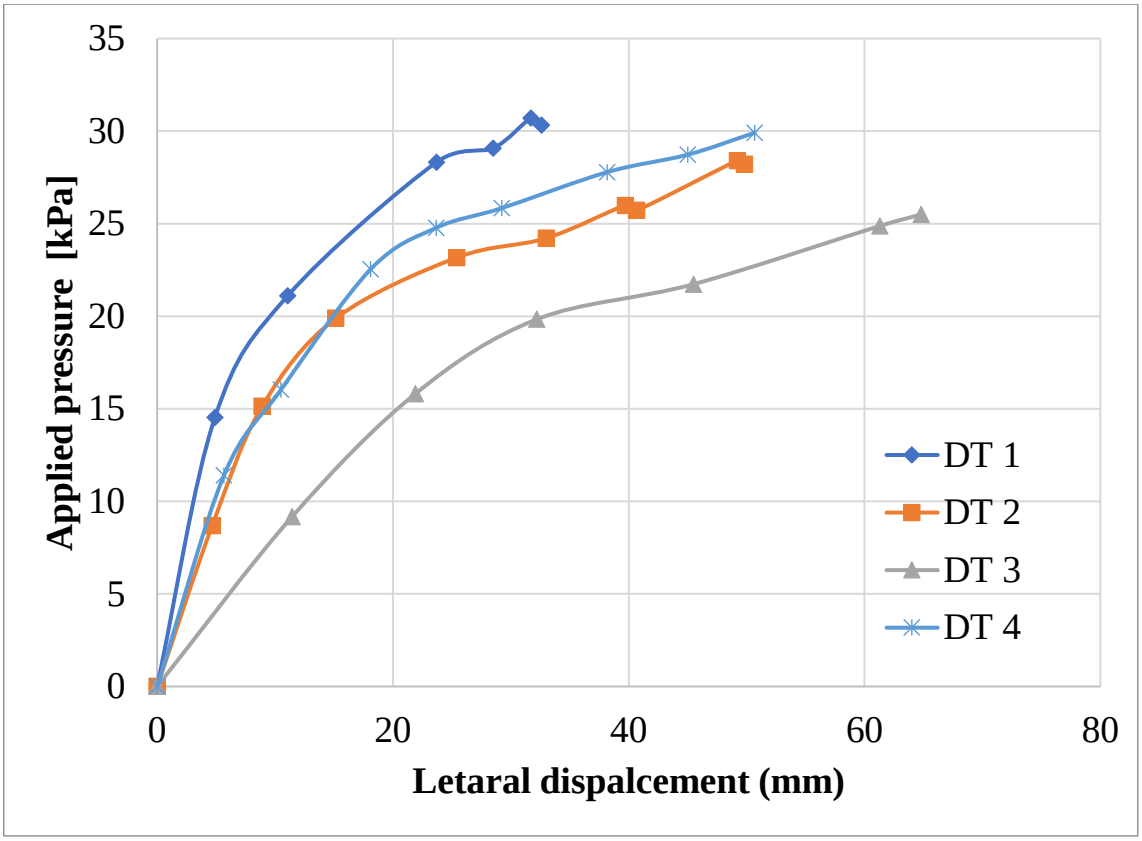

Figure 7.1. Applied load and lateral displacement response for dry soil models.

The saturated model results are shown in Figure 7.2. ST1 in the figure represents the saturated sand model that worked as a control model. By comparing the results of the other models in Figure 7.2 with the control model, we can reach the following conclusions:

- ST2 represents the second model. The results show that the model reached a higher applied load than the control model while the displacement was the same as the control model. Its response was weaker than the control model before reaching 50% of the lateral displacement. The results showed that the backfill had a small effect on the model.
- ST3 represents the third model. In this model, the backfill was extending from the sheet pile to the middle of the loading plate. The results show a higher resistance with low lateral displacement that reached 61% of the control model in addition. It showed two major failures. The cause of the high resistance is due to the high permeability of the mix that made the backfill mix lose the water faster when the load was applied, which eventually increased the resistance.

- ST4 represents the fourth model. The results show that the fourth model reached the highest load with displacement equal to 89 % of the control (CLEAN SAND) model. The backfill in this model extended from the sheet pile to the end of the loading plate, forming a high permeability layer under the loading plate. Due to this layer, the effect of the water is reduced.

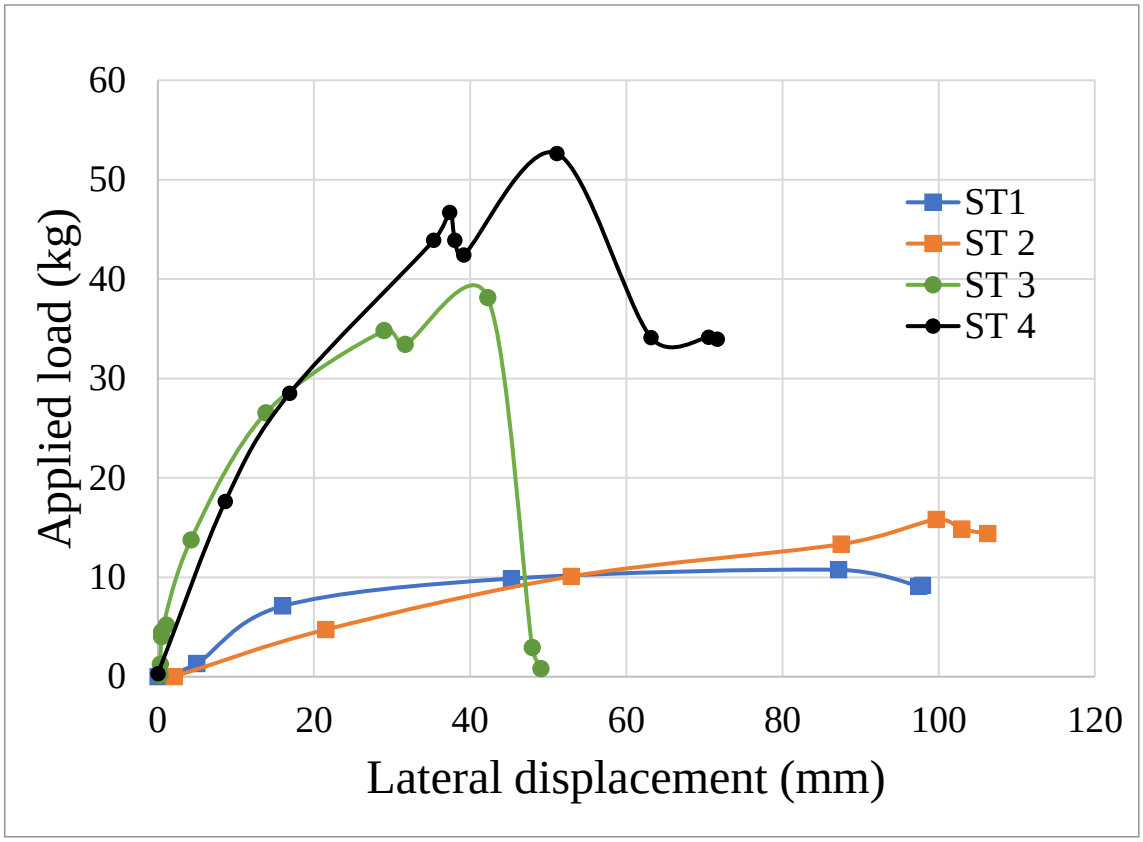

Figure 7.2. Applied load and lateral displacement response for saturated models.

7.1. Recommended Future Studies

- For design optimization, direct shear results can be used to build a constitutive model for the granulated rubber-sand mix.
- The response of the sand-granulated rubber backfill material behind the sheet pile can be tested in dynamic conditions. Examine the ability of the granulated rubber in improving the dynamic response characteristics of sandy soil
- The response of the sand-granulated rubber backfill material as a liquefaction countermeasure for residential buildings can be studied as a low-cost technique to prevent vibration and liquefaction-induced damage to residential buildings.

REFERENCES

Aksoy, Hüseyin Suha, Nichirvan TAHER, and Halmat AWLLA. 2021. “Shear Strength Parameters of Sand-Tire Chips Mixtures.” Gümüşhane Üniversitesi Fen Bilimleri Enstitüsü Dergisi (July).

Al-Neami, Mohammed Abdullateef. 2018. “Stabilization of Sandy Soil Using Recycle Waste Tire Chips.” International Journal of GEOMATE 15(48): 175–80.

Amanta, Adyasha Swayamsiddha, and Satyanarayana Murty Dasaka. 2021. “Evaluation of Engineering Properties of Sand–Tire Chips Mix.” Indian Geotechnical Journal. https://doi.org/10.1007/s40098-021-00552-5.

Banzibaganye, G, A Becker, and C Vrettos. 2019. “Static and Cyclic Triaxial Tests on Medium Sand and Tire Chips Mixtures.” Proceedings 17th African Regional Conference on Soil Mechanics and Geotechnical Engineering (October).

Chevalier, Bastien, Yohei Tsutsumi, and Jun Otani. 2019. “Direct Shear Behavior of a Mixture of Sand and Tire Chips Using X-Ray Computed Tomography and Discrete Element Method.” International Journal of Geosynthetics and Ground Engineering 5(2): 1–12. http://dx.doi.org/10.1007/s40891-019-0160-3.

D. Pradeep Kumar, S. Bali Reddy and A. Murali Krishna. 2014. “Evaluation of Optimum Mix of Sand-Tire Chip Mixtures for Geotechnical.” (December).

Ding, Yu et al. 2021. “Experimental Investigation on Static and Dynamic Characteristics of Granulated Rubber-Sand Mixtures as a New Railway Subgrade Filler.” Construction and Building Materials 273: 121955. https://doi.org/10.1016/j.conbuildmat.2020.121955.

Gill, Gourav, and Ravi Kant Mittal. 2019. “Use of Waste Tire-Chips in Shallow Footings Subjected to Eccentric Loading-an Experimental Study.” Construction and Building Materials 199: 335–48. https://doi.org/10.1016/j.conbuildmat.2018.12.024.

Hazarika, Hemanta et al. 2020. “Tire-Chip Reinforced Foundation as Liquefaction Countermeasure for Residential Buildings.” Soils and Foundations 60(2): 315–26. https://doi.org/10.1016/j.sandf.2019.12.013.

Jamshidi, R., I. Towhata, H. Ghiassian, and A. R. Tabarsa. 2010. “Experimental Evaluation of Dynamic Deformation Characteristics of Sheet Pile Retaining Walls with Fiber Reinforced Backfill.” Soil Dynamics and Earthquake Engineering 30(6): 438–46. http://dx.doi.org/10.1016/j.soildyn.2009.12.017.

Kaneda, K., H. Hazarika, and H. Yamazaki. 2018. “Examination of Earth Pressure Reduction Mechanism Using Tire-Chip Inclusion in Sandy Backfill via Numerical Simulation.” Soils and Foundations 58(5): 1272–81. https://doi.org/10.1016/j.sandf.2018.06.002.

Kim, Byung Tak, and Gil Lim Yoon. 2011. “Laboratory Modeling of Laterally Loaded Pile Groups in Sand.” KSCE Journal of Civil Engineering 15(1): 65–75. www.springer.com/12205 (March 20, 2021).

Lambert, S., L. Bałachowski, and P. Gotteland. 2005. “Strength Characteristics of Tyre Chips-Sand Mixtures.” Studia Geotechnica et Mechanica Vol. 27(nr 1-2): 55–66.

Lesniewska, D., and D. Muir Wood. 2011. “Photoelastic and Photographic Study of a Granular Material.” Geotechnique 61(7): 605–11.

Liu, Lulu, Guojun Cai, and Xiaoyan Liu. 2020. “Investigation of Thermal Conductivity and Prediction Model of Recycled Tire Rubber-Sand Mixtures as Lightweight Backfill.” Construction and Building Materials 248: 118657. https://doi.org/10.1016/j.conbuildmat.2020.118657.

Marto, Aminaton, Sayyed Yaghoub, and Zolfeghari Far. 2013. Article in Electronic Journal of Geotechnical Engineering Shear Properties of Sand-Tire Chips Mixtures. https://www.researchgate.net/publication/260390260 (March 20, 2021).

Masad, Eyad, Ramzi Taha, Carlton Ho, and Thomas Papagiannakis. 1996. “Engineering Properties of Tire/Soil Mixtures as a Lightweight Fill Material.” Geotechnical Testing Journal 19(3): 297–304.

Mashiri, M. S., J. S. Vinod, and M. Neaz Sheikh. 2016. “Constitutive Model for Sand–Tire Chip Mixture.” International Journal of Geomechanics 16(1): 04015022.

McGown, A., K. Z. Andrawes, and M. M. Al-Hasani. 1978. “Effect of Inclusion Properties on the Behaviour of Sand.” Geotechnique 28(3): 327–46.

Mittal, Ravi Kant, and Gourav Gill. 2018. “Sustainable Application of Waste Tire Chips and Geogrid for Improving Load Carrying Capacity of Granular Soils.” Journal of Cleaner Production 200: 542–51. https://doi.org/10.1016/j.jclepro.2018.07.287.

Ravichandran, Nadarajah, and Lea Huggins. 2014. “Applicability of Shredded Tire Chips as a Lightweight Retaining Wall Backfill in Seismic Regions.” : 3496–3505.

Reddy, S. Bali, and A. Murali Krishna. 2015. “Recycled Tire Chips Mixed with Sand as Lightweight Backfill Material in Retaining Wall Applications: An Experimental Investigation.” International Journal of Geosynthetics and Ground Engineering 1(4).

Sandford, Thomas C, and Michelle M Cribbs. 1997. “Shear Strength and Compressibility of Tire Chips for Use as Retaining Wall Backfill.” : 29–35.

Shariatmadari, N., S. M. Zeinali, H. Mirzaeifar, and M. Keramati. 2018. “Evaluating the Effect of Using Shredded Waste Tire in the Stone Columns as an Improvement Technique.” Construction and Building Materials 176: 700–709. https://doi.org/10.1016/j.conbuildmat.2018.05.090.

Silva Araujo, Gregorio Luis, Jaime Alberto Suarez Moreno, and Jorge G. Zornberg. 2021. “Shear Behavior of Mixtures Involving Tropical Soils and Tire Shreds.” Construction and Building Materials 276: 122061. https://doi.org/10.1016/j.conbuildmat.2020.122061.

Tabrizi, Mohammad Karamad et al. 2019. “Experimental Investigation on the Behavior of Fine-Grained Soils Containing Waste Rubber Tires under Repeated and Static Loading Using Direct Shear Apparatus.” Construction and Building Materials 223: 106–19. https://doi.org/10.1016/j.conbuildmat.2019.06.159.

Tatlisoz, Nilay, Craig H. Benson, and Tuncer B. Edil. 1997. “Effect of Fines on Mechanical Properties of Soil-Tire Chip Mixtures.” ASTM Special Technical Publication 1275(December 2015): 93–108.

Tsiavos, Anastasios et al. 2019. “A Sand-Rubber Deformable Granular Layer as a Low-Cost Seismic Isolation Strategy in Developing Countries: Experimental Investigation.” Soil Dynamics and Earthquake Engineering 125(May): 105731. https://doi.org/10.1016/j.soildyn.2019.105731.

Warith, M. A., E. Evgin, and P. A.S. Benson. 2004. “Suitability of Shredded Tires for Use in Landfill Leachate Collection Systems.” Waste Management 24(10): 967–79.